Air-Sea Interaction over the Agulhas Current and Implication for South African Weather

M Rouault • JRE Lutjeharms • AM Lee-Thorp • MR Jury
M Majodina

Report to the Water Research Commission
by the
Department of Oceanography
University of Cape Town

WRC Report No 374/1/99

Disclaimer

This report emanates from a project financed by the Water Research Commission (WRC) and is approved for publication. Approval does not signify that the contents necessarily reflect the views and policies of the WRC or the members of the project steering committee, nor does mention of trade names or commercial products constitute endorsement or recommendation for use.

Vrywaring

Hierdie verslag spruit voort uit 'n navorsingsprojek wat deur die Waternavorsingskommissie (WNK) gefinansier is en goedgekeur is vir publikasie. Goedkeuring beteken nie noodwendig dat die inhoud die siening en beleid van die WNK of die lede van die projek-loodskomitee weerspieël nie, of dat melding van handelsname of -ware deur die WNK vir gebruik goedgekeur of aanbeveel word nie.

AIR-SEA INTERACTION OVER THE AGULHAS CURRENT AND IMPLICATION FOR SOUTH AFRICAN WEATHER

Final report to the
WATER RESEARCH COMMISSION
By The
DEPARTMENT OF OCEANOGRAPHY
UNIVERSITY OF CAPE TOWN

Rouault, M., Lutjeharms, J.R.E., Lee-Thorp, A.M., Jury, M.R. and Majodina, M.

August 1998

WRC Report No : 374/1/99

ISBN No : 1 86845 489 4

Contents

List of Figures

List of Tables

Acknowledgements

We would like to thank the Chief Director of of the Weather Bureau for the help by that institution. The collaboration for all matters related to radiosondes was essential for the success of the project. We offer special thanks to Elizabeth Poppitch, Tom Roos, Sydney Marais and Piet King from the Weather Bureau who launched the radiosondes and helped with the data.

We would also like to thanks Dr Vere Shannon, director of the Sea Fisheries Research Institute for making shiptime, data and technicians available. We are particularly indebted to Robert Robertson, Donald Alexander, Pieter Claassen, Didi Van Royeen and Patrick Folley of the Sea Fisheries Research Institute for their technical assistance in installing the instrument package and for modifying the DDS software.

We would like to thank Prof Geoff Brundrit, head of the Oceanography Department that hosted the project. Special thanks to Koos Williams, John Joseph, Penny Krohn, Lesley Staegeman, Lesley Elley and Shirley Hutchings.

The success of the research cruises during which these data were collected was due to the hard work and dedication of a large number of people all mentioned by name in the relevent data reports.

We would like to thank Prof K. Katsaros, Dr Yves Quilfen and S. Pouliquen from the Department of Oceanography from Space at IFREMER, France, for the ERS-1 data.

We would like to thanks Dr Chris Fairall, Dr Jim Edson and Prof Ken Davidson who advice on the instruments and methods and made their software avalaible.

We would also like to thank members of the steering commitee whose inputs were beneficial to the project and in particular Dr George Green of the Water Research Commission for his support, help and encouragement.

Executive summary

Recent statistical results have demonstrated that the oceanic environment of Southern Africa plays an important regulating role in the climate of the subcontinent. Statistical teleconnections between oceanic temperature anomalies and precipitation over South Africa's summer rainfall region have been demonstrated. A research programme to investigate the physical mechanisms of ocean atmosphere interaction in those areas that have been identified as crucial to Southern Africa climate and rainfall started in 1993.

The main goal of this program was to perform high quality measurements and use up to date methods to quantify the air-sea exchange in those areas. We assembled a portable air-sea interaction measurement system. The system includes a Gill sonic anemometer, an Ophir infrared hygrometer, an Eppley pyranometer, an Eppley pyrgeometer and a Vaisala temperature and relative humidity probe. The turbulent fluxes of momentum, sensible heat and latent heat are calculated in real time using the bulk method and the inertial dissipation method. Both intrumentation and methods are state of the art and only the Ophir hygrometer gave us serious problems. The system was installed on the research vessel S.A Agulhas and tried with success during a 6 weeks cruise (the SAAMES 3 cruise) in the Roaring Forties during the 1993 winter. The system was then used in a coastal meteorology experiment in November 1993 and set up on a mast on top of a lighthouse at the end of a jetty. Ship time being scarce for dedicated air-sea interaction cruises, we decided to evaluate a low cost automatic air-sea interaction measurement system that could go on the three research vessels, S. A. Agulhas, Africana and Algoa. A relative humidity probe was added to an existing set of meteorological measurement devices aboard the research vessel S. A. Agulhas to provide an automatic, unmanned, air-sea interaction system. Measurements during the Marion Island relief cruises across the Agulhas Current with this new intrumentation were complemented by radiosonde releases made by the South African Weather Bureau. Radiosoundings provide vertical profiles of air temperature, humidity and wind. These data are useful to understand physical processes and to verify the results of numerical models. Furthermore they provide input data for radiation transfer models to calculate radiation budgets, and to develop and validate remote sensing techniques.

The highlight of this program was the Agulhas Current Air-Sea Exchange Experiment (ACASEX). It was the first dedicated air-sea interaction experimental cruise in the Agulhas Current. It took place during autumn 1995 to study the influence of the Agulhas Current on the atmospheric marine boundary layer. ACASEX resulted in a thorough investigation of the exchange between ocean and atmosphere, the net heat budget of the ocean, the structure of the marine atmospheric boundary layer as well as the behavior of the Agulhas Current and the upwelling cell at Port Alfred.

The portable air-sea interaction measurement system was again used during the ACE recovery experiment in April 1996. We also took part in 2 cruises of opportunity, the ACE cruise in 1995 and the ACE recovery cruise in 1996. Being guests on a foreign research vessel, it was not convenient to use our system and we used their meteorological instruments to collect data above the Agulhas Current.

Most of our measurements have shown that the core of the Agulhas Current, about 50 km wide, transfers about 5 times as much water vapour to the atmosphere as the surrounding water, all year long. Moreover the structure of the marine atmospheric boundary layer is very different offshore, above the core of the current and above the colder inshore water. The atmospheric

stability parameter is usually unstable above the current, stable above the inshore cold water and near neutral offshore. This creates an important heterogeneity at the mesoscale. This heterogeneity will create a problem for General Circulation Models whose hypothesis of homogeneous turbulence between 2 grids points, will be seriously challenged south of Africa.

The SAAMES 3 was a multi-disciplinary cruise on the research vessel S. A. Agulhas during the austral winter of 1993. The aim of the physical oceanographic component of the research cruise was to identify a warm eddy south of the Subtropical Convergence in the region south of Africa and to investigate its interaction with the Subtropical Convergence, with the ambient Subantarctic water masses and with the overlying atmosphere. Mesoscale oceanic features are believed potentially to have considerable effects on the overlying atmosphere, notwithstanding their relatively small lateral dimensions. We collected air-sea exchanges measurements over a warm eddy of subtropical origin found in the subantarctic south of Africa. Air-sea interaction measurements were made jointly with radiosonde launches and oceanographic measurements. These observations were made in winter, further enhancing the already strong ocean-atmosphere contrasts. The eddy was a substantial source of heat for the atmosphere as a result of latent heat fluxes of up to 500 Wm^{-2}, sensible heat fluxes of up to 350 Wm^{-2} and low short wave radiation inputs due to cloud coverage. The vertical heat flux from the ocean to the atmosphere in these mesoscale oceanic features is an order of magnitude higher than shown in climatology. Satellite altimetric data suggest that the eddy remained relatively stationary for a number of months. ERS-1 satellite wind measurements from this period show that the eddy had a persistent influence on the mesoscale wind field, increasing wind speeds whenever high differences between air and sea temperatures created unstable atmospheric conditions and high values of turbulent heat flux. Modification of air-sea interaction characteristics across the Agulhas Front, with a sea surface temperature difference of 8°C, were investigated during the cruise. It showed large differences of the air-sea exchange from the warm side to the cold side leading to decrease in wind strength on the colder side.

The East London 1993 experiment was a multi-disciplinary study of the lower atmospheric environment west of East London in November 1993. The study region falls in a transition zone between the dry area to the west and the sub-humid vegetated areas bordering the Agulhas Current to the east. Instrumented aircraft surveys were flown in the surface layer between the southeastern Karoo and the warm SW Indian Ocean. Meanwhile measurements were taken at the East London harbour jetty with our air-sea interaction measurement system. The goal was to characterize moisture inputs from the Agulhas Current to the adjacent plateau. Radiosonde data were used to quantify the humidity content of the atmospheric layer. Satellite composites of sea surface temperature (SST), vegetation reflectance and cloud temperatures were used to describe the physical environment following a prolonged drought and a brief wet spell. Cool upwelled water along the coast lies adjacent to sea surface temperatures > 24°C offshore, where gale force winds were measured by the aircraft. Aircraft and radiosonde data quantified the depth of the atmospheric moist layer and reveal how the sub-humid front is shifted east-west by large scale weather systems. Some aircraft sections illustrate sharp spatial gradients and changes in surface fluxes of order 100 $Wm^{-2}.(10\ km)^{-1}$. Inland penetration of moisture depends on background zonal winds and depth of the marine layer. Aircraft turbulent covariance estimates were used to identify high surface heat fluxes over the inland arid Karoo. During easterly winds, moisture fluxes are greatest over vegetated coastal mountains in a plume 2 km deep. Surface moisture fluxes over the Agulhas Current and coastal mountains are double those over the cold inshore waters and inland desert. The injection of moist unstable air increases the convective potential, during ridging anticyclone weather conditions.

The Marion Island Relief Cruises are part of a routine annual program to supply the base on Marion Island. Calculation of the turbulent fluxes of momentum, latent and sensible heat requires the simultaneous measurement of wind speed, sea surface temperature, air temperature and air humidity. Except for air humidity, these parameters are measured and stored aboard the three research vessels, S.A. Agulhas, Africana and Algoa. These vessels average approximately 200

days at sea each year and could gather valuable air-sea interaction data. Our seas are too rough to have an array of air-sea interaction buoys such as the Tropical Atmosphere Ocean (TAO) array of buoys deployed in the Pacific during TOGA. This array allowed investigators to study air-sea interaction processes, calibrate satellite and validate model output. This provides ample motivation for a shipboard, automatic air-sea interaction monitoring scheme. The simple addition of an air humidity probe to the existing suite of instruments on any of these platforms completes a low-cost, automatic, air-sea interaction measurement system. A relative humidity probe was installed aboard the S.A. Agulhas to provide such a system in 1994. Radiosonde releases made by the South African Weather Bureau aboard this vessel link the surface forcing to the remainder of the atmosphere providing invaluable data above the Agulhas Current at a very low cost and without having to spend 6 weeks to gather 4 days of data. In 1995 the full resolution of the radiosonde data was saved and stored during the cruise instead of the 10 mandatory points used for forecasting purpose. The operation was repeated in 1996 and 1997 with extra radiosonde ascents made by the SAWB personel above strategical areas of the Agulhas Current.

The Agulhas Current Air-Sea Exchange Experiment (20 April to 5 May, 1995) was the first dedicated air-sea interaction cruise to investigate the horizontal variability of ocean atmosphere interaction over the Agulhas Current and adjacent sea. ACASEX resulted in a thorough investigation of the exchange between ocean and atmosphere, the net heat budget of the ocean, the structure of the marine atmospheric boundary layer as well as the behavior of the Agulhas Current and the upwelling cell at Port Alfred for different wind conditions. Approximately 20 transects across the Agulhas Current were carried out in the area where the Agulhas Current separates from the coast, namely between Port Elizabeth and Port Alfred. To link surface measurements to the marine atmospheric boundary layer, radiosondes were launched 4 times a day. Oceanographic measurements were carried out in support of this program. Surface heat fluxes increased by over 200 Wm^{-2} over the current from a negligible amount over the shelf whilst the sensible heat flux reversed sign. A characteristically stable boundary layer over the cool shelf waters was replaced by an unstable convective boundary layer over the current. For both westerly and easterly wind cases the mean specific humidity and potential temperature of the boundary layer increased significantly with a concomitant boundary layer deepening over the current. In the presence of alongshore winds an atmospheric moisture and thermal front developed over the inshore SST front. This is attributed to the horizontal gradient in the surface heat fluxes at the time.

When air is advected towards the coast the surface latent heat flux increased from approximately 160 Wm^{-2} over the seaward border to 270 Wm^{-2} over the current (approximately 80-90 km wide) and decreased dramatically to approximately 40 Wm^{-2} over the cool shelf. This spatial heat flux gradient is reflected in the overlying atmosphere by a transition in atmospheric stability from the warm current to the cool continental shelf. A convective boundary layer over the current was replaced by a stable boundary layer over the cool shelf where a deep residual moisture layer indicated the former vertical extent of convective eddies. A progressive accumulation of moisture occurred within the boundary layer as the airmass was advected over the current. Mean specific humidity and precipitable water vapour content in the boundary layer over the shelf were 20-25 % higher than over the seaward border of the current. The results give credence to the assertion by many investigators that moisture uptake above the Agulhas Current may contribute significantly to moisture convergence and rainfall over the interior of South Africa.

During the cruise a transition in cumulus was observed above the Agulhas Current during a period of anticyclonic ridging. Clear conditions over the shelf were replaced by active, coupled cumuli above the current and partly cloudy conditions above the seaward border. Negligible or even downward heat exchanges occur over the shelf whilst strong atmospheric heat and moisture gains occur over the current. This sets up a transition in stability of the boundary layer and potential cumulus formation. Thermodynamic considerations adequately account for this cumulus transition. The vertical extent of cumulus is influenced by the atmospheric stability and limited by the subsidence inversion. Thus cumulus cloud lines also demonstrate a temporal evolution which is

determined by the wind and subsidence field of the ridging anticyclone. The transition in cumulus may increase the vertical extent of this atmospheric moisture front through vertical redistribution of heat and moisture.

Another important result was that neglecting the speed of the Agulhas Current in the calculation of the wind stress, sensible and latent heat flux could lead to large errors in the estimation of those fluxes. The mistake would be the same as a mistake induced by a 2 m/s error in the wind speed measurement.

To better illustrate the effect of the Agulhas current on the weather, we present two vertical contour plot of moisture from Port Elizabeth to the offshore edge of the Agulhas Current. The moisture data were obtained by releasing radiosondes from Port Elizabeth to the offshore edge of the Agulhas Current during two transects. On the 29 of April (bottom figure) the wind was almost parallel to the coast and to the Agulhas current. The accumulation of moisture is clearly visible above the Agulhas Current. (about 120 to 220 km from Port Elizabeth). Above the continental shelf and Port Elizabeth the air was a lot drier. An atmospheric moisture front above the inshore edge of the Agulhas Current was present.

On the 28 of April the wind was blowing from the Agulhas Current to Port Elizabeth. advecting a considerable amount of moisture above the continental shelf and Port Elizabeth. The precipitable water and the moisture increased by about 25 % above Port Elizabeth and the continental shelf, and the mixed layer deepened substantially. An atmospheric moisture front above the inshore edge of the Agulhas Current was created.

On the 28 and 29 the wind speed was about 5 to 10 m/s and moisture production and advection would be greatly enhanced at higher wind speed not uncommon in the area.

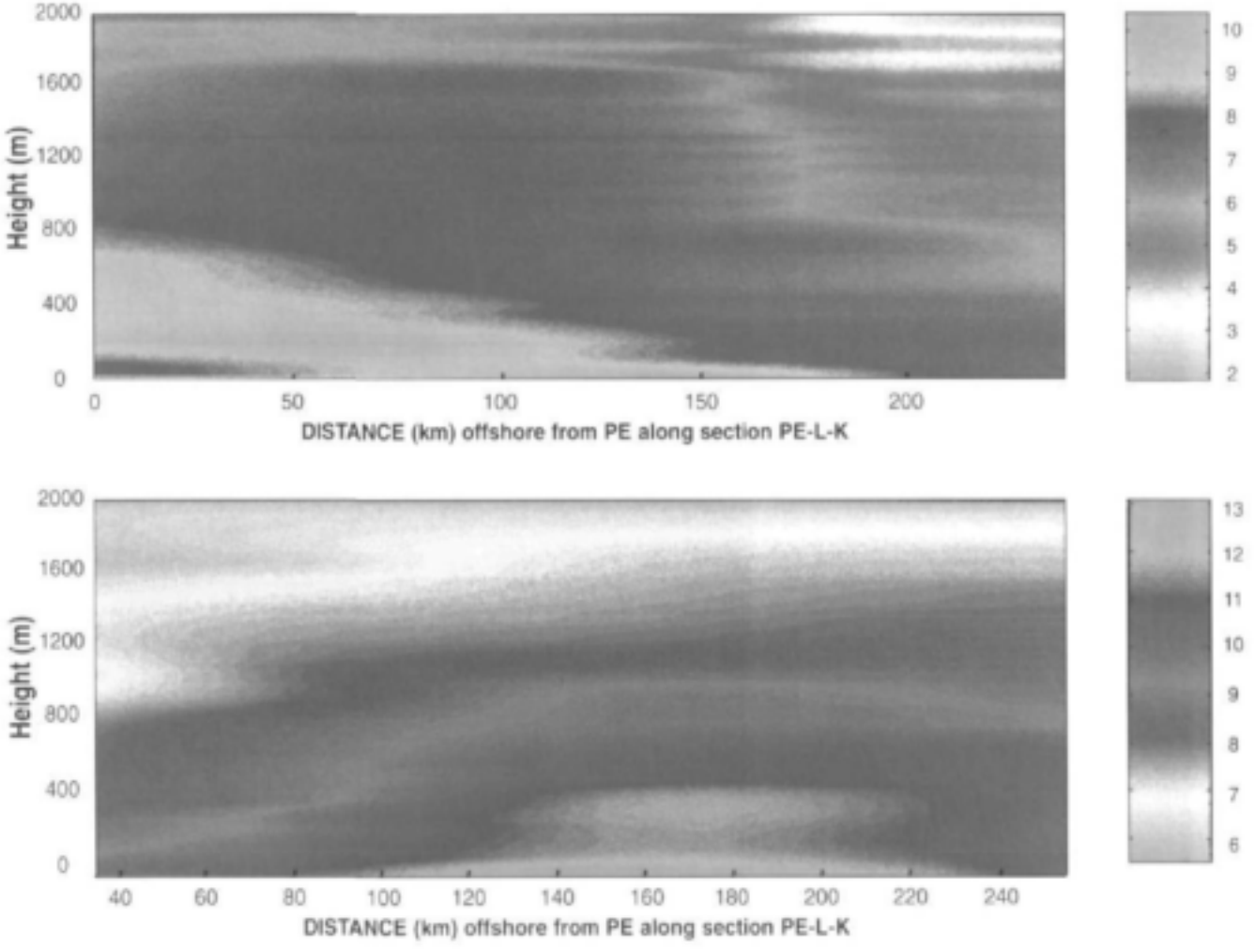

Figure 0.1: Colour contour plots of the specific humidity (g/kg) above Port Elizabeth, the continental shelf and the Agulhas Current on 28 April (top) and 29 April (bottom). On 28 April, southerly winds advected moisture accumulated above the Agulhas Current towards Port Elizabeth leading to a 25 % increase in precipitable water in the first 2 kilometers of the atmosphere. On 29 April, easterly along current wind led to local latent heat release above the current, deepening of the moisture layer and the formation of an atmospheric moisture front above the inshore edge of the Agulhas Current.

Chapter 1

Introduction

1.1 Motivation

Being for the greater part surrounded by ocean, it is to be expected that the weather and climate of Southern Africa is strongly influenced by these water masses. Recent statistical correlations (Walker, 1990; Jury et al., 1993) have demonstrated that heat losses in the Agulhas Current and Agulhas retroflection play an important regulating role in the weather and climate of the subcontinent. Anomalies of sea surface temperatures in the South Atlantic and South Indian oceans are geographically extensive and have a life-time of weeks to years. Furthermore, significant statistical teleconnections between these oceanic temperature anomalies and precipitation over South Africa's summer rainfall region have been demonstrated (Walker, 1990; Jury et al., 1993) Having established statistical connections, an understanding of the actual processes involved becomes important if ocean variability is to be used in future to predict rainfall patterns over land.

In order to investigate the interaction between ocean and atmosphere in those key ocean areas, a dedicated research programme has been instituted of which this document is the final report. To understand the coupling of the ocean and atmosphere, to calibrate satellite detected meteorological parameters and to improve air-sea interaction parameterization in the current numerical models, it is mandatory to have high resolution and accurate measurement of sea surface temperature, wind speed, air temperature and humidity, short and long wave radiation and to use them to calculate the turbulent and radiative fluxes and the net heat budget at the air-sea interface. Knowledge of the turbulent fluxes allows us to describe the structure of the lower part of the marine atmospheric boundary layer, i.e. vertical profiles of air temperature, humidity and wind. To link those surface measurement to the rest of the marine atmospheric boundary layer (MABL), radiosondes must be used. The interaction between the atmosphere and the oceans takes place in the (MABL) and the oceanic mixed boundary layer. The MABL layer is about 1 to 3 km thick while the oceanic mixed layer is less than a hundred meters deep. Both are decoupled from the remainder of their fluid bodies by a stratified layer called an inversion in the atmosphere and a thermocline in the ocean. The atmospheric boundary layer is currently better understood than the marine boundary layer. It is composed of a few millimeters thick laminar layer, a surface layer where the turbulent fluxes of momentum, latent and sensible heat are almost constant and a mixed layer up to the inversion zone. The surface layer is supposed to be horizontally homogeneous and processes are essentially turbulent.

The turbulent fluxes of momentum (wind stress), sensible heat and latent heat at the air-sea interface are important in numerous aspects of oceanography and meteorology. The latent heat flux is the energy flux connected with the vertical transport of water vapour, the evaporation. Oceanic evaporation leads to the latent heating of the atmosphere and participates in the creation of hurricanes and cyclones. Water vapour is advected above the continents by physical processes not well understood and depending on ocean-atmosphere interactions. Only a fraction of it precipitates above the continents. Consequently the global cloud coverage, precipitation rates and their

distribution depend mainly on the latent heat fluxes over the ocean. In turn evaporation leads to significant cooling of the upper ocean. The sea surface temperature field and the related thermohaline circulation depend on the net heat budget at the surface. Evaporation and precipitation at sea are the main forcing of the thermohaline circulation of the oceans. Oceanic motion is mainly due to atmospheric forcing by wind. This oceanic motion again affects the seasonal and climatic atmospheric temperature distribution. Gas exchange between the oceans and the atmosphere is directly regulated by sea state, wind speed and the air-sea temperature difference. Water vapour is a greenhouse gas; it plays an important role in the radiative balance of the atmosphere. On a smaller scale, latent and sensible heating in a strong convective regime, radiative heating and precipitation all have a strong influence on storm dynamics and regional circulation.

Satellite imagery and computer manipulation have succeeded in simulating roughly the coupling between the atmosphere and the oceans. Numerical simulation also yields interesting results but gross parameterization of boundary conditions, limitations due to the size of the modelling grid and the present impossiblity to take into account all the time scales involved prohibits a good description of exactly those small scale phenomena which are responsible for the ocean-atmosphere engine. Ideally, to understand the influence of air-sea interaction on a large scale, high quality in situ measurements have to be made jointly with satellite observations and the product should be assimilated in atmospheric general circulation model. The feedback between the fluxes and the different scales involved are responsible for the complication of the theory. Yet, there still is a lot of room for experimental studies and research programmes of measurements in this field, especially over the Agulhas Current

1.2 Background

Recently, researchers have undertaken air-sea interaction investigations in Southern African waters with both a climatological (Walker and Mey, 1988; Walker, 1990; Jury and Levey, 1993; Jury et al., 1993) and a meteorological (Jury and Courtney, 1991; Jury, 1993; Jury, 1994; Jury and Walker, 1988; Mey et al., 1990) emphasis.

Climate studies have, of necessity, tended to treat air-sea interactions over the adjacent oceanic region as a black box. This is due to the fact that too few dedicated air-sea interaction studies have been undertaken with the result that a conceptually reliable and useful model has yet to be proposed. As shown below there are large knowledge gaps in our understanding of ocean-atmopshere coupling mechanisms in the oceanic region adjacent to the subcontinent.

Differences in sea surface temperature (SST) between the cool shelf waters and the warm Agulhas Current (Pearce, 1977) offer the possibility of a semi-permanent mesoscale circulation system that can interact with transient weather systems (Jury, 1993). Indeed satellite images frequently show the presence of a line of deep cumulus clouds organized in the alongshore direction over the Agulhas Current either as singular cloud lines or as cloud streets (Lutjeharms et al., 1986).

Aircraft observations (Jury and Courtney, 1991) along a NW - SE cross-section of the northern edge of the Agulhas Current near the eastern Agulhas Bank during uniform, light, zonal (westerly) flow were composited to elucidate the mean boundary layer structure (Jury, 1993). The flight path covered a SST front of $8°C.(40\ km)^{-1}$. For zonal westerly flow (airflow from the cooler shelf waters to the Agulhas Current), typical of the winter season, the following results were obtained (Jury and Courtney, 1991; Jury 1993).

- The surface heat and momentum fluxes increased by a factor of 5.
- A warming and moistening of the boundary layer had implications for a subsequent deepening over the Agulhas Current
- Airflow accelerates over the front and decelerates downstream resulting in divergence, subsidence, clear weather formation over the front and convergence, convection and cumulus

formation over the current.

- Mixing through the boundary layer is accomplished by convective eddies of some 3 km horizontal extent.
- A low-level jet exceeded geostrophic values by about 50 % and indicates the presence of a thermal front in the atmosphere.
- These features are quasi-stationary.
- A thermal internal boundary layer (TIBL) associated with a clearly defined top is defined by the vertical wind variances (i.e. vertical gustiness). The depth of the TIBL increases with fetch downstream.

Schumann (1989) questioned the relationship between wind speed and pressure and particularly whether geostrophy applies to the South African coastline. Jury's (1993) derivation of the surface fluxes was obtained from the lowest aircraft flight level at 100 m. A question arises as to whether these measurements were made within the surface layer.

The meteorology of the Agulhas Bank is in fact highly variable over time, alternating between easterly and westerly flow. Easterly flow is required to initiate upwelling near the surface (Schumann et al., 1982). A direct consequence is that alternating wind stress may partially control the surface expression of the Agulhas Current and related SST front in the region. This has implications for the secondary circulations observed by Jury (1993). Transient anticyclones initiate shallow easterly flow whose characteristics within the boundary layer are quite unlike the westerly wind regime (Jury, 1994).

During easterly flow the airmass has already undergone modification over the warm Agulhas Current. Composite aircraft results for a single level across the Agulhas Current in this region distinguish the characteristics of easterly flow (Jury, 1994). In that case winds increase sharply toward the Agulhas Current whilst rotating clockwise toward the coast. The inshore zone is generally characterized by light winds.

Moving south of the Agulhas Bank, the Agulhas Current enters the retroflection region. It is well known that for the globe as as whole, maximum oceanic heat losses to the atmosphere occur over western boundary currents at mid-latitudes (Budyko, 1963; cited in Walker and Mey, 1988). It is to be expected that the Agulhas Current will experience greatest energy losses to the atmosphere in that region where high SSTs are continually exposed to cold air outbreaks. The Agulhas Retroflection area is such a region. Walker and Mey (1988) have used VOS (Voluntary Observing Ship) data to construct a heat flux climatology for this region. Unlike the Gulf Stream in the northern hemisphere that exhibits a pronounced annual heat flux cycle with maximum losses in winter (Bunker, 1976; cited in Walker and Mey, 1988) the Agulhas Retroflection Region (ARR) is continually exposed to cold, unsaturated, maritime air embedded within the westerlies (Walker and Mey, 1988). Their results are outlined below.

- A high heat flux core (200-225 Wm^{-2}) within the Agulhas Retroflection Region is found at 37°-41°S, 16° - 22° E.
- The latent heat flux exceeds the sensible heat flux by up to 90%.
- A weak, semi-annual heat flux cycle shows maximum losses in winter and spring.
- Spatial heat flux gradients are more pronounced in summer. This means that locally, cyclogenesis may not be as seasonally dependant as in the northern hemisphere.
- Spatial heat flux gradients are determined primarily by SST variability.
- Magnitudes of SST (and heat flux) variability on an interannual cycle exceed those of the intra-annual cycle.

It was concluded that heat loss from the ocean to atmosphere in this region was an important climatic factor (Walker and Mey, 1988). Subsequent investigations (Jury and Walker, 1988; Mey et al., 1990) have attempted to quantify and understand these exchange processes.

Meteorological observations from an aircraft survey in the retroflection region have shown the response of the MABL to a SST front of 6°C at the edge of the Agulhas Current (Jury and Walker, 1988). Significant boundary layer modification was demonstrated as the cool westerly flow encountered the warm current. A number of processes contributing to MABL modification were shown to be operating simultaneously on this occassion.

- Turbulent heat fluxes were enhanced over the warmer water.
- Divergence in the near-surface horizontal winds occurred. (This was attributed to daytime thermal entrainment onto the continent (sea breeze)).
- The surface layer wind accelerates over the SST front in a sea breeze like fashion.
- A mesoscale sea-breeze structure existed when synoptic-scale forcing was weak and intitiated a singular N-S cloud line.
- A boundary layer height growth and warming rate of 60m.°C^{-1} (SST) and 1°C (100 km)$^{-1}$ was found.

Whilst daytime thermal entrainment has been proposed as a mechanism for divergence of near-surface horizontal winds, the structure observed (Jury and Walker, 1988; Figures 3 and 4) closely resembles the expected anticyclonic wind-field structure. Jury and Walker (1988) also proposed that the MABL growth characteristics are influenced by synoptic scale divergence and subsidence of transient anticyclones. which serve to constrain the vertical extent of eddies.

Since lowest aircraft data were measured at a height of 70 m, these data were interpolated to 10 m values assuming a neutral atmosphere, before deriving bulk fluxes. Transfer coefficients of C_H=1.2 $\times$ 10^{-3}, C_E=1.5 $\times$ 10^{-3} and $C_H = C_E$=0.85 $\times$ 10^{-3} were used for unstable and stable conditions respectively.

A more descriptive study within the greater Agulhas Retroflection Region (Mey et al., 1990) has shown that under a westerly wind regime surface heat flux processes are enhanced under the simultaneous occurrence of strong winds and a cold air outbreak (a maximum of 828 Wm^{-2} was found). Their results for westerly zonal flow are outlined below.

- The MABL is characterized by strong low-level baroclinicity and low static stability.
- Surface lapse rates are superadiabatic as a result of surface warming.
- Dramatic increases in wind speed over the ARR-STC (Subtropical Convergence) SST front are associated with increased turbulent heat flux over the warm water.
- For the case where the wind blew along the ARR-STC front a jetlike flow parallel to the front and observed vertical wind shear were both closely related to the meridional gradient in SST.
- When a zonal wind blew perpendicular to the SST front (from cold to warm), marked vertical wind shear was replaced by a boundary layer in which winds were well-mixed.

Bulk fluxes were derived from three-hourly, shipboard observations (Mey et al., 1990). This is less than ideal as bulk flux derivations are intended for bulk averaged variables. Three-hourly observations are instantaneous readings made once every three hours and are a poor substitute. The air-sea flux parametrization scheme was identical to that of Walker and Mey (1988). No data were available for intercomparison. A maximum heat loss of 828 Wm^{-2} compares with values found for the Gulf Stream (Bane and Osgood, 1989). Slowly ascending radiosondes were released to elucidate

the boundary layer structure. The boundary layer top was then defined by a sudden change in slope of the dewpoint isotherm (Mey et al., 1990). However, at the time of the study, radiosonde ascents (undertaken by the South African Weather Bureau) were designed for operational forecast purposes only. This meant that only data from specific pressure levels (about 10 levels within the first 3000 m) were recorded, regardless of the ascent rate. This, coupled with an inadequate definition of the boundary layer height weakens the argument that boundary layer deepening was observed. The subsidence inversion height was erroneously identified as the boundary layer top and the study failed to demonstrate low static stability as the lapse rate of most vertical profiles did not exceed the dry adiabatic lapse rate (Mey et al., 1990; Figure 6).

Mey et al. (1990) argued that the observed processes may operate to enhance cyclogenesis by enhancing low-level baroclinicity and increasing the "tilt" of a westerly trough (Holton, 1979, p. 126; Mey et al., 1990). Furthermore the destabilized MABL is a source of energy to the region of frontal uplift. Whether this area sustains cyclogenesis remains to be tested. Nevertheless, the above discussion highlights the climatic importance of the Agulhas Retroflection Region.

Under an easterly wind regime air-sea transfer processes over the ARR and the Agulhas Current proper were quite unlike the westerly scenario (Mey et al., 1990).

- The airmass had already undergone modification over the warm current.
- Downward heat fluxes had implications for low-level stability and reduced surface wind stress.
- This situation is associated with a ridging (transient) anticyclone.

Having established some of the features within the boundary layer of the Agulhas Current over parts of its domain, various authors (eg. Walker, 1990; Jury et al., 1993) have used this information to construct a climatology of atmospheric control and interaction by the Agulhas Current.

As the Agulhas Current flows south from its source region of mostly subtropical atmospheric influence, it enters into a region whose atmospheric controls become increasingly dominated by mid-latitude influences (Preston-Whyte and Tyson, 1988). Coastal summer conditions are dominated by transient anticyclones which initiate shallow sub-tropical easterly flows. In winter, topographically trapped coastal lows track anticlockwise along the coast from west to east, often preceding mid-latitude westerly depressions whose influence is increasingly felt southwards.

Jury et al. (1993) have undertaken a statistical study of the influence of the Agulhas Current on summer rainfall along the southeast coast of the subcontinent between 28° - 34° S and 26° - 33° E in the transition region of sub-tropical/temperate influence.

- They found a strong correlation between adjacent coastal rainfall and SST (r = +0.88), and shelf-width (r= -0.92).
- Rainfall was found to decrease in a NE-SW gradient in conjunction with a NE-SW decline of maximum sea-surface temperature within the core of the current.
- These results indicate the influence of the proximity and temperature of the warm Agulhas Current adjacent to the coast, on the local rainfall.

Jury et al. (1993) have provided a model in which essentially two mechanisms are thought to produce alongshore variations in coastal rainfall. They are

- The modification of onshore moving air by surface heat fluxes, and
- The interaction between transient weather systems and the embedded mesoscale circulation over the Agulhas Current.

Under strong synoptic conditions the following model may be appropriate (Jury et al., 1993). Where the shelf is narrow, the Agulhas Current flows close to the coast. If the shelf is narrow or

wide, the fetch length over the relatively cooler shelf waters is limited or increased respectively. Recall that observations (Jury and Courtney, 1991; Jury, 1993) have shown the sharp decrease in surface heat fluxes in this inshore zone. The resultant increase in stability has implications for moisture uptake and wind stress. This feature is complemented by the fact that where the shelf is narrow the escarpment rises steeply along a narrow coastal plain. Where the shelf is wide the escarpment rises gently along a wide coastal plain. Where the shelf is narrow, orographically forced convection therefore may provide a complementary influence.

Jury (1993) has suggested that quasi-stationary, secondary convergent circulations are embedded within the Agulhas Current. Under light winds associated with gentle synoptic forcing or a more alongshore component of flow sustained convergence over the surface heat core is complemented by a subsiding cell near the front. Jury et al. (1993) have postulated that the position of the subsiding limb is indirectly influenced by shelf width. Where the shelf is wide, the quasi-stationary zone of subsidence is located on the inshore edge of the current and suppresses rainfall. Where the shelf is narrow, the steep orographic upslope (and subsequent uplift) may counteract subsidence . The results indicate the possible role played by the Agulhas Current in air-sea interactions in this region, leading to inputs of heat and moisture into the sub-tropical airmass, and the modification of transient weather systems.

It remains to be shown that the quasi-stationary circulation features observed by Jury (1993) occur also during the summer rainfall months when airflows are predominantly easterly. The analysis of Jury (1993) occurred during westerly flow associated with transient mid-latitude depressions, systems known to be inherently baroclinic (Holton, 1979). Easterly airflows are associated with transient anticyclones and constitute an essentially barotropic environment quite unlike that of westerly flow.

Walker (1990) has examined statistical relationships between South African summer rainfall and SST variability in the surrounding oceanic current regimes. Her analysis includes the entire summer rainfall region. Those results pertaining to the Agulhas Current circulation system are discussed below.

Wetter summers occurred with relatively higher SSTs in the Mozambique/Agulhas Current region. The ocean warming along the east coast and southern reaches of the Agulhas Current System is accompanied by stronger easterly winds in the South Indian Ocean especially in the area of Madagascar where large north-easterly anomalies were found. This suggests that the Indian Ocean Anticyclone is displaced polewards and westwards of its mean summer position. A concomitant poleward shift of the wind stress curl zero line in turn has implications for the Agulhas Current and will be discussed later. In particular the waters of the Agulhas Current may penetrate directly westward into the Southeast Atlantic Ocean. Walker (1990) has discussed ways that air-sea interactions may operate under these conditions and has outlined two mechanisms that may enhance summer rainfall. They are

- Increased moisture convergence over the interior.
- Tropical-temperate trough formation.

The simultaneous occurrence of a warmer Agulhas Current (hence a warmer, moister boundary layer) and stronger onshore winds increases moisture convergence over the tropical and sub-tropical interior. Further south, cyclogenesis occurs in association with intensified SST gradients in the ARR and resultant differential temperature advection (Holton, 1979). The highly dynamic nature of the boundary layer processes in the ARR has been discussed earlier. On a synoptic scale it is postulated that the tendency for intensification of mid-latitude low-pressure systems in the ARR might facilitate the formation of tropical-temperate troughs. These troughs are aligned in a NW-SE direction across the interior and are responsible for between 50 % and 90 % of South Africa's rainfall during most months (Harrison, 1984). The tendency is for the contribution of this synoptic type to increase during wetter (summer) months. Tropical-temperate troughs are associated with

cloud bands which connect tropical and temperate circulations (Preston-Whyte and Tyson, 1988; Harrison, 1984). This system provides a conduit for the poleward transfer of momentum and energy.

Walker's postulation that stronger onshore advection of warmer, moister air under large-scale, enhanced easterly circulation may enhance rainfall through increased moisture convergence over the interior is supported by the findings of Jury et al. (1993) for the coastal regions where highest SSTs are associated with highest levels of summer rainfall. It remains to be shown, however, that Agulhas Current warm events in the ARR (Walker, 1990) are indeed related to enhanced local cyclogenesis and to increased tropical-temperate trough formation. The former is likely to be a prerequisite for the latter. Since interannual SST variability in the ARR exceeds the intra-annual variability (Walker and Mey, 1988) this region is expected to play a role on a climatic as well as synoptic scale. Boundary layer processes in this region may even impact beyond South African climate. Apart from the role in modulating South African rainfall, such processes are likely to play a small role in the global atmospheric circulation of the southern hemisphere. On a global scale it may modulate the atmospheric exchange of momentum and energy between the tropics and the high-latitudes by virtue of its influence on cloud band formation. It is primarily this exchange which drives the global atmospheric circulation. It is apparent therefore that the air-sea interactions over the Agulhas Current may influence South African climate in two ways (Walker, 1990; Jury et al., 1993).

- Deepening, moistening and warming of the boundary layer has implications for moisture convergence and rainfall.
- Local cyclogenesis in the ARR may favour tropical-temperate trough formation.

It is worthwhile emphasising that to date our knowledge of air-sea interaction mechanisms over the Agulhas Current has been gleaned from just three meteorological experiments (Jury and Walker, 1988; Mey et al. 1990; Jury and Courtney, 1991). These shipboard pioneering studies used outdated instrumentation and methods and it was a goal of this project to bring up to date methods and instrumentation.

The next chapter describes the instruments used in that study. Chapter 3 describes the methods used to quantify the exchange at the air sea interface. The following chapters describe the different experiments in which we participated.

Chapter 2

Instrumentation

2.1 The air-sea interaction portable system

The first aim of this research project was to develop a system that employed up to date devices, methods and softwares necessary to infer radiation and turbulent fluxes at the air-sea interface in the Marine Atmospheric Surface Layer (MABL). Design of the system was motivated by six factors: cost, accuracy, ruggedness, speed, flexibility and extensibility. In order to calculate the turbulent fluxes, measurements of wind velocity, temperature and humidity are required. For the radiation fluxes, incoming and outgoing short wave and long wave radiation have to be measured or calculated. The following sections describe the instruments required and the software designed for the air sea interaction measurement system. A schematic of the devices is presented in Figure 2.1.

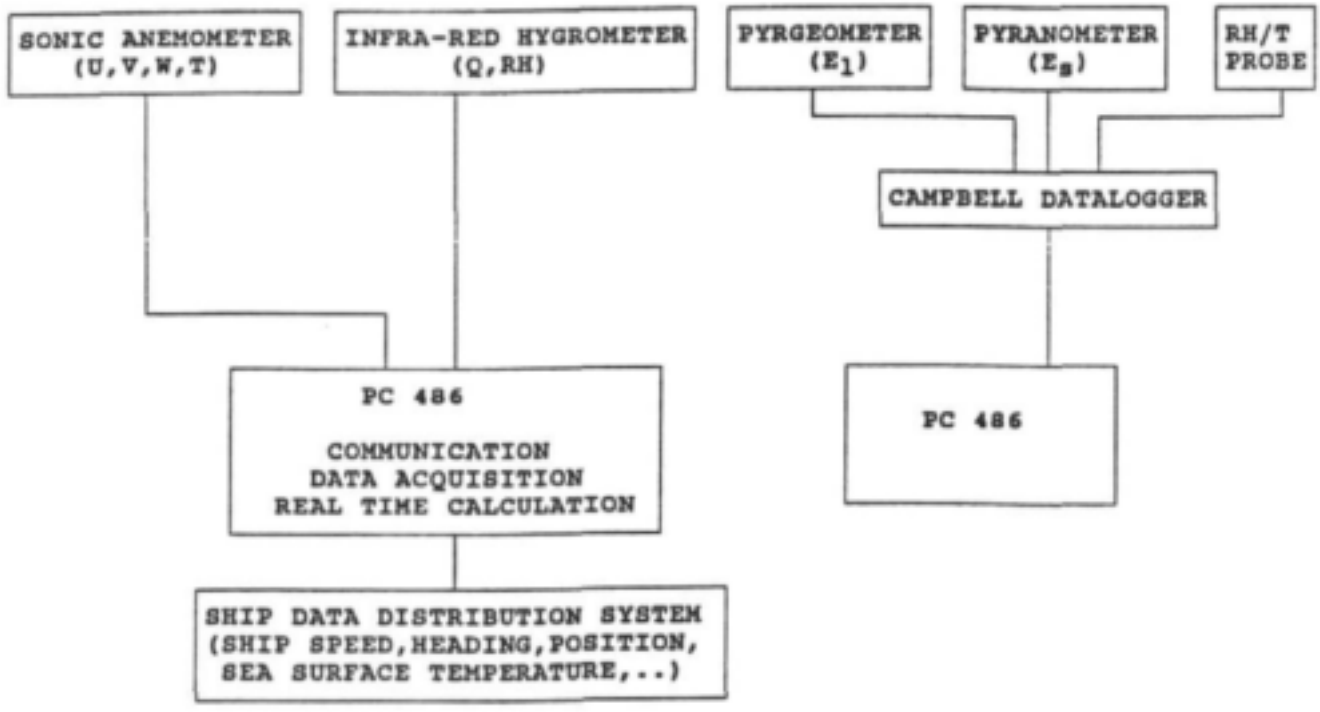

Figure 2.1: Schematic of devices for the portable air-sea interaction system

2.1.1 Fast response sensors and acquisition software

To be able to use the inertial dissipation method to calculate the turbulent fluxes, it is necessary to have fast response measurement of the wind speed, humidity and temperature and to perform Fast Fourier Transform while sampling the fast response devices

2.1.1.1 Sonic anemometer

The ultrasonic anemometer has become a standard instrument for turbulence and boundary layer research. It enables reliable fast response measurements of both u, v and w components of wind velocity, and temperature. It is rugged in the sense that it has no moving parts and possesses a stable absolute velocity calibration. It is not subject to sea-salt degradation which plagues the microthermal temperature sensors (De Cosmo, 1991) and possesses a significantly higher frequency response than traditional propeller anemometer problems which are plagued by problems of inertia.

The Gill ultrasonic anemometer (Figure 2.2) consists of a sensing head with six ultrasonic transducers arranged in three pairs above a cylindrical housing. A pair of transducers act as alternating transmitters and receivers sending

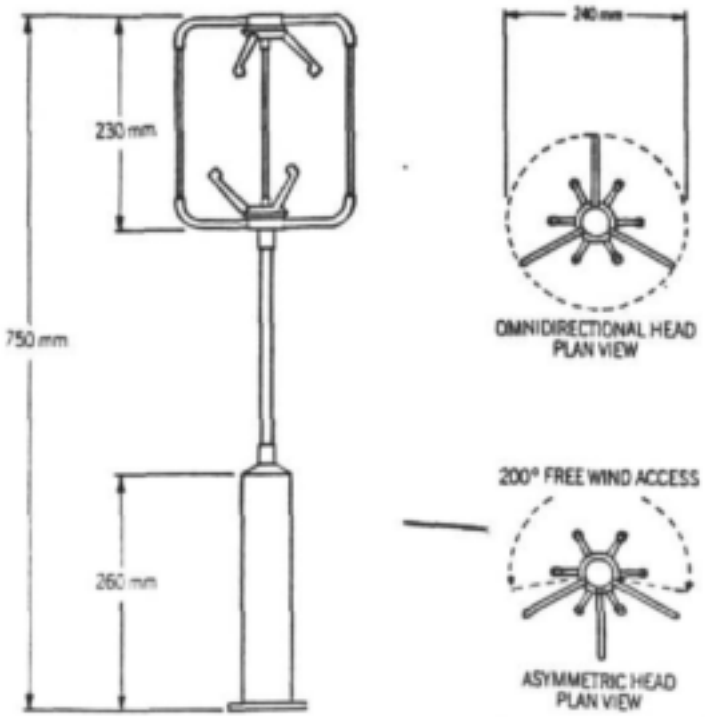

Figure 2.2: Gill ultrasonic anemometer with transducers (top) and cylindrical housing (below).

pulses of high frequency ultrasound between themselves. If a traveling sound wave is carried through the air along a fixed path length L between a pair of transducers then the time of propagation in one direction is given by

$$t_1 = \frac{L}{c + v} \tag{2.1}$$

and in the other direction by

$$t_2 = \frac{L}{c + v} \tag{2.2}$$

where c is the speed of sound and v is the speed of the fluid medium. By inverting and subtracting, v is solved explicitly

$$v = \frac{L}{2}\frac{t_2 - t_1}{t_1 t_2} \tag{2.3}$$

Conversely, by inverting and subtracting

$$c = \frac{L}{2}\frac{1}{t_1 + t_2} \tag{2.4}$$

The speed of sound is useful for calculating air temperature with a rapid response. Since the transducer pairs do not have to conform to cartesian axes the electronics perform a transformation to calculate velocities in a u, v, w format. Serial communication at 4800 baud conforms to the RS422 format an ISO (International Standards Organisation) standard. A power supply and interface unit (PSIU) powers the anemometer and converts the signal to RS232 format (another ISO standard) for serial input to the PC. The model purports to have an instantaneous windspeed resolution of $\pm$ 0.02m/s at a serial output data rate of 20.833 Hz. The sonic thermometer is not free from the effects of flow distortions about the transducers and the supporting frame, and wind speed measurements need to be corrected using calibration coefficients determined at GILL. The velocity crosstalk effect on temperature values were corrected using the recommendation of Kaimal et al.(1991).

2.1.1.2 Infrared hygrometer

For many years, the most commonly used fast-response hygrometer employed in turbulent flux research has been the the Lyman-alpha. However, many difficulties in calibration, window degradation due to sea-salt and temperature contamination preclude the reliable use of the Lyman-alpha hygrometer for automated data acquisition systems in harsh environments (Fairall et al., 1990).

The OPHIR Corporation IR-2000 hygrometer (Figure 2.3) measures the humidity along a path by the attenuation of infrared radiation along that path. The measurement is made by the comparison of absorbing and non-absorbing frequencies and therefore the calibration of this device is inherently more stable than the Lyman-alpha. With daily cleansing the rugged sapphire window avoids many of the salt contamination problems of the traditional Lyman-alpha type. The basic equation relating apparent absolute humidity ρ_* to the IR-2000 measured Transmissivity Ratio R_C is

$$R_C = \frac{C_{2.6} - C_{ref}}{C_{2.5} - C_{ref}} = A_0(1 + A_1 T_{can})e^{-\kappa\rho_*^{\beta}} \tag{2.5}$$

where $C_{2.6}$ is the raw count output from the 2.6μm vapour (absorbing) channel and $C_{2.5}$ is the raw count output from the 2.5μm (non- absorbing channel), C_{ref} is the raw count from the reference (blank) channel, T_{can} is the IR-2000 internal housing temperature in degrees Celsius, and A_0, A_1, κ and β are calibration coefficients. Through the use of an adjacent, non-absorbing channel (2.5μm), instrument drifts are corrected. Serial communication at 9600 baud conforms to the RS422 standard which is interfaced with the PC comport via an RS422/RS232 converter. The IR-2000 can be operated in a number of different modes. In CONTINUOUS mode the IR-2000 outputs a steady stream of raw counts at 20 Hz while in QUERY 7 mode it outputs an average ratio R_C over the previous one second. Unfortunately this device had many problems. During the SAAMES 3 cruise and the East London Experiment the device did not give good results during the daytime. It was sent back to the factory which found the calibration factor to be wrong. During the ACASEX and ACE cruise the device stopped transmitting the data for short periods. Moreover the turbulence humidity spectra produced were wrong for some unknown reason. It is also difficult to use this device operationally because of the sea spray contamination that will eventually set in a few hours after high wind speed conditions have started.

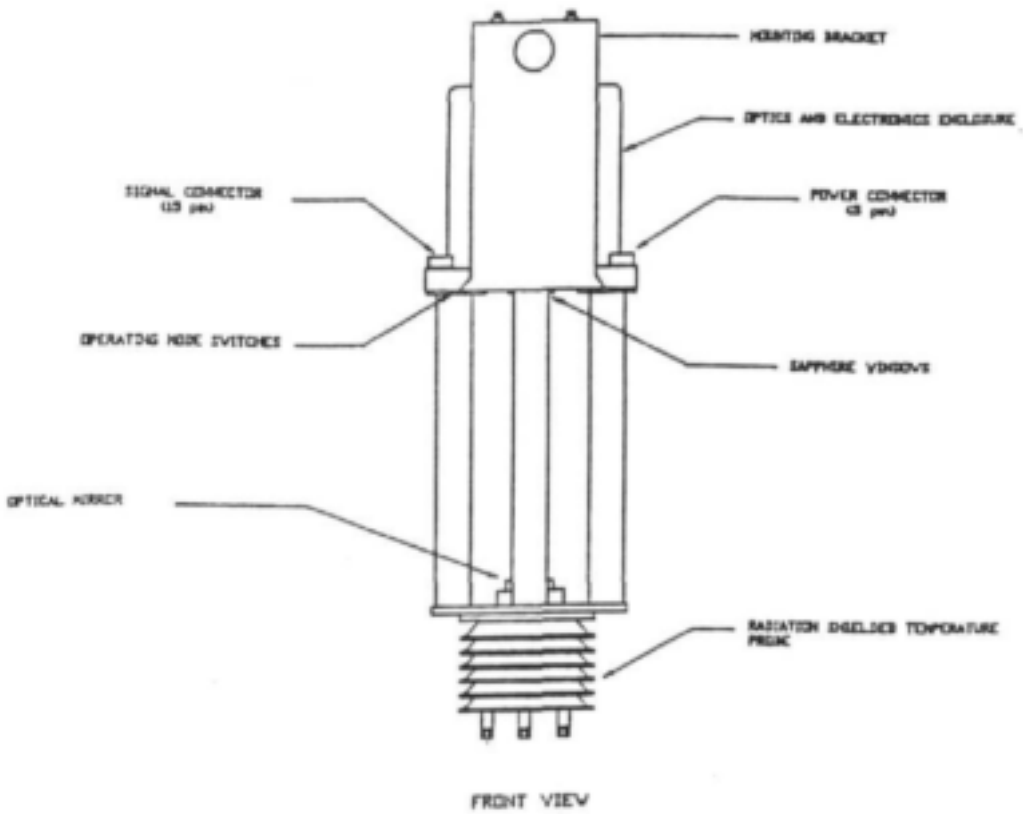

Figure 2.3: OPHIR IR-2000 hygrometer

2.1.1.3 System computer

The system was designed around a 50 MHz Intel 80486 (486) processor PC but will run comfortably on a 286 or 386. It uses two serial ports (COM1 and COM2) which are standard with any PC.

2.1.1.4 System software

The real-time data acquisition and processing package was written in the highly functional C language. C is the language favoured by UNIX programmers due to its speed and low-level hardware interface capabilities. The use of C is consistent with the fundamental aim of this research project (viz. a fast, reliable, extensible and flexible data acquisition system that could run on a PC). The system BIOS can be used in two modes for data acquisition (viz. polled and interrupt-driven). The program uses an interrupt-driven serial communications library (ie. the system BIOS is used in interrupt mode).

It is beyond the scope of this project to comprehensively discuss interrupt-driven communication and only a short description is given. In the data link (transmission) level data frames are exchanged between the modem and the UART (Universal Asynchronous Receiver/Transmitter) located on that serial port. Upon receiving a frame the UART strips off the start, stop and parity bits. It then notifies the CPU (Central Processing Unit) that a byte of data has arrived. It accomplishes this by means of an interrupt. When the CPU is interrupted it immediately transfers control to a specified area of memory where an Interrupt Service Routine (ISR) is located by indexing into an Interrupt Vector using a key for that device (serial port). The indexed value usually contains the start address of the ISR (ie. it contains the address of the first instruction of that ISR). It is the task of the ISR to save the host process status, the address of the next instruction, contents of CPU registers, accumulators etc. The ISR then transfers the data byte to a data buffer within main

memory and reloads the CPU registers before returning control of the CPU to the host process. The host process can then continue as if it had not been interrupted. Alternatively, the CPU or ISR can choose to ignore an interrupt until the UART's internal buffer has been filled. The INS16450 and INS16550 UART's both have 16-byte buffers and the latter can be programmed to interrupt at different trigger levels.

Interrupt-driven mode of operation can be easily conceptualized as a process that captures data from the serial ports in the background. This background process is transparent to the host process (ie. the host process is unaware that the background process is continously capturing data from the serial ports).

2.1.1.5 Conceptual model

This section is a very broad outline of the step by step operation of the system. Once serial communication has been established the two devices (sonic anemometer and hygrometer) are synchronised for fast (20 Hz) data transmission. This synchronisation is necessary as the two devices do not transmit data at precisely the same frequency. The two devices are sampled at 20 Hz for 12.8 s. The mean is then removed from each of the 256 values of wind speed, temperature and humidity. The data is filtered using the Hamming Window to remove any high frequency spikes. A 256-point Fast Fourier Transform is performed on the variance of each parameter time series. The spectral variance is then summed for later averaging. The IR-2000 is then operated in QUERY 7 mode which outputs mean values of the previous one second's worth of temperature, specific humidity and relative humidity data. This serves to compare the mean of the data obtained from the IR-2000 in QUERY 7 mode with the mean calculated from the fast data. The two devices are then resynchronised and the cycle continues. A timeout occurs after ten minutes, the spectral variance and other neccessary parameters are averaged and along with various quality control parameters is written to disk. The inertial dissipation, hybrid and bulk methods are applied respectively, and the results are dumped to the screen. Such real-time feedback is of critical importance to researchers in the field.

2.1.1.6 User interface

The motivation behind real-time calculation of data is to monitor the devices and have real-time feedback of the fluxes of interest (eg. water vapour flux) and other meteorological parameters describing the ASL.

The user interface is a Windows and Pop-Ups type interface. This simple windowed system assists assimilation of all the current data at a glance. There are two main windows for the ten minute and ten second mean parameter values respectively. Raw data windows for the sonic anemometer and hygrometer repectively, allow the operator to view the processed raw data as it arrives. A useful feature is the Host window which allows the user to interact with the IR-2000. It has been mentioned that the IR-2000 can be operated in a number of modes and the full complement of interactive commands is enabled using this window. This provides an extremely useful monitoring and debugging tool.

2.1.1.7 Troubleshooting and quality control

Quality control is assisted by the IR-2000 which appends to the raw counts, a number of engineering units associated with the operation of the device. This allows plenty of seemingly redundant real-time checking of data and serves to improve the robustness of the system. Although it is impossible to correct errors, it is possible to detect them when they occur and take appropriate corrective measures. A less likely source of problems is in the data link level (ie. the level of the background process) and concerns transmission errors. The low level interface of the C language allows such errors to be read off the status byte of the line control register (LCR) of the UART (Universal

Asynchronous Transmitter/Reciever) found on that port. Such transmission errors include framing, parity and overrun errors. The system continually monitors the carrier signal and the operator is immediately notified if a device goes down. Error detection is a useful tool in quality control and can go some way towards ensuring confidence (doubt) in field data.

2.1.1.8 Extensibility

We evaluated a number of communications libraries before designing the system. Although most C serial communications libraries allow the simultaneous operation of four serial ports (at high baud rates) the library selected (see appendix A) also provides a low level hardware interface and access to most of the UART registers. The third serial port is used for the Data Distribution System (DDS) on the fleet of DEA research vessels. The fourth serial port is therefore available for any further improvements or extension to the system. In particular, the fourth serial port could link to the Campbell Datalogger which samples slower sensors and provides additional information about the heat budget at the ocean surface. Such a setup would make full use of the available resources of a PC thus allowing a second PC to be kept for backup purposes.

2.1.1.9 Cost and flexibility

The system flexibility lies primarily in its robust implementation of the inertial dissipation method for calculating air-sea fluxes, with the hybrid and bulk methods serving as a backup. As mentioned earlier the inertial-dissipation method is suitable for all research platforms and can therefore service a wide variety of coastal and oceanic meteorology studies. The system does not require expensive computing power or hardware interfacing equipment. The project has already saved the purchase of the highly expensive HP data acquisition system and an FFT card.

2.1.2 Slow response sensors and acquisition software

2.1.2.1 Radiation measurements

To calculate the net heat budget at the surface, measurement of the incoming short wave and long wave radiation is required. The outgoing long wave radiation is calculated as a function of the sea surface temperature and the outgoing short wave radiation is taken as a fraction of the incoming short wave radiation (7 %). The incoming short wave radiation is measured with an Eppley precision spectral pyranometer (Figure 2.4). It has a thermopile detector with a long term stability. It has two hemisphere with the inner hemisphere blocking the infrared radiation from the outer one. The incoming long wave radiation is measured with an Eppley precision infrared radiometer (Figure 2.5). It measures the exchange of radiation between a horizontal blackened surface and the sky. Both devices are sampled with a Campbell CR10 dataloger system. The datalogger can be used to sample other device such as the HMP35D Vaisala humidity and temperature sensor.

2.1.2.2 Backup relative humidity and temperature measurement

This was supplied by a Vaisala HMP35D relative humidity (RH) sensor housed in a radiation shield. This intrument utilises a HUMICAP, a thin-film capacitive sensor that has become a research standard (Mesiä, 1993). The humidity and temperature are sampled with the datalogger every 10 s, averaged and stored independently from the fast response devices.

2.1.2.3 CR10 datalogger

The CR10 is a measurement and control system protected in a sealed and rugged cannister. It provides sensor measurement, timekeeping, communication, data reduction, data and program storage. It interfaces with a wiring panel where the slow response sensor can be powered and sampled.

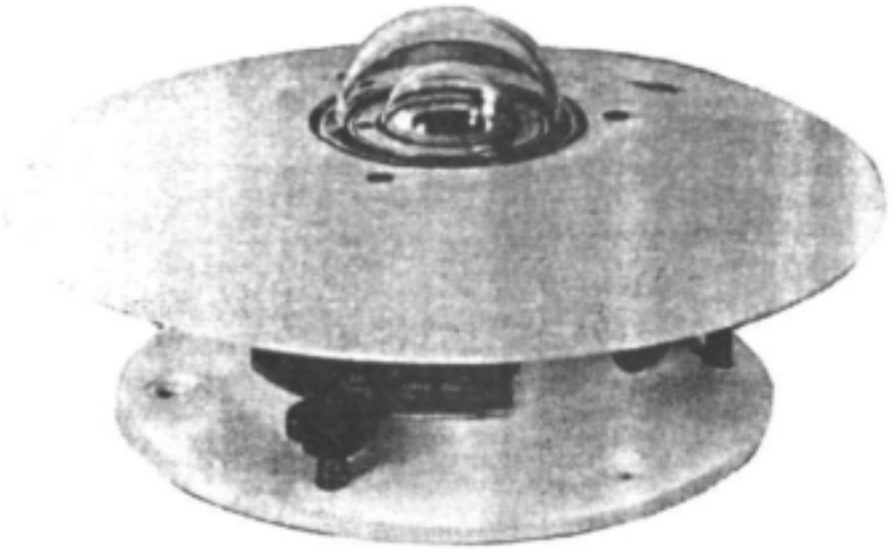

Figure 2.4: Eppley precision pyranometer

2.2 Automatic air-sea interaction measurement system

The fleet of DEAT vessels is equipped with a number of physical devices which measure a variety of useful geophysical information. A Data Distribution System (DDS) samples these data at 1 second intervals. The values obtained are averaged over 1 minute and stored with relevant information such as time, date, latitude and longitude. Whilst automatic measurement does not necessarily represent any technological advance, it has enabled the collection of high resolution data that has been used in an air-sea interaction study for this region. Such high resolution data will be shown to be an improvement over the traditional 3-hourly meteorological observations employed in previous studies such as in Mey et al. (1990).

Parameters of particular interest are air pressure, wind speed, wind direction, air temperature, sea surface temperature and air humidity.

Three-hourly surface observations were undertaken on the Marion 1994 and Marion 1995 cruises by the South African Weather Bureau. These data are used for comparative purposes or can serve as a backup.

2.2.1 Wind speed and direction

Wind speed and direction were sampled at 1 seconds intervals, averaged over 1 minute and stored. This represents a wind vector relative to the mean ship motion. Therefore wind vectors were simultaneously readjusted against the ship movement vector to obtain an absolute wind vector (i.e. relative to the ground).

An Aerovane-type anemometer (Fritschen and Gay, 1979) was used to measure the wind speed and direction. Two types of Aerovanes were used. This information is summarized below together with the manufacturer's accuracy specifications. Whilst it may be considered that this type of anemometer is less influenced by atmospheric turbulence, possesses low inertia and pursues wind direction well (with little swing) there are uncertainties about its performance at low wind speeds (starting speed of less than 2 ms^{-1}) and response to ship's

Figure 2.5: Eppley precision infrared radiometer (pyrgeometer)

Table 2.1: Instruments used aboard DEA vessel

MAKE AND MODEL	PARAMETER	ACCURACY
KOSHIN-VANE KA-101	WIND SPEED, DIRECTION	1 ms^{-1}, 5°
FURUNO FW-200	WIND SPEED, DIRECTION	1 ms^{-1}, 5°
AANDERA 3145	AIR TEMPERATURE	0.1°C
PT-100	AIR TEMPERATURE	0.1°C
VAISALA HMP35D	RELATIVE HUMIDITY	1%
AANDERA 2810	AIR PRESSURE	0.2 hPa
SEACAT SBE 3	SST	0.01°C

direction. Hence there is a bias in the calculation of the absolute wind speed during these periods.

2.2.2 Air temperature

An Aandera 3145 platinum resistance sensor (M94, ACASEX) and a standard PT100 sensor (M95) were utilised for the DDS data (Table 2.1). The air temperature probes were housed in radiation shields.

Three-hourly observations of dry and wet-bulb temperatures were made by the South African Weather Bureau from two Yellow Springs Instruments (YSI) platinum resistance thermistors (Table 2.2) each housed in a Stevenson Screen. The Stevenson screen is a slatted white wooden box which is also designed to eliminate radiation errors. Resultant errors on the temperature sensors are associated with poor ventilation, ship exhaust heat contamination and sea spray contamination of the wet bulb temperature. From 1996 there was a serious calibration problem with theses devices on both the S.A. Agulhas and Algoa with over-estimation of the air temperature by 1 to 2°C. Also the location of this probe aboard the ship is far from ideal. Errors in results from psychrometers

Table 2.2: Instruments used for SAWB observations

MAKE AND MODEL	PARAMETER	ACCURACY
YSI 44203	AIR TEMPERATURE	0.2 °C
YSI 44203	WET BULB TEMPERATURE	0.2 °C
VAISALA PA 11	AIR PRESSURE	0.3 hPa

arise especially from errors in the wet-bulb temperature as a result of heat conduction, ventilation and sea salt contamination which tend to influence this sensor more (Fitschen and Gay, 1979).

2.2.3 Relative humidity

This was supplied by a Vaisala HMP35D relative humidity (RH) sensor housed in a radiation shield. This intrument utilises a HUMICAP, a thin-film capacitive sensor that has become a research standard Mesiä (1993).

2.2.4 Air pressure

Air pressure was supplied by an Aandera 2810 air pressure sensor.

2.2.5 Sea surface temperature

This was supplied by a Seacat SBE 3 located at the ship's water intake.

2.3 Upper-air data

Boundary layer characteristics in this study were provided by radiosonde ascents. Whilst radiosondes provide high vertical resolution compared to aircraft they will sample the local mixed layer top (not necessarily equal to the average mixed layer top). Furthermore a radiosonde does not necessarily represent a vertical spot measurement as it will advect with the mean wind.

The Vaisala RS80 Omega Sounding System provided the vertical profiles of wind speed and direction, temperature and relative humidity. During M94 radiosonde ascents were undertaken on a twelve-hourly basis (twice-daily). During M95 ascents were released aproximately three to six-hourly. During ACASEX ascents were chosen to coincide with the region of interest.

It is unfortunate that, until 1995, the system of radiosonde data capture used was designed for operational forecast purposes only. The result has been a vertical spatial data sparseness (about 10 values for the first 3000 m) which was suitable for forecast purposes but less than ideal for investigating boundary layer dynamics. In most cases, however, the data have been sufficient to delineate the surface layer, the inversion height and the mean characteristics of the atmospheric mixed layer. This low resolution data applies only to the 1994 Marion Island cruise (M94). Thereafter, we were able to persuade the SAWB to modify their data capture system to store the full resolution radiosonde data. The refinement has since been implemented and vertical resolution is now on the order of 4 mb (roughly 50 m to 60 m).

Rawinsonde wind data from M95 and ACASEX was rejected. M95 wind data was found to be unrealistic (due to a software problem). During ACASEX water entered the housing enclosing the tracking antenna pre-amplifier with the result that the tracking signal could not be received.

In 1996, five extra radiosondes launches were done above the Agulhas Current. Unfortunaly, the ship came back 3 weeks earlier without warning us and the return leg radiosonde were not done by SAWB. In 1997, five extra radiosondes were done above the Agulhas Current.

2.4 Aircraft measurement system

The flight navigation system aboard the aircraft consisted of a Trimble TNL2000 Global Positioning System (GPS) for 1 s updates of position, aircraft track and ground speed. With the addition of true air speed and aircraft heading, wind velocity could be derived. Pressure and radar altimeters gave height above sea and ground level. An accelerometer and pitch rate gyroscope sensitive to aircraft motions was used in conjuction with a Rosemount angle of attack vane to determine vertical gusts. The angle of attack vane adequately measures high frequency vertical eddies in the airflow, whilst the accelerometer and pitch gyro account for departures of the aircraft from its intended track caused by low frequency eddies. When analysed together, aircraft motion can be subtracted from vane deviations to provide reliable estimates of the vertical gust (w') at specified sampling periods. Fast response sensors monitored air temperature (Rosemount) and specific humidity (Lyman-alpha), which were archived together with vertical gust, position, height, etc, at 10 Hz using a PC. Dewpoint temperatures were measured with a cooled mirror (EGG) sensor as a cross check of the Lyman-alpha. Further details of this system are available in Jury et al. (1993).

Chapter 3

Methods

3.1 Turbulent fluxes of sensible, latent heat and momentum

Turbulent fluxes of momentum, sensible and latent heat are not measurable parameters but are derived from values of meteorological parameters (wind speed, air and sea temperature and air humidity).

3.1.1 Bulk method

The simplest method used to obtain the vertical turbulent fluxes of momentum heat and water vapor at the surface of the marine atmospheric boundary layer is the bulk method. The turbulent fluxes are estimated with transfer coefficients which relate the fluxes to the means of routinely measured variables (Fairall et al., 1996).

The bulk formulae for wind stress, sensible heat and water vapor fluxes are:

$$\tau = \rho_a C_D (U - U_s)^2 \tag{3.1}$$

$$Q_H = \rho_a c_p C_H (U - U_s)(T_s - \Theta) \tag{3.2}$$

$$Q_v = \rho_a C_E (U - U_s)(q_s - q) \tag{3.3}$$

where U, Θ and q are mean wind speed, potential temperature and specific humidity respectively measured at some reference height z_r. U_s is the sea surface current speed. In the case of the Agulhas Current, U_s cannot be neglected. With current velocity up to 2 m/s the error on the turbulent fluxes can be very important at low wind speed. For instance if we have a 2 m/s eastward current velocity and a westerly wind speed of 4 m/s, neglecting the current velocity will lead to a 50 % underestimation of the water vapor and sensible heat fluxes and 225 % underestimation of the wind stress. U_s can be measured by an Acoustic Doppler Current Profiler (Rouault et al., 1996). C_D is the drag coefficient. C_H and C_E are the dimensionless Stanton and Dalton numbers, also called transfer coefficients for heat and water vapor. ρ_a is the air density. c_p is the specific heat of air at constant pressure.

$$\Theta = T_a + 0.0098 z_r \tag{3.4}$$

where T_a is the air temperature at z_r.

$$q_s = 0.98 q_{sat}(T_s) \tag{3.5}$$

T_s and q_s are mean sea surface temperature and specific humidity (assumed to be saturated) at the sea surface, qs is calculated from q_{sat} the saturation specific humidity at the surface. The factor 0.98 is introduced to account for the reduction in water vapor pressure due to salinity (Fairall et al., 1996). Instead of using the turbulent water vapor fluxes, we will present the turbulent latent

heat fluxes, Q_E in the result section. That way we will be able to compare the sensible, latent and radiative fluxes with the same units (Wm^{-2}).

$$Q_E = L_v Q_v \tag{3.6}$$

L_v is the latent heat of vaporisation.

In the lower part of the marine atmospheric boundary layer, the surface layer (a few tens of meters) the turbulent fluxes are considered to be constant and the average values of wind speed, temperature and water vapor are expected to vary logarithmically with height. Thus the surface fluxes and scalar quantities for the surface layer can be derived from measurement of the meteorological parameters at only one height within this layer. The vertical profiles of wind velocity, temperature, and humidity above the oceans in the constant flux layer are (Stull, 1988):

$$\overline{U}(z) - U_s = \frac{u_*}{\kappa}\left(\ln\frac{z}{z_0} - \phi_m\left(\frac{z}{L}\right)\right) \tag{3.7}$$

$$\overline{T}(z) - T_s = \frac{T_*}{\kappa}\left(\ln\frac{z}{z_{0T}} - \phi_T\left(\frac{z}{L}\right)\right) \tag{3.8}$$

$$\overline{q}(z) - q_s = \frac{q_*}{\kappa}\left(\ln\frac{z}{z_{0q}} - \phi_q\left(\frac{z}{L}\right)\right) \tag{3.9}$$

where κ is the Von Karman constant and taken to be 0.4. u_*, T_*, q_* are the friction velocity and scaling parameter for temperature and water vapor. u_* is called the friction velocity, z_{0T} and z_{0q} are calculated as a function of the Reynolds number according to Liu et al. (1979) and modified by Fairall et al. (1996). z_0, the roughness length, reflects the roughness of the sea, and is related to the wave field using the relation of Smith (1988)

$$z_0 = 0.011u_*^2/g + 0.11\nu/u_*.$$

ϕ_m, ϕ_T, ϕ_q are called stability functions and were determined empirically as a function of the stability parameter, $\zeta = z/L$. L is the Monin-Obukhov length.

$$L = \frac{Tu_*^2}{\kappa g\left(T_* + 0.61Tq_*\right)} \tag{3.10}$$

The stability parameter is analogous to the Richardson number, which is the ratio of the work done by the buoyant force to the rate of shear production of turbulent energy. It takes into account both the temperature and em moisture dependence of air parcel buoyancy and is affected by the friction velocity, u_*. The stability influences the vertical exchange of energy and momentum and thereby the vertical distribution of wind, temperature and humidity in the boundary layer. A positive number of the stability means that the conditions are stable and the stratification will act against the turbulence. Between 0 and -0.3 the stability is neutral. It usually happens when the air temperature is less than the sea temperature and for average to strong wind speed when the mixing is mainly due to the shear. If the stability is less than -0.3 the conditions are unstable with convective activity: the buoyant force begins to dominate the mixing process. We are using the stability function that obeys the convective limit prescribed by Fairall et al. (1996). The turbulent fluxes can be related to the scaling parameters u_*, T_*, q_* using the Monin-Obhukov similarity theory (Stull, 1988).

$$\tau = \rho_a u_*^2 \tag{3.11}$$

$$Q_H = -\rho_a c_p u_* T_* \tag{3.12}$$

$$Q_E = -\rho_a L_V u_* q_* \tag{3.13}$$

Using the former equation one can express the transfer coefficients in the bulk formulation as:

$$C_D = \kappa^2 / \left(\ln \frac{z}{z_0} - \phi_m(\zeta) \right)^2 \tag{3.14}$$

$$C_H = \kappa^2 / \left(\left(\ln \frac{z}{z_{0T}} - \phi_T(\zeta) \right) \left(\ln \frac{z}{z_{0T}} - \phi_m(\zeta) \right) \right) \tag{3.15}$$

$$C_E = \kappa^2 / \left(\left(\ln \frac{z}{z_{0q}} - \phi_q(\zeta) \right) \left(\ln \frac{z}{z_{0q}} - \phi_m(\zeta) \right) \right) \tag{3.16}$$

One can calculate the surface fluxes using equation (3.1), (3.2), (3.6) and (3.14), (3.15), (3.16) with an iterative process, starting with an arbitrary value of the flux corresponding to neutral atmospheric stability to obtain an estimate of the Monin-Obukhov length (3.10) and the stability parameter. From this, the transfer coefficients and the fluxes are recalculated and reentered into the iterative process. A solution is obtained after a few iterations. The algorithm developed by Fairall et al. (1996) for the TOGA-COARE experiment is used here. It includes a separate module to calculate the real sea surface temperature (skin temperature) from the measured bulk sea surface temperature which is usually the temperature of the ship intake a few metres below the surface. Scenarios such as light winds, gustiness velocity, actively convective regimes and the contribution of sensible heat flux due to rain which are not covered by traditional bulk models, are accounted for in this algorithm. This algorithm allows one to calculate the vertical profiles of wind velocity, temperature and humidity above the oceans at any height of the constant flux layer even if the meteorological parameters are measured at different heights. Results will be presented at a standard height of 10 m. The parameters necessary for the bulk flux calculations were averaged over 10 minutes before applying the bulk formulae. Estimation of fluxes with the bulk method shows great variability depending on the accuracy of the measurement devices, the flow distortion generated by the ship and the accuracy of the exchange coefficients used (Blanc, 1987). The absolute wind speed is calculated from the measured relative wind speed and the ship speed and direction. This requires knowledge of the ship exact position and motion at least every 10 s to get a correct estimate of the 10 mn averaged absolute wind speed.

3.1.2 Inertial dissipation method

The inertial dissipation method has become a new standard after a validition campaign that took place during the HEXOS experiment [14,15]. One of the main advantage of the method is that it uses the relative wind speed only. Therefore it is not necessary to know the current speed or absolute wind speed which require accurate measurement of the ship position, speed and heading

Within the inertial subrange of isotropic turbulence, the variance spectra for velocity, temperature and humidity can be expressed as a function of wavenumber magnitude, k:

$$S_u(k) = 0.25 C_u^2 k^{-5/3} \tag{3.17}$$

$$S_T(k) = 0.25 C_T^2 k^{-5/3} \tag{3.18}$$

$$S_q(k) = 0.25 C_q^2 k^{-5/3} \tag{3.19}$$

C_u^2, C_T^2, C_q^2, are the structure function parameters for velocity, temperature and humidity. The structure function parameters are defined in terms of the differences in the meteorological variables at location r and $r + d$ (where d is a spatial separation in the inertial subrange).

The scaling parameter can be related to the local rate of dissipation through the budget equation for turbulent kinetic energy, temperature variance and moisture variance. The rate of dissipation of velocity, temperature and humidity are related to the stucture function parameters. Therefore the scaling parameter can be related to the structure function parameter:

$$u_* = \left(\frac{C_u^2}{f_u(\zeta)} z^{2/3} \right)^{1/2} \tag{3.20}$$

$$T_* = \pm \left(\frac{C_T^2}{f_T(\zeta)} z^{2/3} \right)^{1/2} \tag{3.21}$$

$$q_* = \pm \left(\frac{C_q^2}{f_q(\zeta)} z^{2/3} \right)^{1/2} \tag{3.22}$$

f_u, f_T, f_q are empirical structure function determined during experiments.

$$fu = \begin{cases} 4(1 - 0.5\zeta)^{2/3} & \zeta < -2 \\ 4(\phi_m - \zeta)^{2/3} & -2 < \zeta < 0 \\ 4\left(1 + 2.5\zeta^{2/3}\right) & \zeta > 0 \end{cases} \tag{3.23}$$

$$f_T = \begin{cases} 4.9(1 - 6.2\zeta)^{-2/3} & \zeta < 0 \\ 4.9\left(1 + 2.5\zeta^{2/3}\right) & \zeta > 0 \end{cases} \tag{3.24}$$

$$f_q = f_T \tag{3.25}$$

By calculating the velocity, temperature and humidity spectral variance and using equation 3.20, 3.21, 3.22 iteratively, it is possible to estimate the turbulent flux. The iteration is done on the stability parameter starting with a neutral value of 0.

The variances are calculated using Fast Fourier Transforms of high frequency measurements of the fluctuation of the relative wind speed, temperature and humidity. The relative wind speed, temperature and humidity are measured 20 time per second for 12 seconds to get 256 point in order to be able to perform a Fast Fourier Transform. We calculate the mean for this time period and subtract each of the 256 values from this mean to get the fluctuating part of the measured variables. It is the Fast Fourier Transform of the fluctuating part that give the turbulence spectra as a function of wave number or frequency. Those spectra are calculated every 12.8 s for 10 mn, averaged and stored with the means of the other meteorological parameters. The frequency f is related to the wave number k and the relative wind speed U using Taylor hypothesis of frozen turbulence:

$$k = 2\pi f / U \tag{3.26}$$

In the inertial subrange, the spectra are supposed to vary linearly as a function of the frequency with a $-5/3$ slope. Theoretically, it is possible to calculate the structure functions using any set of frequency and corresponding variance spectrum. Practically, we are using the measured discrete spectrum between 2 and 4 Hz (about 20 points). Using equation 3.17, 3.18, 3.19, 3.26 the structure functions are

$$C_u^2 = 4 \left(\frac{2\pi}{U} \right)^{2/3} \frac{1}{N} \sum_{f=f_1}^{f_N} f^{5/3} S_u(f) \tag{3.27}$$

$$C_T^2 = 4 \left(\frac{2\pi}{U} \right)^{2/3} \frac{1}{N} \sum_{f=f_1}^{f_N} f^{5/3} S_T(f) \tag{3.28}$$

$$C_q^2 = 4 \left(\frac{2\pi}{U} \right)^{2/3} \frac{1}{N} \sum_{f=f_1}^{f_N} f^{5/3} S_q(f) \tag{3.29}$$

This method is less sensitive to flow distortion and ship motion than the eddy covariance method. The method produces a true turbulence statistic and gives a more direct estimate of the fluxes than the bulk method. Also the time average used in the method is shorter than for the eddy covariance

method. Another advantage is that the method is using the relative wind speed which means that one can get an estimate of the wind stress without knowledge of the current velocity or the absolute wind speed. During the different experiment we found that the temperature spectrum calculated with the ultrasonic temperature does not follow the -2/3 law in the inertial part of the spectrum. Therefore it was not possible the use the inertial dissipation method to calculate all the turbulent fluxes

Nevertheless it is possible to estimate the turbulent fluxes using an iterative hybrid method where the turbulent flux of momemtum is calculated using the inertial dissipation method (Fairall et al, 1990) and the turbulent fluxes of sensible and latent heat are calculated using a bulk method developed by Fairall et al (1996) for the TOGA-COARE experiment. The iteration is done on the stability parameter. That way it is possible to calculate the fluxes using only the ultrasonic anemometer and the Vaisalla HMP35D humidity and temperature sensor without knowledge of the ship speed and position, surface current or absolute wind speed. Another problem arose when vibration of the mast at about 3 HZ was introduced a spike in the velocity spectrum. In that case the structure functions were calculated with 10 points instead of 20. Recent studies using the inertial dissipation method discard results when the ship maneuvers or is not underway at full speed and when the relative wind speed is not blowing within 30 degree from the bow (Yelland and Taylor, 1996). These bad conditions happened each time we launched a radiosonde. Moreover, use of the inertial dissipation method implies stationary and horizontally homogeneous conditions that may not be respected above the SST front. Therefore it is very difficult to use the inertial method or the hybrid method operationally to get a continuous estimate of the fluxes.

3.1.3 Eddy covariance method

The turbulent fluxes are defined by the following relations

$$\tau = \rho_a \overline{w'u'} \tag{3.30}$$

$$H = \rho_a c_p \overline{w'T'} \tag{3.31}$$

$$E = \rho_a L_v \overline{w'q'} \tag{3.32}$$

where τ is the momentum flux in units of Newtons per square meter; H and E are the fluxes of sensible heat and latent heat respectively in units of Watts per square meter; ρ_a is the air density; w is the vertical component of the wind; u is the streamwise wind vector; T is the temperature; and q is the specific humidity. The primes indicate a perturbation from the mean and the overbar indicates an average over an infinite ensemble. Assuming stationarity and ergodicity the direct covariance method can be used to estimates the fluxes by cross correlating simultaneous measurements of w' with u', T' or q' over some finite averaging period (Edson et al., 1990). The covariance method has been used extensively over land (Fairall, 1990) and from aircraft but with the exception of the straightforward application over the ocean has been limited to fixed towers as in the HEXOS experiment (Edson et al., 1990) Until recently the covariance method has not been used on a ship platform due to the effects of flow distortion (Edson et al., 1990) and platform motion. The measured wind velocity components therefore almost always require significant correction. An approach suitable for correcting contaminated atmospheric signals is a system not unlike an aircraft inertial navigation system (INS). However, the cost of such a system is prohibitive and even a compromise system represents both cost and real-time maintenance obstacles. It has yet to be shown that systems employing the covariance method do indeed obtain independent, high speed measurements of u, T and q which are significantly correlated in time (ie. sampling these parameters at the same frequency does not guarantee simultaneous sampling). Therefore extreme care must be taken to ensure that sampling start times coincide exactly. The assumption of stationarity and ergodicity presents another sampling problem. Since this method is based on covariance statistics, a longer sampling period is needed (typically 50 minutes) to approximate the ensemble average. Such

long sampling periods may violate the assumption of stationarity and obscure important mesoscale processes within the MABL.

3.2 Upper air parameterization

3.2.1 Humidity

Whilst the saturation water vapour pressure, es, is usually considered to be strictly a function of temperature, Buck (1981) described a small pressure enhancement effect. The enhancement correction, called the enhancement factor is made to correct for the very small pressure effect on water vapour. Buck (1981) suggested a suite of enhancement factors for varying meteorological ranges of interest. Bolton (1980) suggested a formulation for the saturation vapour pressure

$$es(T_a) = 6.112 \exp\left(\frac{17.67 T_a}{T_a + 243.5}\right)$$

(air temperature T_a in °C) is sufficiently accurate for most meteorological purposes.

The most appropriate enhancement factor (i.e. for the temperature range −20 to 50 °C) (Buck, 1981; Table 2) does not always encompass the full range of temperatures during radiosonde ascents. At the surface where measurement errors may be large (eg. Fritschen and Gay, 1979) the achieved error reduction is insignificant. Therefore the formulation of Bolton (1980) is preferred over that of Buck (1981).

The water vapour pressure, e, in pascals is then found by

$$e = es(T_a)\frac{RH}{100}$$

where RH is the relative humdity.

The mixing ratio, r, in $\mathrm{kg.kg^{-1}}$ is the ratio of the mass of water vapour to the mass of dry air, and reduces to

$$r = 0.622\frac{e}{P - e}$$

(P in pascals) The specific humidity, q, in $\mathrm{kg.kg^{-1}}$ is the ratio of the mass of water vapour to the mass of moist air given by

$$q = 0.622\frac{e}{P - 0.378e}$$

The psychrometer-like arrangement of the SAWB is also used to calculate the water vapour pressure from

$$e = es(T_w) - 0.000660(1 + 0.00115T_w)(T_a - T_w)P$$

(P in pascals and T_a and T_w, the dry and wet-bulb temperature in $°C$) (Fitschen and Gay, 1979).

3.2.2 Virtual potential temperature

Buoyancy is one the driving forces for turbulence in the boundary layer. The virtual temperature of a moist air parcel is the temperature of a dry air parcel which has the same density. It takes into account the water vapour effect on air parcel density. Thus variations of virtual temperature can be studied in place of variations in density. The study of virtual potential temperature is not just an attractive but also a necessary means of describing the structure of boundary layer (Stull, 1988).

The virtual potential temperature (in Kelvin) for unsaturated air is (after Stull, 1988):

$$\theta_v = \theta(1 + 0.61r)$$

and for cloudy air

$$\theta_{vc} = \theta(1 + 0.61r - r_L)$$

where the liquid water loading r_L, the ratio of the mass of liquid water to the mass of dry air, serves to reduce the virtual potential temperature.

The potential temperature θ is defined by

$$\theta = T_K \left(\frac{P_0}{P}\right)^{0.286}$$

where T_k is the air temperature in Kelvin, P_0 and P the air pressures in pascals at the surface and reference level P. Potential temperature is conserved during dry adiabatic processes. An air parcel sinking dry adiabatically from some reference level P will warm according to the dry adiabatic lapse rate before attaining a temperature θ at P_0 (Preston-Whyte and Tyson, 1988; p 21).

The (unsaturated) virtual potential temperature will be used to describe the nature of the boundary layer. The cloudy virtual potential temperature will be used to compare model cloud densities to the environmental density. The mixed layer (with top z_i) will be defined as the layer above the surface where the virtual potential temperature profile is approximately adiabatic. The convective boundary layer (CBL) is defined (after Betts and Albrecht, 1987) as the layer above the surface that is convectively coupled to the surface. This includes the surface layer, mixed layer and entrainment zone.

3.2.3 Equivalent potential temperature

The equivalent potential temperature, θ_e, is especially useful as a tool in conserved variable analysis and diagnosing the origin of airmasses (Betts and Albrecht, 1987, Section 3.2.5). This is defined by Holton (1972) as the final temperature attained when a parcel is lifted dry adiabatically to its saturation level, then pseudo-wet adiabatically until all its condensate has precipitated before finally descending dry adiabatically to the surface. θ_e is the final temperature of an air parcel if it is lifted until all of its water vapour is given up to latent heat and it is then brought to the surface.

The method of Bolton (1980) will be used to calculate θ_e. The lifting condensation level, T_L the temperature an air parcel would attain when lifted dry adiabatically to its condensation level is found by

$$T_L = \frac{1}{\frac{1}{T_K - 55} - \frac{\ln(RH/100)}{2840}} + 55$$

The equivalent potential temperature is then

$$\theta_e = \theta \exp\left[\left(\frac{3.376}{T_L} - 0.00254\right) \times r\left(1 + 0.81 \times 10^{-3} r\right)\right]$$

.

3.2.4 Boundary layer quantification

In order to describe the mean scalar quantities of the boundary layer the following two properties are defined (after Katsaros et al. (1994))

$$\overline{\theta}_e = 1/z_i \int_0^{z_i} \theta_e(z)\, dz$$

$$\overline{q} = 1/z_i \int_0^{z_i} q(z)\, dz$$

where z_i is the mixed layer height. When the boundary layer was not actively convective, a residual layer (Stull, 1988; p 14) was identifiable. The top of the residual layer was then taken as the limit

of integration. When the boundary layer was stable there was no defined boundary layer top. In this case the inversion was chosen as the limit of integration.

Changes in $\overline{\theta}_e$ and $\overline{q}$ along an atmospheric trajectory over short time intervals are due to turbulent surface fluxes and entrainment.

3.2.5 Conserved variable analysis

A conserved variable diagram is a plot of one conserved variable against another (Stull, 1988; p 548). A particularly useful conserved variable diagram is the $\theta_e - r_T$ plot (Betts and Albrecht, 1987). For unsaturated air, this reduces to a $\theta_e - r$ plot. Mixing lines are straight lines on this diagram, advective processes do not move parcel points and radiative and precipitation processes are easily identifiable (Betts and Albrecht, 1987; p 85).

Betts and Albrecht (1987) have discussed how mixing, precipitation and radiative cooling move parcel points on this diagram. Precipitation moves parcel points to a lower r_T at constant θ_e, the radiative process does not change r_T but radiative cooling will move a point to a lower θ_e at constant r_T. Mixing lines are straight lines on this diagram.

The convective boundary layer profiles were classified according to synoptic conditions and composited. A simple averaging technique was used which has the effect of eliminating kinks but also smoothing repeated features.

3.2.6 Convective available potential energy

Cloud convective available potential energy was calculated to illustrate potential cumulus formation and decay. The cloud convective available potential energy (CAPE) is (Stull, 1988)

$$CAPE = \int_{z=z_{LFC}}^{z_{LOC}} \frac{g}{\theta} \Delta\theta_v(z)\, dz$$

where

$$\Delta\theta_v = \theta_{vcloud} - \theta_{venviron}$$

The cloud temperature can be estimated by assuming dry adiabtic ascent from the surface until the lifting condensation level, T_L (a good approximation for cloud base), and wet adiabatic ascent thereafter until the limit of convection (LOC). The mixing ratio was considered to be everywhere saturated within the cloud. The liquid water mixing ratio, r_l was calculated from the liquid water mixing ratio lapse rate $\Gamma_l = \frac{dr_l}{dz}$ (Albrecht et al., 1990).

$$\Gamma_l = -\frac{dr_s}{dz} = \frac{(0.622 + r_s)\, r_s L_v}{R_d T a^2} \Gamma_W - \frac{r_s P}{P - e_s} \left(\frac{g}{RdT_a} \right)$$

L_v is the latent heat of vaporisation, R_d is the specific gas constant for dry air and Γ_W is the wet adiabatic lapse rate calculated from Betts and Bartlo (1991). The liquid water mixing ratio may be assumed to vary linearly with height for thin clouds (Albrecht et al., 1990).

$$r_l = \Gamma_l (z - z_B)$$

For deeper clouds this assumption is unreasonable. Therefore the liquid water content was calculated as an integral.

This gives a theoretical upper limit on CAPE. However, many convective thermals have undiluted cores allowing the actual cloud base to be close to the lifting condensation level calculated from surface-layer air (Stull, 1988; p 551). Calculation of CAPE is highly sensitive to the humidity of the air parcel at its initial level since this affects the value of T_L and the resultant air parcel trajectory.

3.2.7 Precipitable water content

The precipitable water content (also known as the total water path) was analysed to determine synoptic variations and the contribution of the moisture in the boundary layer to this quantity. The water vapour path (given in metres) is

$$(\Delta z)_v = \frac{1}{\rho_l} \int_0^{ztop} \rho_a(z)\, r(z)\, dz$$

where ρ_l and ρ_a are the densities of water and dry air respectively. The latter is a "partial density" (Stull, 1988).

$$\rho_a = \frac{P - e}{R_d T_a}$$

Boundary layer estimates of $(\Delta z)_v$ were obtained by choosing $ztop = z_i$.

The liquid water path (given in metres) is

$$(\Delta z)_l = \frac{1}{\rho_l} \int_0^{ztop} \rho_a(z)\, r_l(z)\, dz$$

where r_l is the liquid water mixing ratio obtained assuming wet adiabatic ascent above cloud base. Following Betts and Albrecht (1988), cloud base was chosen as the saturation level of air at the base of the mixed layer. Cumulus clouds have a liquid water profile that is rarely adiabatic. Observations for these clouds show that the true liquid water content occurs as a fraction of its adiabatic value (Warner, 1970) Therefore the liquid water profile, r_l, was adjusted to a fraction of its adiabatic value using Warner (1970, Table 1).

Chapter 4

The 1993 SAAMES 3 cruise

4.1 Introduction

One of the regions that are most strongly implicated in the control of rainfall of South Africa is the region overlying the Subtropical Convergence (STC) south of Africa, in particular near the the Agulhas retroflection region (Jury, 1995). This region has some unusual characteristics in terms of current dynamics and air-sea interaction.

The Agulhas Current retroflects sharply south of Africa to flow back into the South West Indian Ocean as the Agulhas Return Current (Lutjeharms and van Ballegooyen, 1988). At the retroflection, Agulhas rings are shed at irregular intervals by current loop occlusion. These rings are the largest observed in the world ocean (Olson and Evans, 1986). The vigorous ring-spawning process and the intensity of these rings create a region with exceptionally high levels of mesoscale variability.

Downstream of the retroflection, the Agulhas Return Current exhibits similarly high levels of variability that extends as a tongue along the STC up to at least 70°S longitude. This variability is due to meanders in the Agulhas Return Current (Lutjeharms and van Ballegooyen, 1984) and in the STC, and eddies formation along these two features. The shedding of warm eddies into Subantarctic waters has its origins in the Agulhas Return Current. These eddies carry vast amounts of heat and may thus be important components of the meridional heat flux of the ocean.

The warm water carried into the region south of Africa by the Agulhas Current contributes to very high ocean-to-atmosphere heat fluxes for the region as a whole (Bunker,1976). In situ measurements of heat fluxes in circulation elements of the Agulhas retroflection (Mey et al., 1990) have been shown to exceed climatological values by a factor of 4 (Walker and Mey, 1988). Lutjeharms and Gordon (1987) have estimated a rate of heat loss of 157 Wm^{-2} for a newly shed Agulhas ring whereas (Van Balleygooyen et al., 1994) have calculated a value of between 20 and 100 Wm^{-2} for a range of Agulhas rings and eddies of various ages. It is important to establish more reliable figures. Firstly, the heat loss to the atmosphere of these features is needed to determine the remaining contribution to the oceanic global thermohaline circulation and the meridional heat flux. Secondly, since this region has been recognised as one that affects the weather over southern Africa, the air-sea interaction mechanisms need to be understood better.

Recent efforts in modelling the effects of those eddies on the weather pattern and climate have been carried out. Gutowski et al. (1996) have studied the effect of SST heterogeneity typical of Gulf stream rings on Atmospheric General Circulation Models (AGCM). They found that introducing this heterogeneity in AGCM can lead to differences of up to 50 % in latent heat flux for the northen hemisphere summer. Xie et al. (1996) have studied the effect of a mesoscale heat source similar to Agulhas or Gulf stream eddies on the atmosphere. It modifies the weather pattern mainly by increasing surface wind speed above and downstream of the heat source.

4.2 Observations

As part of the South African contribution to WOCE (World Ocean Circulation Experiment) and to JGOFS (Joint Global Ocean Flux Study) a multi-disciplinary cruise on the research vessel S. A. Agulhas was planned for the austral winter of 1993 (Lutjeharms et al., 1994). This cruise was to be a follow-up on a similar one carried out previously as part of the same program, but in summer (Rigg et al., 1992). In both cases the aim of the physical oceanographic component of the research cruise was to identify a warm eddy south of the STC in the region south of Africa and to investigate its interaction with the STC, with the ambient Subantarctic water masses and with the overlying atmosphere.

Satellite remote sensing in the thermal infrared was used to identify and locate such a warm eddy south of the STC before the vessel's departure from Cape Town on 21 June 1993. A line of XBT (Expendable Bathythermograph) stations was carried out in a southerly direction (Figure 4.1) to intersect this eddy, named Lesley, and to confirm its location. This was followed by a number of CTD (Conductivity-Temperature-

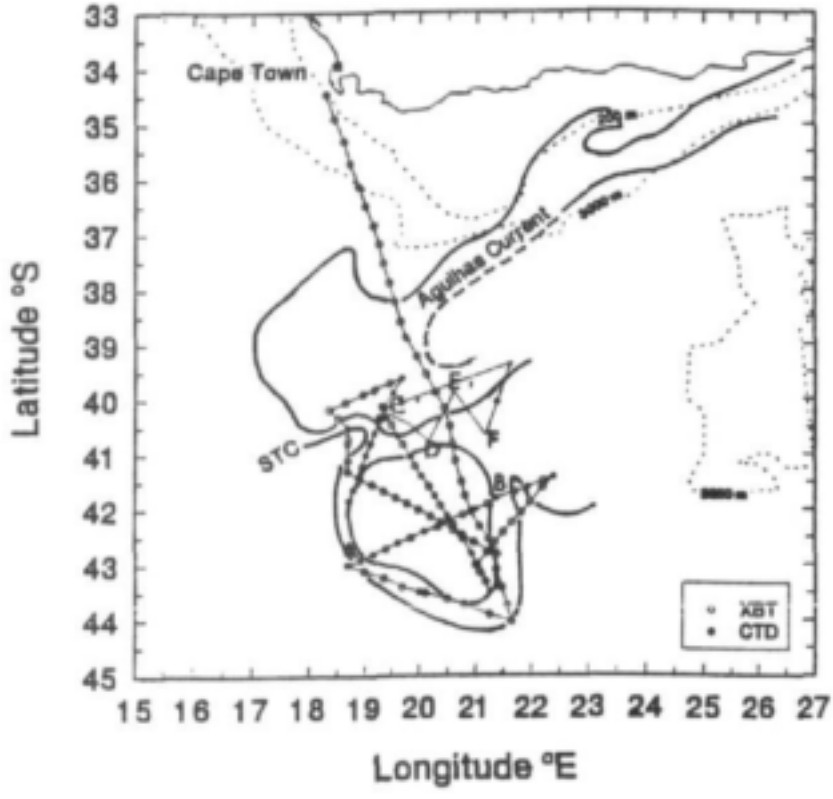

Figure 4.1: Ship track and station positions of the research vessel S.A Agulhas from 21 June to 14 July 1993 with location of the Agulhas Current, Eddy Lesley and the STC (STC). Measurements are presented along transect AB, CDEF.

Depth) lines across the feature and an hydrographic exploration of the adjacent STC. The sea surface temperatures observed are shown in Figure 4.2. Particularly noteworthy is the thermally very intense frontal nature of the STC. A drop from 20°C to 10°C was observed over a distance of less than 70 km. Highest surface temperatures in the eddy itself exceeded only 17°C. Since it is assumed that this eddy had been part of the Agulhas Return Current shortly before, substantial surface cooling must have taken place. This is substantiated by a mixed layer to a depth of 250 m in the upper waters with a uniform temperature of 16°C, not shown here.

The eddy was evident as a disturbance in the surrounding thermal and haline fields to a depth of 1 000 m, the greatest depth to which measurements were made. Judged by the slopes of the

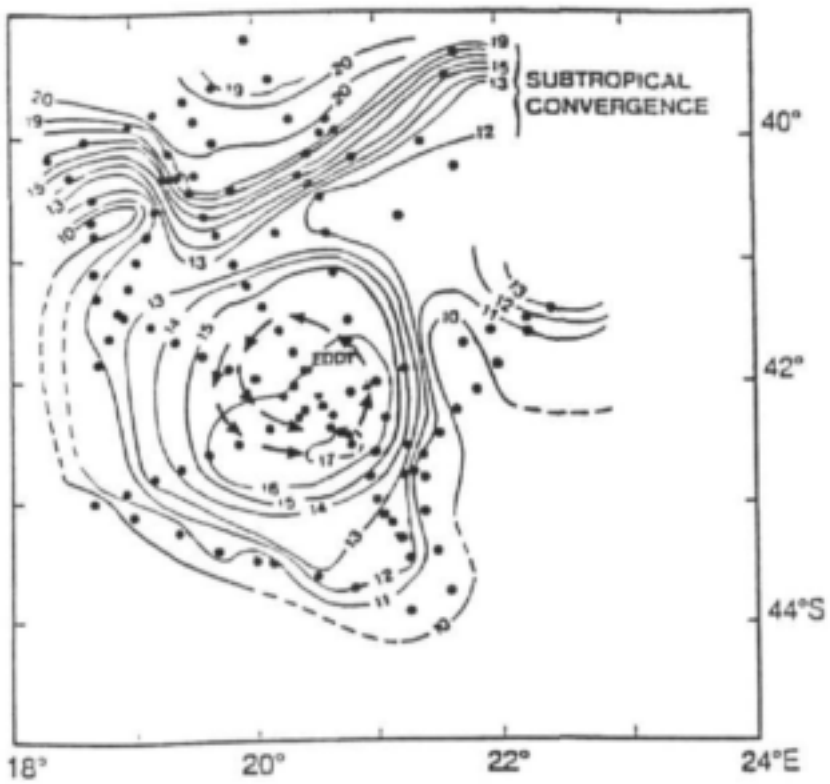

Figure 4.2: The distribution of the sea surface temperature in the region of Eddy Lesley. Dots represent the locations of hydrographic stations, arrows the trajectories of a buoy deployed during the cruise.

10°C isotherm, a good proxy for the dynamic heights in this ocean regime, the eddy was nearly circular with a diameter of about 230 to 250 km. Its rotation rate, as measured by the Lagrangian motion of a surface drifter placed in the eddy (Lutjeharms et al., 1994), was about 1 day giving an azimulthal velocity greater than 1 m/s. Both the location and dimensions of the eddy were similar to those observed in such eddies in this region previously (Lutjeharms and Gordon, 1987, Rigg et al., 1992) leading to the hypothesis that the eddy observed during this cruise was fairly representative of these recurrent mesoscale features.

4.3 Measurement and methods

During the cruise, measurements were made continuously of the sea surface temperature, air temperature and specific humidity, wind speed and direction, short wave radiation and long wave radiation. This allows the calculation of the turbulent fluxes of momentum, sensible and latent heat, the radiative budget and the net heat budget at the sea surface. Oceanographic measurements, XBT and CTD, were carried out. Radiosonde were released every 12 hours and provide vertical profiles. A major problem occurrd when the GPS was down because it then was not possible to calculate the absolute wind speed. This prevented the calculation of the fluxes, of wind speed and direction, humidity and temperature. The Vaisala HMP35D failed at the start of the cruise and the Ophir did not work during daylight due to malfunction. Instead, humidity values were calculated from the SAWB dry bulb and wet bulb temperature.

4.4 Results

4.4.1 Air-sea interaction at the eddy

Two case studies have been chosen to illustrate the great variability of the turbulent fluxes and the net heat budget above the eddy for different meteorological conditions

4.4.1.1 Case 1:

The first case represents measurements made during a transect along the eddy from 25 June at 00:00 GMT to 26 June at 12:00 GMT. The ship track during this transect can be seen on Figure 4.1 (Transect AB). Synoptic pre-frontal conditions prevailed initially. The wind speed was north to north west since 24 June varying from 5 to 10 m/s and brought warm and moist air from the north. On 26 June, as we reached the eastern extremity of the eddy, the arrival of a cold front coincided with an increase in the wind speed with colder and dryer air.

Figure 4.3 shows the different parameters of interest for this transect plotted as a function of time (GMT). They are wind speed and direction, pressure, sea surface temperature, air temperature, air specific humidity, specific humidity at the sea surface, relative humidity, wind stress, latent and sensible heat fluxes, solar radiation (shortwave and long wave), outgoing infrared radiation and the net heat flux. A positive value for the fluxes means a transfer of energy from ocean to atmosphere but a positive value of the incoming short wave and long wave radiation shown here means a gain to the ocean. The mean and standard deviation of the parameters of interest are given in Table 4.1. This table gives averaged values of the parameters of interest measured above the eddy for the two case studies. For this first case, the solar radiation is averaged from from 25 June 0:00 GMT to 26 June 24:00 GMT to be coherent with a full day cycle. On Figure 4.3, the location of the eddy is indicated by the sharp change in SST at about 4:00 GMT (42.728°S, 19.368°E) and at 10:00 GMT on 26 June (41.884°S, 21.266°E). The SST along that transect was almost constant at about 16°C. An interesting feature is the border of the eddy. It had a sea surface temperature higher than the eddy Leslie. This probably was due to past interaction with the Agulhas Current and entrainement of warmer water around the eddy. As we enter the eddy, the difference of temperature between the air and the sea changed sign. On the west side of the eddy the air temperature is slightly

Table 4.1: Mean parameters of interest for case 1 and 2

	Case1		Case 2	
Variable	Mean	Std dev	Mean	Std dev
Wind speed	7.26	2.54	18.37	3.33
Sea Surface Temperature	16.24	0.49	16.05	0.13
Air temperature	14.59	0.78	12.96	1.74
Specific Humidity	10.28	0.45	9.08	1.06
Sea surface Specific Humidity	11.49	0.35	11.34	0.09
Relative Humidity	81.85	3.01	79.51	4.09
Stability	-0.44	0.41	-0.08	0.14
Latent heat flux	35.93	18.14	137.26	52.59
Sensible heat flux	17.17	14.12	67.33	33.36
Bowen ratio	0.46	0.30	0.47	0.13
Visible radiation	46.36	87.89	36.43	80.83
Infrared radiation	325.93	30.35	345.78	19.90
Net heat budget	65.37	95.53	203.63	93.01

higher than the sea. Above the eddy the air is about 1.5°C colder than the sea. This causes the

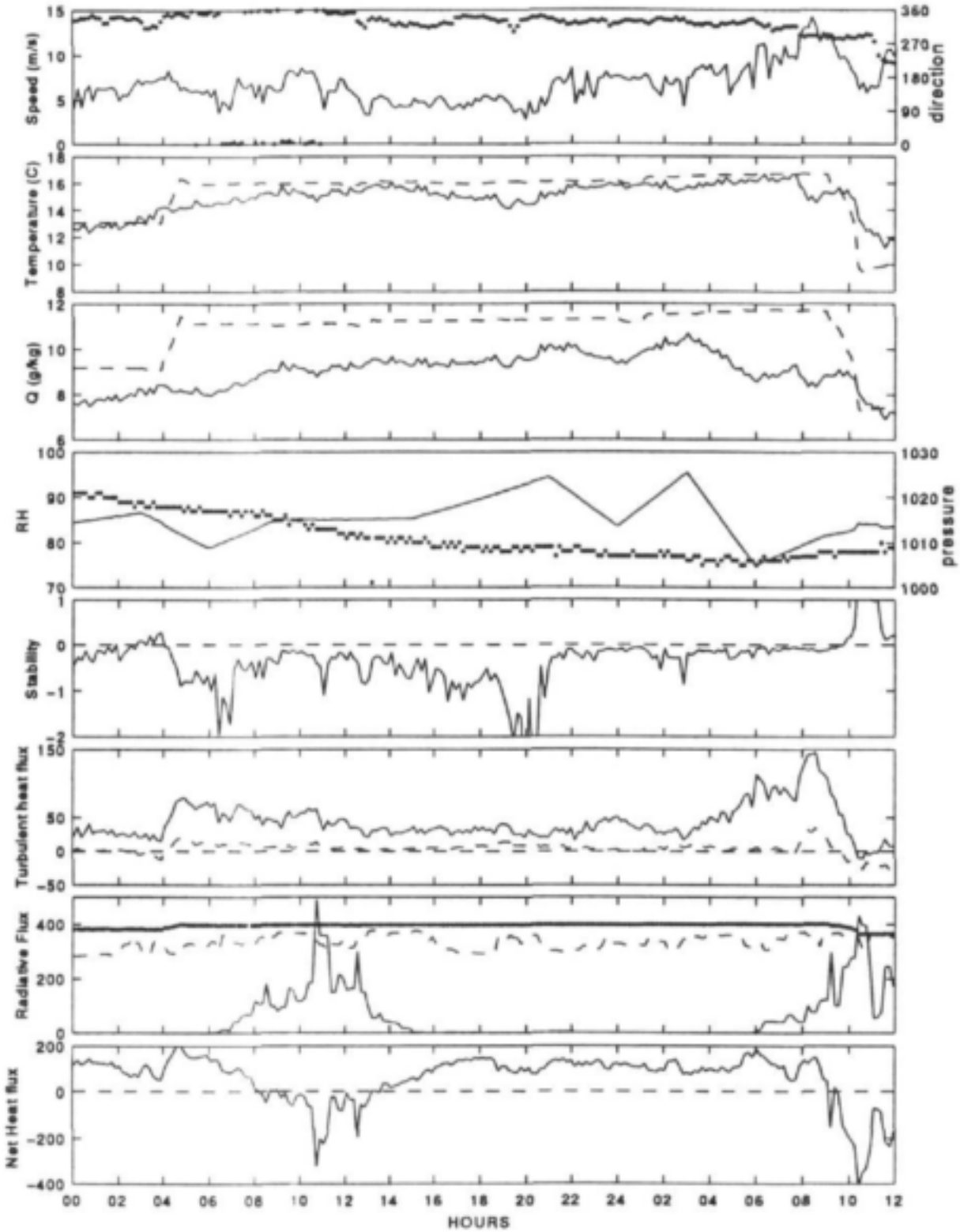

Figure 4.3: Time series of fluxes and meteorological parameters across the eddy (transect AB, South West to North East, see Fig 4.1) for 25 June 00:00 GMT to 26 June 1993 12:00 GMT. The parameters (from top to bottom) are: wind speed (–) at 10 m height and direction (.); air temperature at 10 m height (–) and sea surface temperature (- -); specific humidity at 10 m (–) and saturation specific humidity at the sea surface (- -); relative humidity at 10 m (–) and pressure (.); stability parameter $\zeta = 10/L$ (–); latent heat flux (–) and sensible heat flux (- -); incoming short wave radiation (–), incoming long wave radiation (- -) and upgoing long wave radiation (. .); net heat budget (positive is an ocean loss).

atmospheric stability to be stable on the cold side and unstable above the eddy. Accordingly the latent and sensible heat fluxes increased from about 25 Wm^{-2} to 100 Wm^{-2} from the ocean to the eddy. The same feature can be observered when we left the east side of the eddy where the difference between the sea and air temperature went from about 1.5°C to -2°C and the turbulent heat fluxes decreased from about 180 Wm^{-2} to -10 Wm^{-2}. This show that the eddy can radically modify the atmospheric stability and substantially increases the turbulent heat fluxes. This will create different dynamics of the surface atmospheric boundary layer. In that case relatively warm air was advected from the north and the atmospheric conditions were neutral or unstable above the eddy and stable above the surrounding waters.

The variation of the net heat budget was mainly due to the input of short wave radiation. The difference of temperature and specific humidity between the eddy and the overlying atmosphere was relatively constant thus giving a sensible and latent heat flux varying slightly with the wind speed during the transect. The stability condition above the eddy is generaly neutral being unstable when the wind weakens. The increase in the exchange of latent and sensible energy at the end of the transect is due to the increase in wind speed due to the cold front. This case illustrates the great influence of the eddy on turbulent heat flux and atmospheric stability compared with the surrounding ocean.

4.4.1.2 Case 2:

This case provides 4 days of continuous measurement in the eddy with 3 days in extremely stormy conditions typical of this area in winter. The eddy was entered on 28 June at 11:30 GMT (42.962°S, 20.982°E), before heading to the center of the eddy. 28 June was characteristic of prefrontal conditions with a northerly flow picking up rapidly into gale force. The cold front passed over the ship on 29 June, decreasing the air temperature, with a strong westerly wind. On 30 June a high pressure system ridged around the continent. Tight pressure gradients on the southern limb of the anticyclone maintained strong to gale force westerly winds. The high pressure ridged south and eastward toward the ship on 1 July with decreasing winds when the center of the high pressure was closer. The ship remained on the eddy until 2 July at 06:00 GMT when it reached the northern boundary of the eddy (41.036°S, 19.823°E). On 2 July the high pressure system moved eastward creating northerly winds at the location of the eddy and bringing warm air by the end of the day. During the storm the ship cruised from the center of the eddy to the west and back in a 10 meters swell sea. During the first night of the storm the GPS failed, preventing the calculation of the absolute wind speed and direction for 8 hours. Nevertheless, the fluxes are calculated using the relative wind speed because the ship was cruising very slowly into the strong wind.

The parameters of interest for the period 28 June to 2 July are presented in Figure 4.4. The mean and standard deviation of the parameters of interest are once again given in Table 4.1. The parameters have been averaged for the period during the storm only, from 28 June 16:30 GMT to 1 July 14:10 GMT, when the wind speed exceeded 10 m/s. For that averaging, we have excluded the period 30 June 2:50 GMT to 6:30 GMT because these observations were taken outside the eddy. Nevertheless it is interesting to see how the turbulent fluxes decrease as the ship leaves the eddy toward the colder ocean. The latent heat fluxes decrease from 120 Wm^{-2} to 40 Wm^{-2} and the sensible heat fluxes decrease from 40 Wm^{-2} to -10 Wm^{-2}. This again illustrates the dramatic effect of the warm eddy on the atmosphere.

The solar radiation is averaged from 28 June 0:00 GMT to 1 July 24:00 GMT to be coherent with a full day cycle. The short wave radiation was very low due to the cloud coverage and one can clearly see that the sensible and latent heat fluxes were the principal components of the heat budget. The difference of temperature between the air and the sea was up to 8°C when cold air from the south was advected above the eddy. The stability parameter was neutral during the whole period due to high wind speed whith the turbulent fluxes driven by the shear force. From 1 July the wind started to decrease and the atmosphere was very unstable due to the extreme difference of

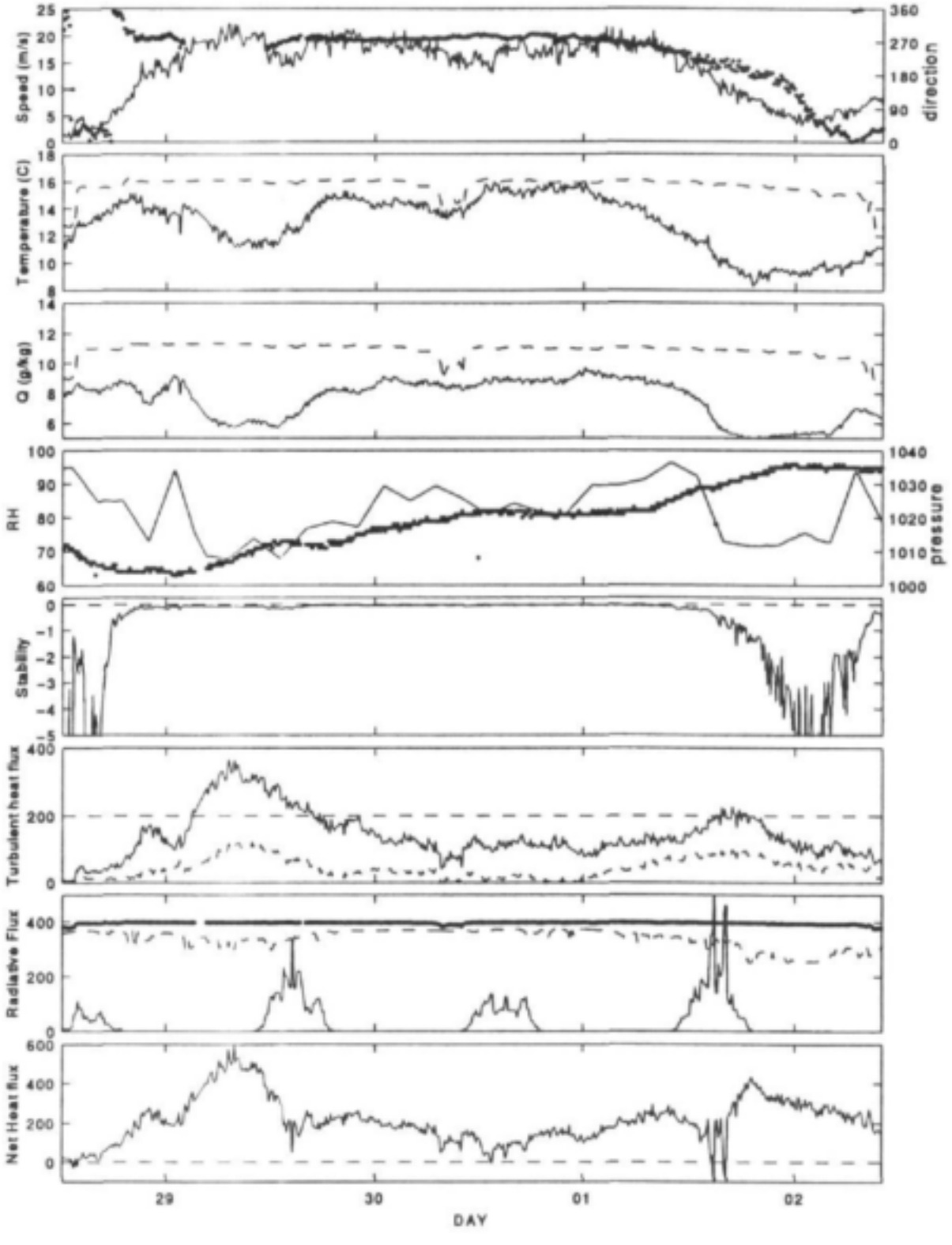

Figure 4.4: Time series of fluxes and meteorological parameters across the eddy from 28 June 00:00 GMT to 2 July 06:00 GMT. The parameters (from top to bottom) are: wind speed (–) at 10 m height and direction (.); air temperature at 10 m height (–) and sea surface temperature (- -); specific humidity at 10 m (–) and saturation specific humidity at the sea surface (- -); relative humidity at 10 m (–) and pressure (.); stability parameter $\zeta = 10/L$ (–); latent heat flux (–) and sensible heat flux (- -); incoming short wave radiation (–), incoming long wave radiation (- -) and upgoing long wave radiation (. .); net heat budget (positive is an ocean loss).

temperature and specific humidity between the air and the eddy. The condition were also unstable at the start of the crossing due to low wind speed and the difference of temperature.

Other observations made during the cruise during different synoptic conditions not shown here illustrate how the eddy is a major source of latent heat fluxes. Heat fluxes increase about five time from the ocean to the eddy especially when westerly, southerly or easterly winds bring cold air above the eddy. During the cruise maximum values of 500 and 350 Wm^{-2} were calculated for the latent and sensible heat flux respectively. During northely condition, not only the fluxes increases but the difference between the air and sea temperature is such that atmospheric unstable condition develop above the eddy when stable or neutral condition can develop above the surrounding oceans

4.4.2 Air-sea interaction modification across the STC

Various crossings of the STC and of the oceanic front situated at the limit of eddy Lesley are reported below. In these cases sea surface temperature gradients across the front were 0.4°C/km. On 4 July the ships started on a zig-zag course eastward along the front (Transect CDEF on Figure 4.1).

The front was crossed at 17:00 GMT (40.401°S, 19.705°E), 22:30 GMT (39.954°S, 20.567°E), 23:00 GMT (39.907°S, 20.639°E)

The meteorological situation during this period was dominated by a high pressure system north east of the ship and the synoptic conditions were dictated by the condition at the trailing edge of a high pressure system bringing warm moist inflow from the north. From 3 July the wind was north-north-west and quite steady bringing warm and moist air from the adjacent Agulhas Current.

On Figure 4.5 is given wind speed and wind direction, air and sea temperature, specific humidity, wind stress and sensible and latent heat fluxes for the frontal crossings. The northerly wind brought warm air over the cold side of the front creating stable conditions. Subsequently a change in the sign of the latent and sensible heat fluxes was observed. The influence of the SST front on air-sea interaction was radical, especially during the first crossing with sea surface temperature drop of 7°C. On the warm side of the eddy the air was about 3°C colder than the sea. On the cold side the air was 1 to 2°C warmer than the sea and the specific humidity decreased towards the cold side. Accordingly the latent heat fluxes decreased from 150 Wm^{-2} to -20 Wm^{-2} and the sensible heat fluxes decreases from 30 Wm^{-2} to -20 Wm^{-2}. The atmospheric stability parameter went from near neutral to stable across the front. The wind speed seems to be weaker over the cold side of the front. In absence of a observational aircraft and without enough radiosonde, it is difficult to know if this reduction in wind speed is due to mesoscale circulation triggered by the SST gradient or if it is due to the reduction of turbulence in the cold side with stable atmospheric condition. The two other crossings show the same trend except that the air temperature gradually increased with the northerly wind. As a result the absolute value of the sensible and latent heat fluxes decreased on the warm side and increased on the cold side.

4.5 Wind fields above the eddy from ERS-1 scatterometer

ERS1 scatterometer surface wind field above the eddy during the cruise are presented for 22 June at 08:20 GMT and 22:10 GMT (Figure 4.6). They are presented together with ECMWF surface wind field for comparisons The scatterometer is an active microwave radar. The resolution is 50 km and data are sampled on a 25 km square grid. Results presented here are the ERS-1 off-line Scaterrometer Products generated at the Institut Francais de Recherche pour l'Exploitation de la Mer (IFREMER) (Quilfen, 1993). A striking feature is the increase in surface wind speed on 22 June at 08:20 GMT and 22:10 GMT. This is in agreement with the results predicted by Xie et al.(1996). His numerical study that shows that a mesoscale heat source such as an eddy will serve to increase the wind speed above and behind it. During the cruise other ERS1 surface wind products above or partially above the eddy were avalaible. Although eddy coverage was poor due to

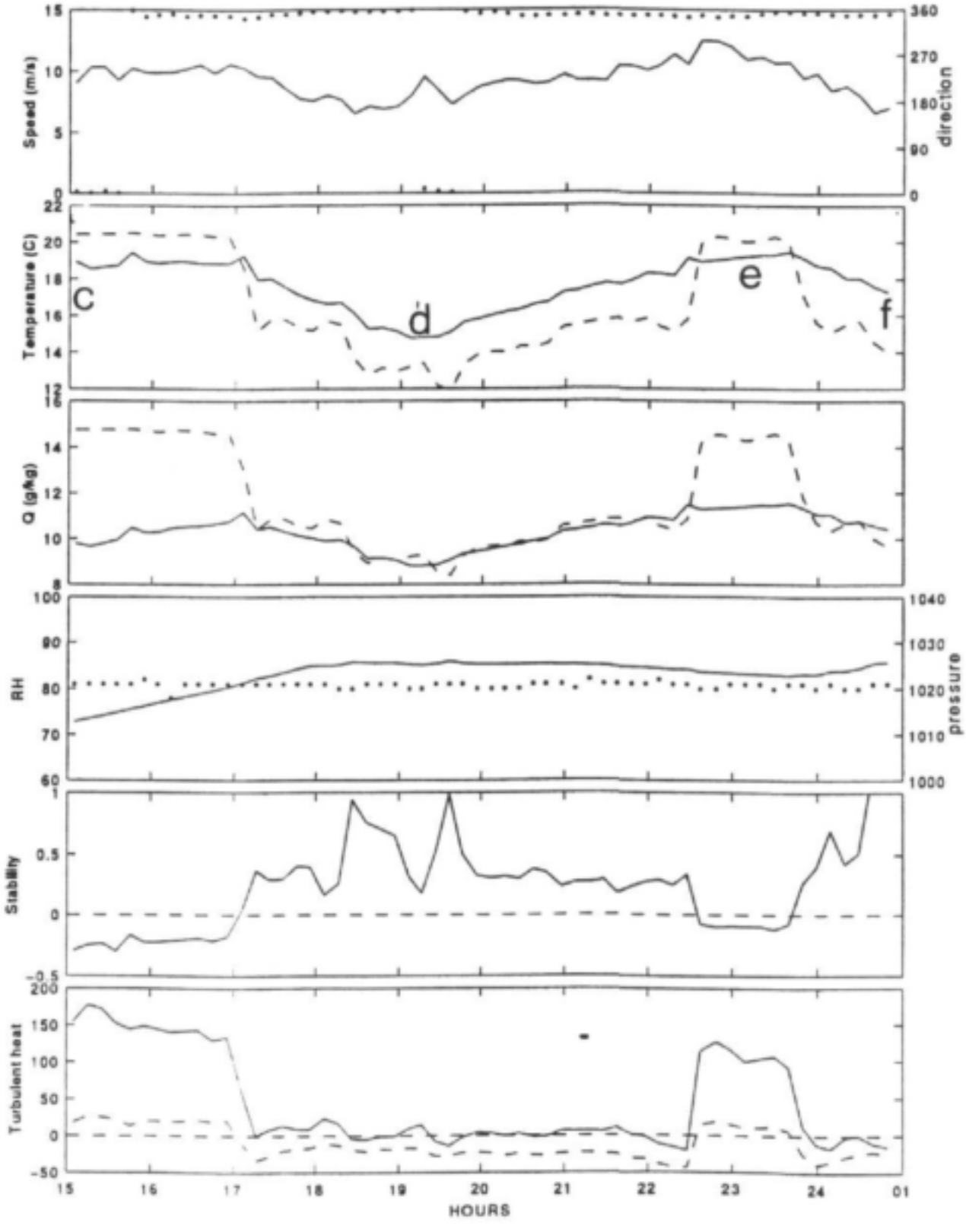

Figure 4.5: Time series of fluxes and meteorological parameters across the Subtropical convergence (transect CDEF, see Figure 4.1) from 4 July 15:00 to 5 July 01:00 GMT. The parameters (from top to bottom) are: wind speed (–) at 10 m height and direction (.); air temperature at 10 m height (–) and sea surface temperature (- -); specific humidity at 10 m (–) and saturation specific humidity at the sea surface (- -); relative humidity at (–) at 10 m and pressure (.); stability parameter ζ = 10/L (–); latent heat flux (–) and sensible heat flux (- -).

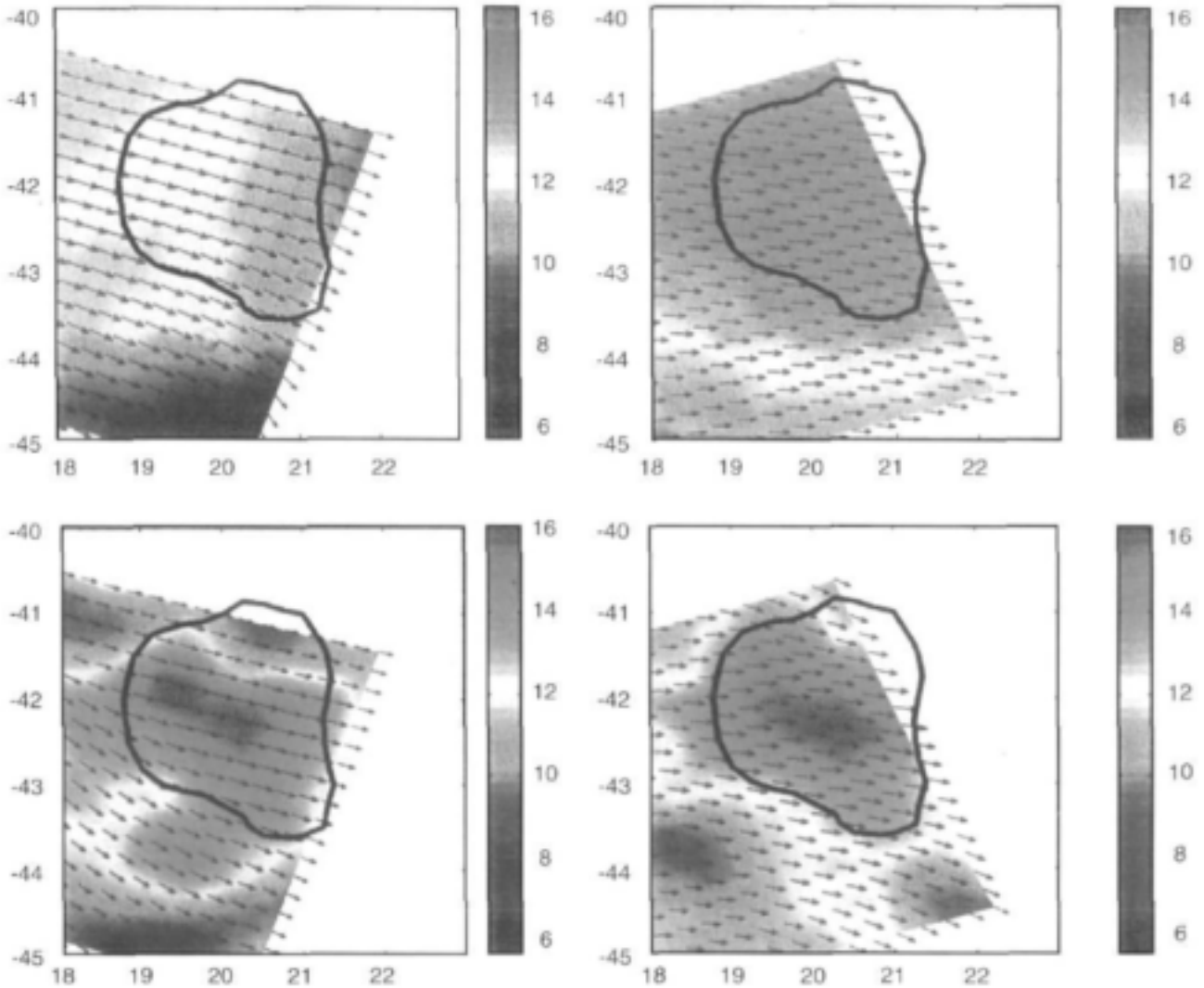

Figure 4.6: ERS1 (bottom) and ECMWF (top) surface wind speed and direction for 22 June 08:20 GMT (left) and 22 June 22:10 GMT (right). The location of the eddy is shown (figure 4.2).

the satellite repeat cycle, the wind speed seems stronger above the eddy. Difference in wind speed between ECMWF and ERS1 was high as can be seen in Figure 4.6. Following those observations we studied all ERS1 products during the 1993 winter when we can assume that the eddy was present. This assumption is not totally arbitrary. A balance between self steering by an anticyclonic eddy and the background advection could achieve this. The ERS-1 data is scarce and irregular but the same pattern was observed for most of the cases with an increase of the wind speed above the eddy and for some case downstream of the eddy especially when the wind is already strong (pre frontal of frontal synoptic conditions).

We present in Figure 4.7 averaged ERS1 wind speed for the winter above the eddy and the warm Agulhas current. They are the ERS1 scatterometer mean wind field products. They are gridded wind field computed from ERS-1 scatterometer observations, interpolated with the kriging method and analysed on a 1° latitude grid (Bentany and al. 1996) . In Figure 4.7, surface wind speed increases above the location of Eddy Lesley and the Agulhas current.

The observations suggest that the surface wind speed increases above the area of SST heterogeneity such as eddy Leslie and the Agulhas Current. The results from the observation have shown that the effect of the eddy is to increase the atmospheric unstability above the eddy and to increase about fivefold the exchange of turbulent fluxes. This should help to transfer the momentum fluxes downward thus increasing the wind at the surface.

Other observational studies in areas of strong SST gradient such as the Gulf stream or the inshore edge of the Agulhas current (Jury and al., Reddy and Ramam, 1994, Rogers 1989, Holt

and Raman, 1990) shown an increase in wind speed and a change in wind direction from the cold side to the warm side. The explanation is that the SST gradients have induced a mesoscale circulation leading to the increase in wind speed. Those situations seems to appear in calm weather. Although the weather in the area in winter is seldom calm those secondary circulations could be partly responsible for the increase in wind speed above the eddy shown in Figure 4.7.

4.6 Conclusion

The data collected during the cruise represent a data set of ocean and atmosphere data that could be used to test different modeling hypotheses. The discrepancy between the ERS1 and ECMWF wind in that area is about 20 %.

This is probably due to the inability of the ECMWF to take into account intense mesoscale features such as an eddy.
The SST gradient across the STC and the eddy are associated with changes in wind speed, atmospheric stability and cloud cover. The subsequent variations in the wind stress and the turbulent fluxes of sensible and latent heat leads to a spatial variation in the structure of the oceanic mixed layer and the surface atmospheric boundary layer. It seems that the eddy is a strong source of heat and especially latent heat to the atmosphere. Because of the difference of temperature the atmosphere is more unstable and turbulent above the eddy. This suggest a reason why the wind seems to accelerate above eddy Lesley, confirming a recent modelling study.

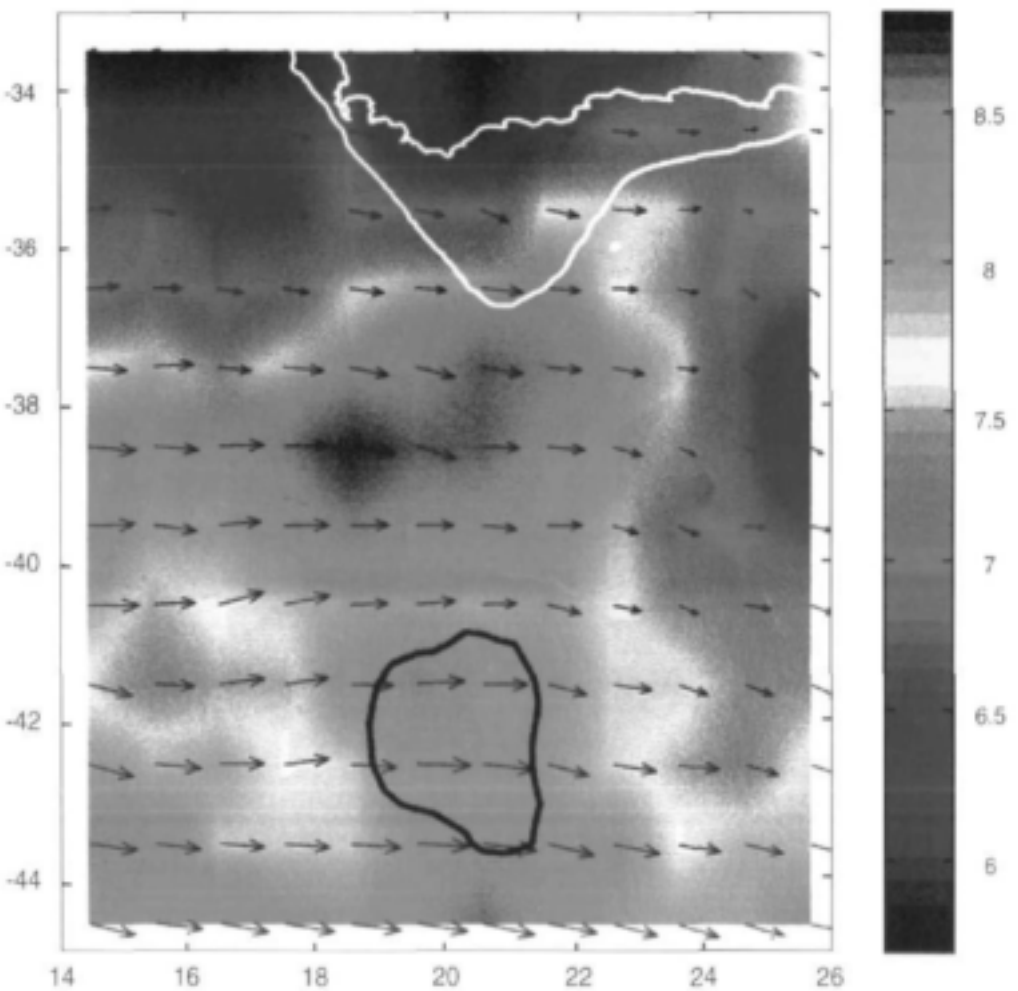

Figure 4.7: ERS1 surface mean wind speed and direction from May to August 1993 above Eddy Lesly and the southern Agulhas Current. The location of the eddy is shown (Figure 4.2).

Chapter 5

Atmospheric boundary layer fluxes and structure across a land-sea transition

5.1 Introduction

The southeastern coast of South Africa (Figure 5.1) is a climate transition zone where the humidifying effects of the warm Agulhas Current to the east lie in contrast to the dry Karoo region in the west. A mountainous escarpment > 1000 m lies 100 to 200 km inland. There are few areas of the world where climatic gradients are as acute. Rainfall in the northeast is > 800 mm and < 300 mm in the west. The vegetation cover varies significantly from year-to-year. The study area has the city of East London near its centre at 33°S, 28°E where the warm Agulhas Current last touches the coast on its south-westward excursion.

The climate of the Eastern Cape has received little attention in comparison to the central plateau of South Africa. Tanga (1992) outlines the main features of climate and rainfall of the region, lying in the transition between summer and all-season convective regimes. A dry continental air mass lies to the northwest, and maritime sub- tropical conditions prevail along the coast and to the east. Transient disturbances of the westerlies determine the temporal pulse of climate. Wet spells are concentrated near convective fronts associated with onshore flow, a marine anticyclone and an interior low pressure cell. Orographically assisted uplift along the windward escarpment may result in flood events, temporal aspects of which have been analysed by Uys (1983). A study of drought in the area was made by Jury and Levey (1993). The rainfall exhibited a bimodal distribution with peaks of 40-50 mm/month in February-March and October-November. Explanations for interannual cycles and seasonal drought were sought in teleconnections with SST, outgoing longwave radiation (OLR) and winds. Westerly winds in the 700 hPa layer increased in dry years, consistent with a meridional band of below normal cloudiness (+OLR). SSTs were below normal to the south and south-east of southern Africa during dry years. Another study by Jury et al. (1993a) found that SST in the Agulhas Current and nearshore environment influence coastal rainfall. Spatial correlations between rainfall and SST over a distance of 1000 km along the south- east coast were +0.88. Where the Agulhas Current is about 10 km from the coast, summer rainfall is > 100 mm/month in association with the onshore advection of thunderstorms by seabreezes. Further to the south-west where the shelf is wider, the Agulhas Current lies > 30 km offshore and a zone of sinking occurs over the cool inshore waters (Jury and Courtney 1991). This inhibits the interaction of marine thunderstorms and convergent seabreezes.

Covariance estimates of heat and moisture fluxes will be presented in the atmospheric boundary layer over a contrasting land-sea transition. It is hypothesised that spatial and temporal changes in turbulence regimes and moisture supply are large and depend on direction of the zonal wind

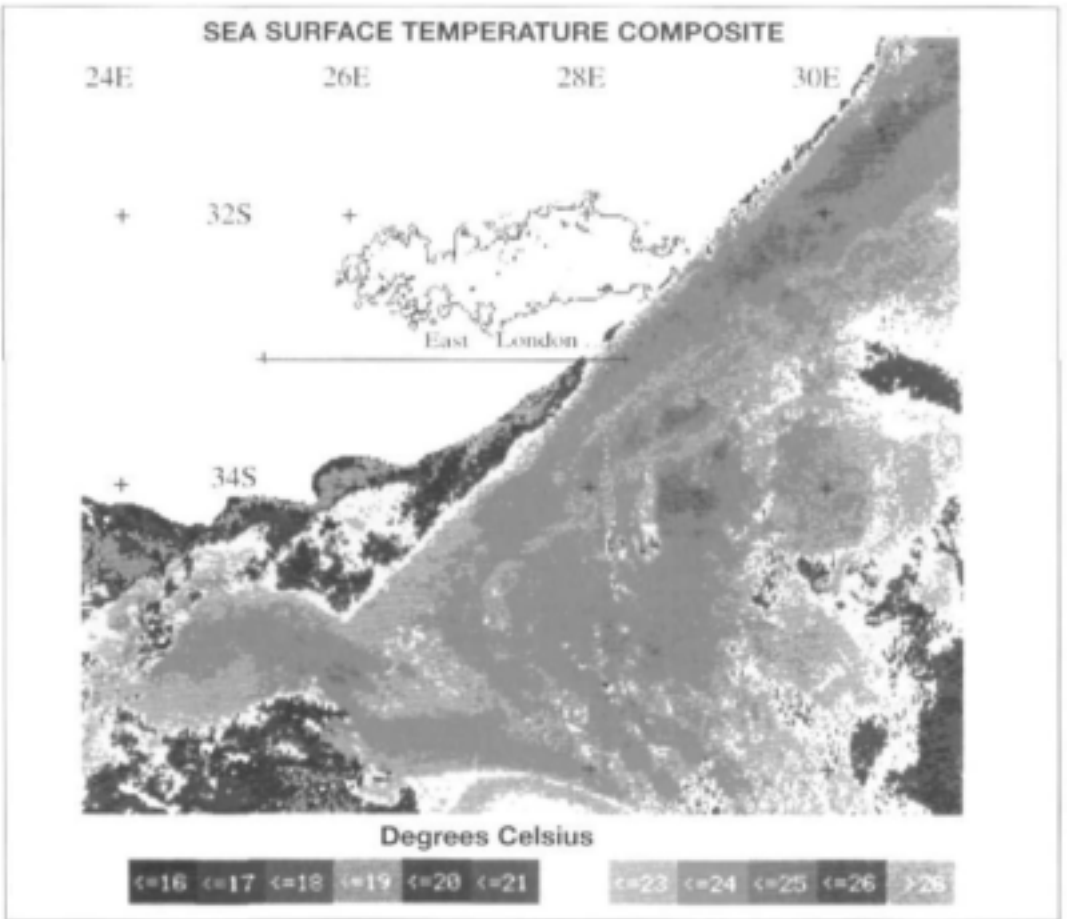

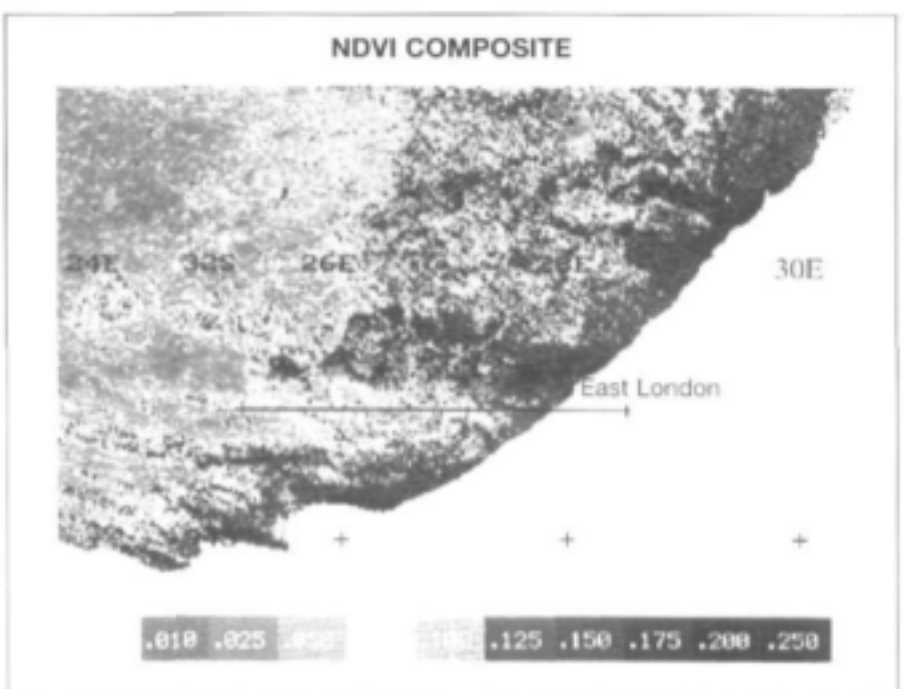

Figure 5.1: Composite maps of satellite (a) SST and (b) NDVI showing the flight track and East London. Composites are based on images for 23, 24, 27, and 28 November 1993.

and depth of the marine boundary layer. A quantitative understanding of surface layer fluxes will ensure that energy exchanges between various scales of weather phenomena are able to be modelled with confidence.

5.2 Data and methods

Satellite composites of sea surface temperature, cloudiness and vegetation reflectance during the study period describe surface gradients in the land-sea transition zone. Regional synoptic weather information was obtained from local sources and supplemented by daily 2.5° gridded ECMWF meteorological data for 1200 UT (14h00 local). The parameters 850 hPa temperature and horizontal wind, and 700 hPa vertical motion are analysed for case study days 23 and 26 November, 1993. The air sea interaction system was set up at the East London harbour breakwater for the estimation of heat, moisture and momentum fluxes over the cooler shelf waters. The breakwater extends about 1 km seawards into the marine environment, so fluxes are representative of cooler shelf waters modified by the nearby coast and breakwater. Aircraft sections were undertaken by means of successive profiles in the boundary layer along 33.1°S to the west of East London (Figure 5.2) Turbulent covariance measurements of temperature, specific humidity and vertical gust were obtained. Regional sea

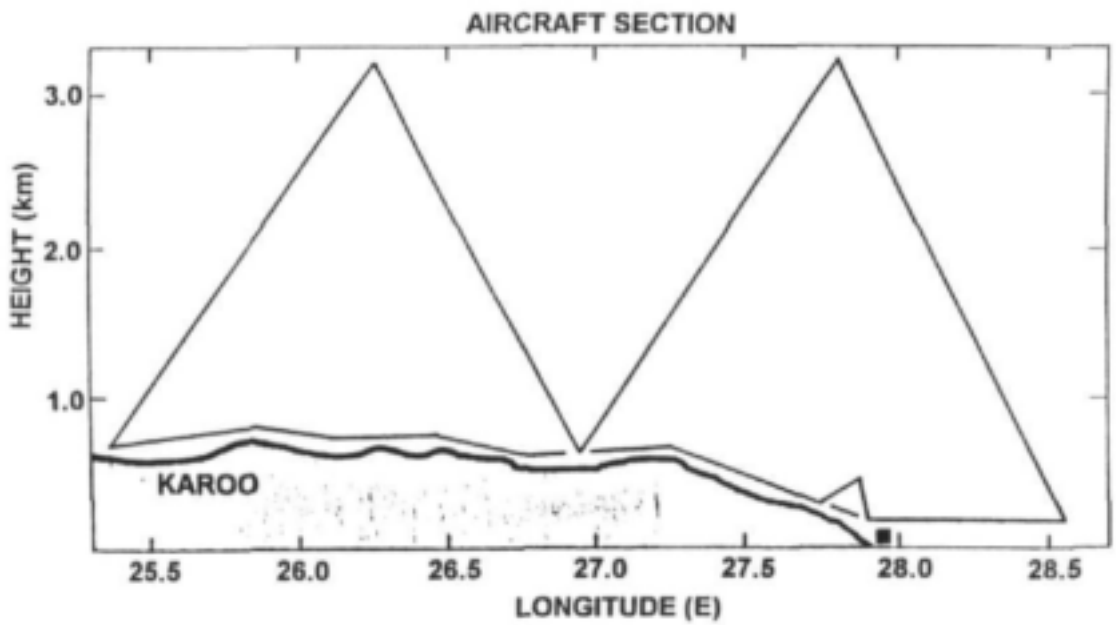

Figure 5.2: Aircraft vertical section for flights conducted from 22-29 November 1993. Small square at coast shows position of coastal weather station.

surface temperature and normalized vegetation index (NDVI) fields were mapped using NOAA-11 Advanced Very High Resolution Radiometer (AVHRR) data. A number of relatively cloud-free days were obtained for the period of intensive surveys: 23, 24, 27 and 28 November 1993. AVHRR data were available for visible, near-infrared and infrared spectral bands at 2 km resolution. Cloud masking was undertaken and a SST algorithm was applied to the thermal infrared data. The NDVI was calculated for each of the four days by applying the standard algorithm (Tucker 1978). Each pixel is examined during the compositing period and co-located maximum values are retained to reduce cloud contamination. Despite the selection of cloud free days and the techniques applied, an area of persistent cloud was found over the steepest escarpment to the north-west of East London. This cloud area was identified from albedo and minimum IR temperature.

The flight navigation system aboard the aircraft consisted of a Trimble TNL2000 Global Positioning System (GPS) for 1 s updates of position, aircraft track and ground speed. With the addition of true air speed and aircraft heading, wind velocity could be derived. Pressure and radar altimeters gave height above sea and ground level. An accelerometer and pitch rate gyroscope sensitive to aircraft motions was used in conjuction with a Rosemount angle of attack vane to determine vertical gusts. The angle of attack vane adequately measures high frequency vertical eddies in the airflow, whilst the accelerometer and pitch gyro account for departures of the aircraft from its intended track caused by low frequency eddies. When analysed together, aircraft motion can be subtracted from vane deviations to provide reliable estimates of the vertical gust (w') at specified sampling periods. Fast response sensors monitored air temperature (Rosemount) and specific humidity (Lyman-alpha), which were archived together with vertical gust, position, height, etc, at 10 Hz using a PC. Dewpoint temperatures were measured with a cooled mirror (EGG) sensor as a cross check of the Lyman-alpha.

A total of eight vertical sections were made by means of successive aircraft profiles from the surface to 3 km elevation (700 hPa) along 33.1°, from 25.2° to 28.5°, an E-W distance of over 300 km (Figure 5.2). The flights were conducted at the time of maximum convective heating, from 10:00-13:00 UT (12h00-15h00 local) in the period 22- 29 November 1993. On the out-bound leg the aircraft first headed low-level over the coastal weather station, then offshore from East London. On reaching the warm core of the Agulhas Current (SST> 24 C), the aircraft turned westward and ascended slowly to 3000 m over a distance of 60 km. A subsequent descending leg brought the aircraft over coastal mountains of elevation 500 m. The aspect ratio of these flight legs was 1:20 and was flown on autopilot so that high frequency eddies could be resolved. The vertical saw-tooth pattern was continued to the Karoo desert some distance inland. The return leg was flown at 100 m above ground level on autopilot at constant power settings, where possible, to obtain reliable surface layer fluxes estimates.

The aircraft sensors and recording systems were calibrated before and after the survey period. 10 Hz meteorological values were initially averaged into 30 s intervals, following removal of linear trends imposed by ascents/descents. The decision to use the 30 s averaging time for covariance products was influenced by the need for discrete measurements in an inhomogeneous environment. This is comparable to averaging times for aircraft surveys of marine turbulence, 1 minute (Said and Druilhet, 1991). In-situ meteorological data were subsequently accumulated into bins of adequate dimensions to characterise turbulent wavelengths from 10 - 10^{-3} m (Wyngaard 1986). Covariance fluxes were estimated from absolute perturbations of the product of vertical gust (w') and temperature (T') or specific humidity (q') over 30 second sampling periods. The aircraft covariance fluxes technique follows the approach of Raynor et al. (1979), Sethuraman et al. (1979), Gamo et al. (1982), Lenschow (1986), Comrie (1988), and Said and Druilhet (1991), except for the 1:20 aspect flight legs which may impose some bias. The sampling strategy enabled the boundary layer to be covered within three hours, thus minimising exposure to the diurnal cycle, and kept flight time within aircraft endurance limits.

Spectral peaks for turbulent covariance parameters were generally in the range 0.5-5 Hz, which for the specified 30 second averaging time provided up to 10 cycles per sample. For analysis of boundary layer structure, aircraft data collected along vertical saw-tooth legs were accumulated into height-distance bins of 100 m x 10 km, respectively, to emphasise stratification. To highlight spatial gradients, a mean (horizontally-averaged) temperature and dewpoint profile for the eight flights was computed and departures for individual flights were analysed. Manual subjective analysis of the section data gave results superior to objective contouring routines, owing to sampling gaps inherent in the vertical saw-tooth pattern.

Variations in regional weather were quite extreme during the intensive survey period of 21 to 30 November 1993. Coastal time series illustrate conditions ranging from warm and humid to cool and dry. Winds varied from 15 m/s southwesterly to 10 m/s northeasterly every couple of days. Hence ensemble averaging of aircraft data into weather regimes was not advisable. The aircraft

data are presented for two contrasting cases: dry westerly on 23 November and moist easterly on 26 November 1993.

5.3 Results

5.3.1 Geographic setting

The SST and NDVI satellite composite images in Figure 5.1 illustrate the in homogenous nature of the underlying surface. SST reflects the presence of the warm Agulhas Current with temperatures > 25°C at the eastern end of the flight track off East London. SST are also > 25°C over a long trajectory to the northeast. Along the coast to the southwest of East London a wedge of cool water (< 19°C) is found. There the Agulhas Current veers offshore in response to a widening shelf, resulting in dynamic upwelling. An area of persistent clouds is outlined to the north of the flight track, which overly the highest coastal mountains of the area (> 1500 m). Within a 400 km radius of East London, the Agulhas Current supplies a 105 km^{-2} area of warm (> 22°C) water which acts as a source of water vapour into the lower atmosphere.

Variations in vegetation reflectance are illustrated in the lower panel of Figure 5.1. Vegetation cover which is green with an NDVI value > 0.15, is found along the coast near East London and to the northeast. Green vegetation underlies the area of persistent clouds, along the escarpment west of East London. Further west the vegetation reflectance changes to yellow and light brown, where the Karoo desert encroaches. NDVI values there are < 0.05. Changes in NDVI beneath the flight track are illustrated in Figure 5.3.

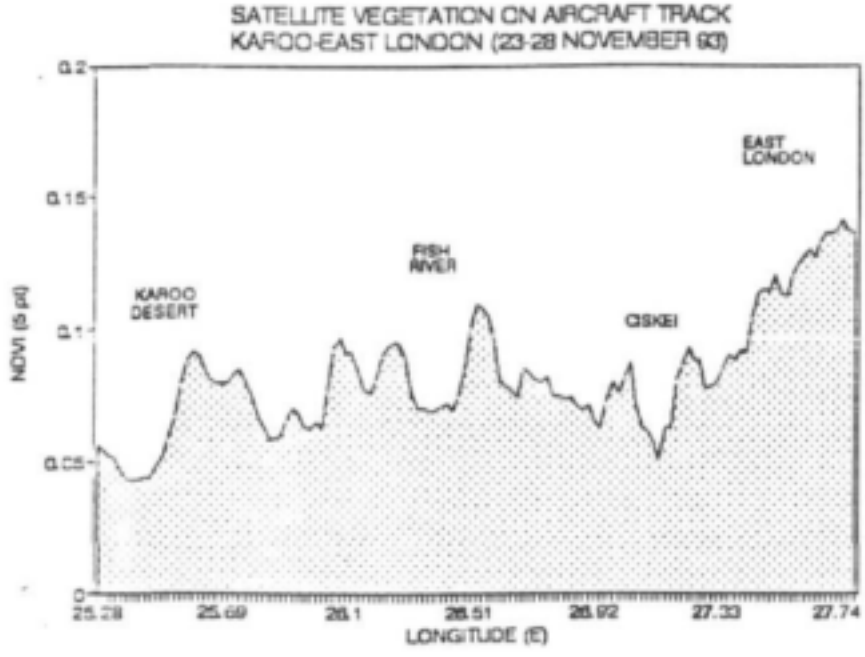

Figure 5.3: Satellite NDVI composite values underlying the aircraft track. A 5 pt filter has been applied. Various place names are provided.

NDVI values reflect green sub-tropical humid conditions in the east. In the hills near 27°E, overgrazing and semi-urban development results in low NDVI values. Further west a gradual decline of NDVI follows the Fish River valley. The trend of vegetation reflectance is contributed primarily by the E-W gradient in mean rainfall. In this land-sea transition zone, differing turbulence regimes are expected.

5.3.2 Coastal time series

Synoptic weather information obtained from the local airport (not illustrated) indicate a range of pressure from 1005 hPa on 21 November to 1022 hPa on 24 November, followed by a gradual decline thereafter. Temperatures varied diurnally from 18-23°C on average and were at a maximum of 27°C on 21 and 27 November and a midday minimum of 19°C on 23 November. Dewpoint temperatures varied diurnally from 16-19°C on average and were at a maximum of 23°C on 21 November and a day-time minimum of 12°C on 23 November. A secondary maximum in dewpoint occurred on 26 November (19°C). The diurnal variation of dewpoint indicates the potential for moisture advection by seabreeze circulations, reflected in increasing wind speeds in the early afternoon hours (Figure 5.4). Wind directions were generally oriented along the coast. As a result of coastal upwelling, SST were about 16°C until 23 November when westerly winds caused warming to 20°C thereafter (see Figure 5.4).

The coastal time series includes comparative airport data. The westerly (23 November) and easterly (26 November) cases are identified on the wind direction plot in the top panel. Coastal wind speeds were about 30% higher than the airport site during easterly events on 21 and 27 November. Temperatures were higher during the daytime at the inland site as expected. The specific humidity was initially about 13 g/kg and declined to a minimum of 7 g/kg on 23 November. Moisture levels at the coast gradually recovered thereafter, peaking on the 26th at 12 g/kg and again on the 29th at 13 g/kg, as local SST increased and humid easterly winds resumed.

Fluxes of latent and sensible heat are illustrated in Figure 5.5. Owing to the cool SST and overlying warmer air, sensible heat fluxes were initially negative and gradually increased to about + 30 Wm^{-2}. Latent heat fluxes were low on 21 November and increased to a peak (> + 100 Wm^{-2}) during westerly winds on 23 November and again during easterlies on the 27th. Due to the presence of cool upwelled water, surface latent heat fluxes were three-fold less over the inshore zone than over the warm Agulhas Current, comparing coastal and aircraft results.

Wind stress was typically around 0.1 $N.m^{-2}$ during the study period, but rose to 0.25 $N.m^{-2}$ on 21 and 27 November (not shown). The stability parameter became increasingly negative on 25 and 26 November, when SST increased and onshore flows brought moist unstable air from the Agulhas Current landwards.

5.3.3 Regional weather setting

The Port Elizabeth radiosonde height-time section for the study period is shown in Figure 5.6. These data are collected about 5 km inland at 34°S, 25.5°E, about 100 km to the southwest of the study area every 12 hours. Dewpoint isotherms and horizontal winds are illustrated from the surface to 700 hPa level (3.1 km). Moist conditions prevailed from 19-21 November and winds swung from easterly to westerly (> 20 m/s) in the upper boundary layer. Dry conditions ensued with the passage of a westerly frontal trough and advection of cool air from the South Atlantic. The 0°C dewpoint isotherm dipped to its lowest level on 24 November. Easterly flow resumed and the depth of moist air gradually increased thereafter. The 10°C dewpoint isotherm rose above 925hPa (800 m) on the 26th when easterly winds extended to almost 2 km depth.

The regional weather is described for the two case study days in Figure 5.6 using ECMWF 12:00 UT (14h00 local) data. On 23 November relatively cool conditions prevailed and 850 hPa temperatures were as low as 5°C to the southwest of the study region. Temperatures over the Karoo along the flight track were about 12°C at 1.5 km. Sinking motions accompanied passage of the trough and winds of up to 22 m/s were observed offshore from East London. In contrast the 26th exhibited relatively warm conditions; temperatures at 850 hPa over the Karoo were > 19°C, and surface temperatures were near 30°C. Rising motions at 700 hPa (3.1 km) were evident within southeasterly winds on the 26th. This flow was up the slope of the coastal mountains across the flight track. The main difference in the synoptic weather was the presence of a marine low < 1008 hPa on the 23rd in contrast to an offshore high pressure cell > 1028 hPa on the 26th.

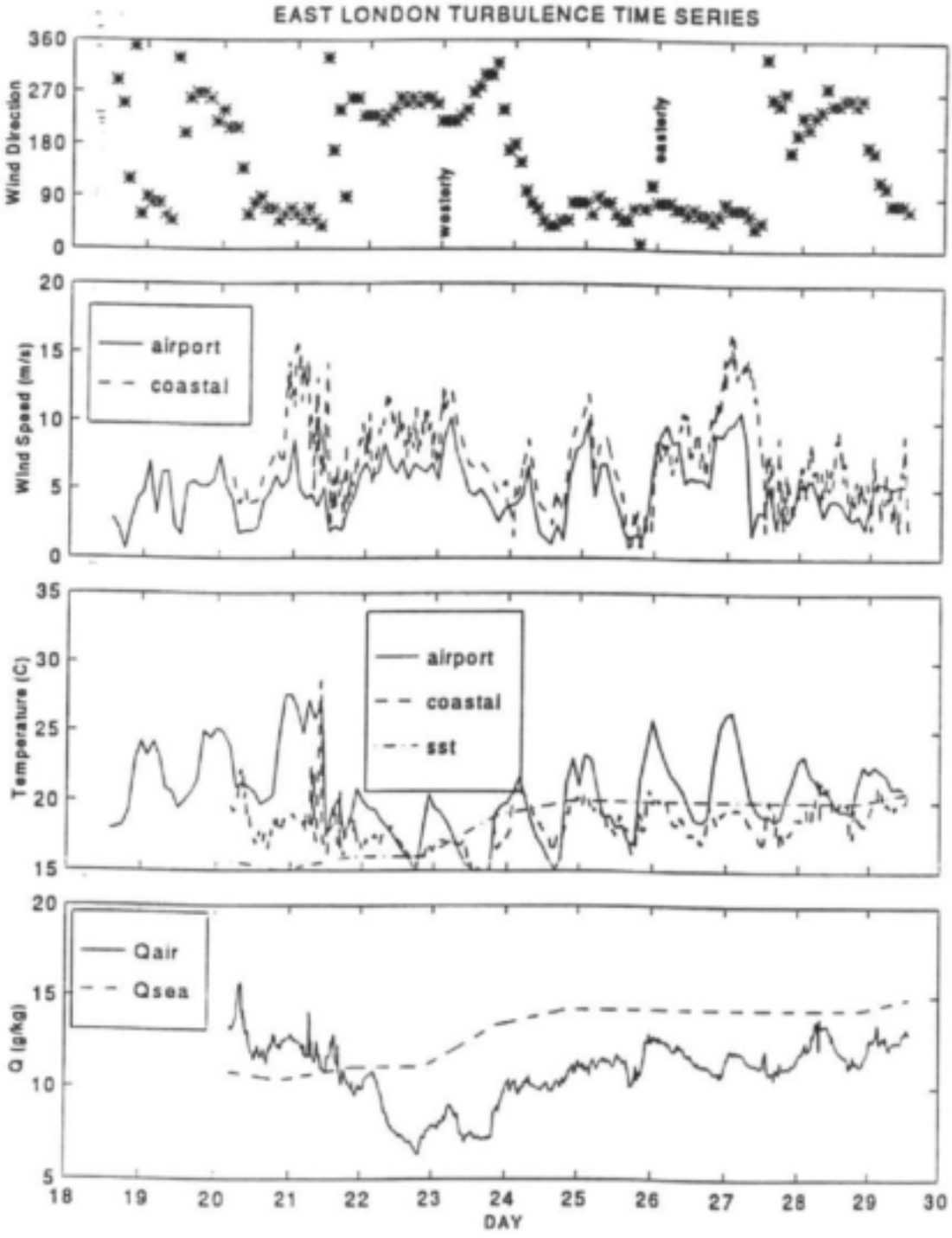

Figure 5.4: November 20-29 continuous time series from the coastal weather station with selected airport data (dashed) for comparison. Parameters are listed on y-axis of each panel. Westerly and easterly cases are identified at top. In bottom panel the saturated specific humidity based on SST is shown by the dashed line.

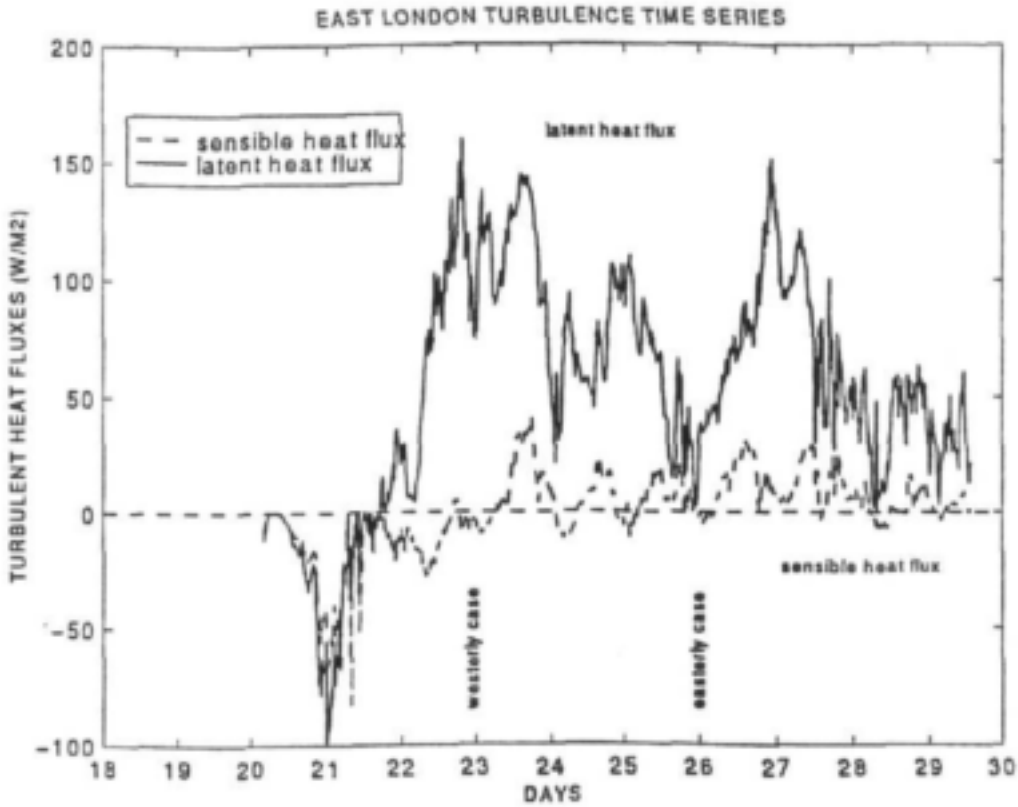

Figure 5.5: November 20-29 time series of latent and sensible (dashed) heat fluxes with cases identified. Units are Wm^{-2}.

5.3.4 Aircraft height-distance sections

Aircraft sections for case study days 23 and 26 November are analysed for departures of the temperature/dewpoint profile from the layer-averaged mean in Figures 5.7 and 5.8. Temperature departures were negative throughout on the 23rd, indicative of advection of cool air over southeastern Africa.

Negative departures reached a peak between 2 and 3 km of -9°C. In the surface layer over the Karoo temperature departures were -5°C. Negative temperature departures over shelf waters reflect diminished sensible heating. Dewpoint departures for 23 November were strongly negative (< -10°C) throughout the lower and upper boundary layer, consistent with sinking motions and the eastward advection of the dry air from the cool South Atlantic. Temperature departures for 26 November (Figure 5.8) were generally positive except over the sea. The warm inland plateau heats the lower 500 m layer by 6-8°C, resulting in departures > +4°C. Over the coastal mountains at 27.5°E warm air mixes through a deeper layer and positive temperature departures extend to the 2 km level. The dewpoint departure field reveals a 300-400 m deep tongue of moisture (> +6°C) extending from the sea to the coastal escarpment near the 1 km level. Positive dewpoint departures were maintained up to the 2 km level and capped by a sharp vertical gradient. Over the inland Karoo, surface dewpoint departures were small (+1 to +4°C) and underlie a moist tongue of +5°C in the 1.5-1.8 km layer around 26.5°E. The interaction of convective heating and the marine wedge of moisture is critical to the turbulent flux field.

Covariance fluxes estimates for heat and moisture are shown in Figure 5.9. In the westerly case, spatial gradients were alleviated by strong dry winds, so these are omitted. In the easterly case high values of $\overline{w'T'}$ were found over the Karoo in a layer from the surface to 2 km. A plume of heat emanated over the coastal mountains near 27 E. A third source of heat was identified over the Agulhas Current. Estimated heat fluxes diminished above the convective boundary layer, > 2.5 km over land and > 1.7 km over the sea. The landward tilt of the 1 and 3 K m/s isolines over the

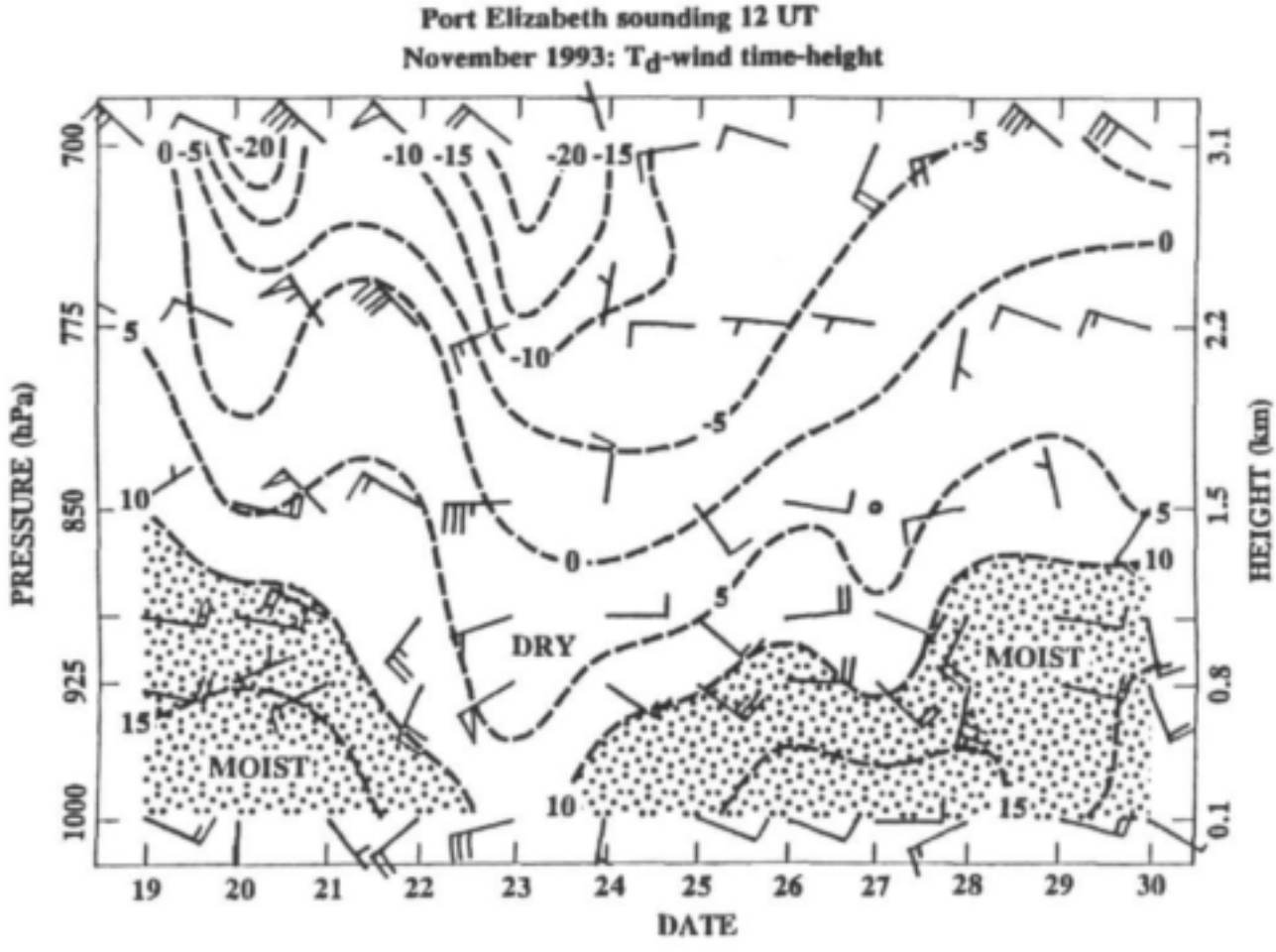

Figure 5.6: Radiosonde height-time series for Port Elizabeth. Dewpoint is contoured and wind barbs are shown in conventional fashion for the period 19-30 November 1993 from the surface to 700 hPa Level. Horizontal wind reference is north up in compass-sense. Moist layer with Td > 10°C is shaded.

coast and escarpment was about 1/60 (Figure 5.9), consistent with a thermal seabreeze.

The covariance flux estimate for moisture exhibits a plume over the escarpment from 26.5-27.5°E in the 1.4-1.9 km layer. The plume extends seaward to lower atmospheric levels with a 1/40 slope over the coast. To the west of the coastal mountains the layer of high moisture flux remained horizontal. Moisture fluxes were low over the desert surface as expected, and in the upper boundary layer. Moisture fluxes were minimal over cool inshore waters, where the coastal weather station was situated. A significant feature of the flux fields is the moist warm plume over the coastal mountains. This pattern was found on another east wind case of 29 November (not shown).

5.3.5 Conclusion

Covariance estimates of heat and moisture fluxes in the atmospheric boundary layer over southeastern Africa have been presented. The study period was characterised by a variety of regional weather and two contrasting cases were illustrated: westerly, cool and dry; and easterly warm and humid. In the former, temperature and dewpoint departures were strongly negative. In the latter, upslope winds injected moisture into the boundary layer preferentially over the coastal mountains. Aircraft covariance fluxes were of order 30 (sensible heat) and 200 (latent heat) Wm^{-2}, as determined from $\overline{w'q'}$ and $\overline{w'T'}$ on the horizontal flight leg nearest the surface, and the usual terms (density, specific heat, vapourisation). Boundary layer fluxes over the coastal mountains in the east wind case exceeded those in the surface layer, due to coalescence of warm moist eddies

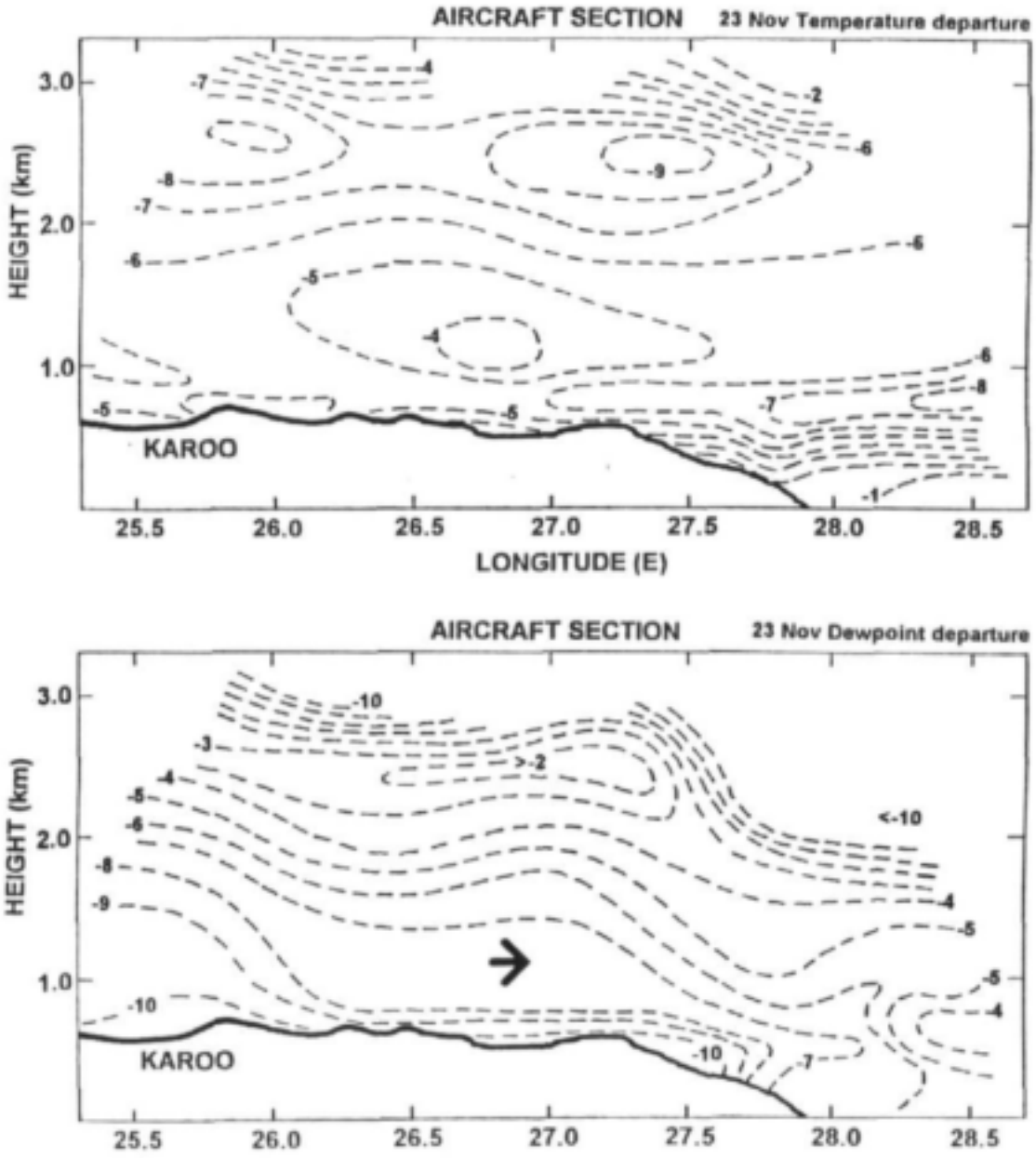

Figure 5.7: Departures of aircraft-derived temperature (top) and dewpoint field from period mean profiles (°C) for westerley case of 23 November 1993. Arrow indicates zonal wind direction. Contour interval is 1°C.

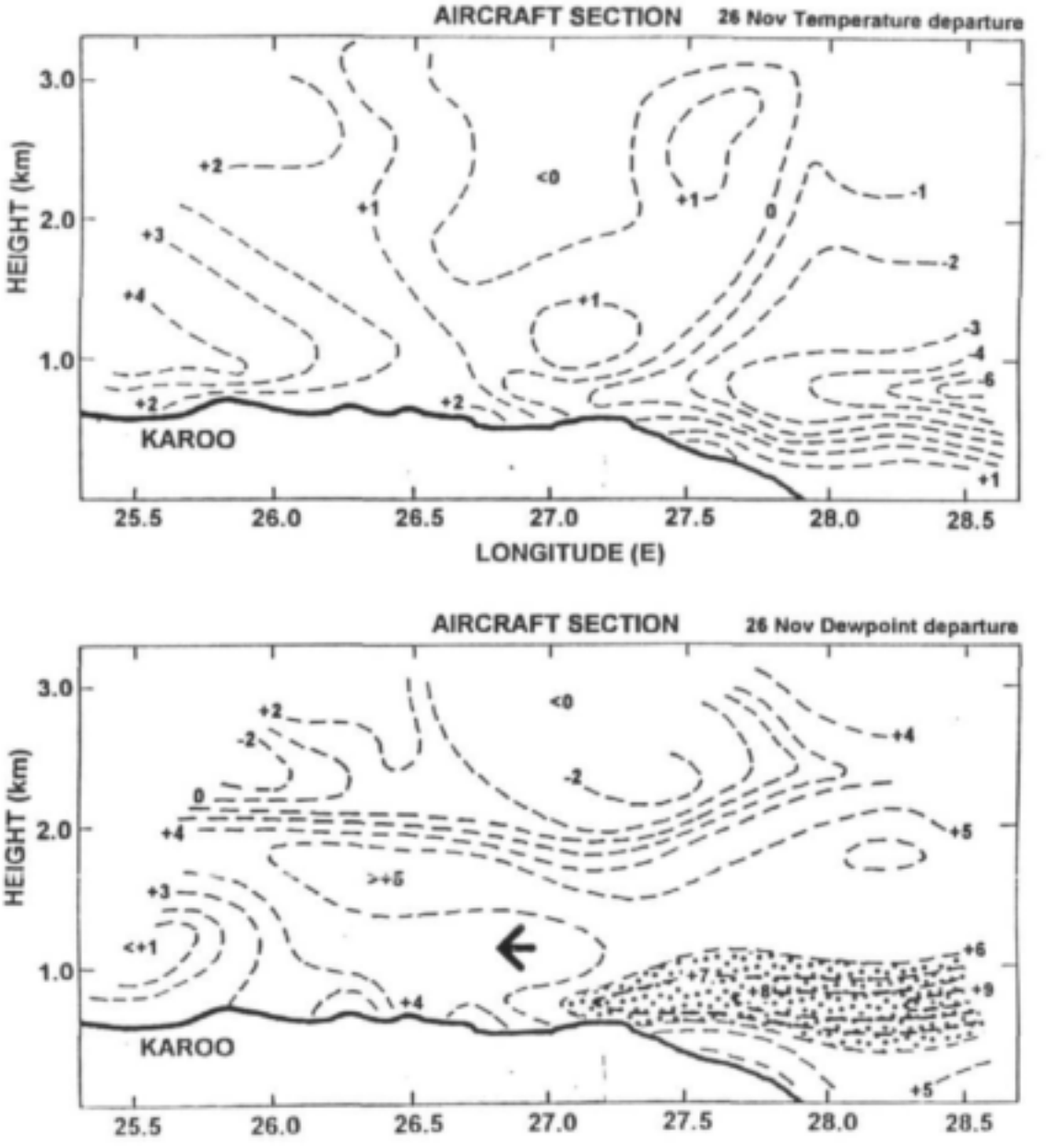

Figure 5.8: Departures of temperature and dewpoint for the easterly case of 26 November 1993 as in Figure 5.7. Shaded region is Td departure > +6°C.

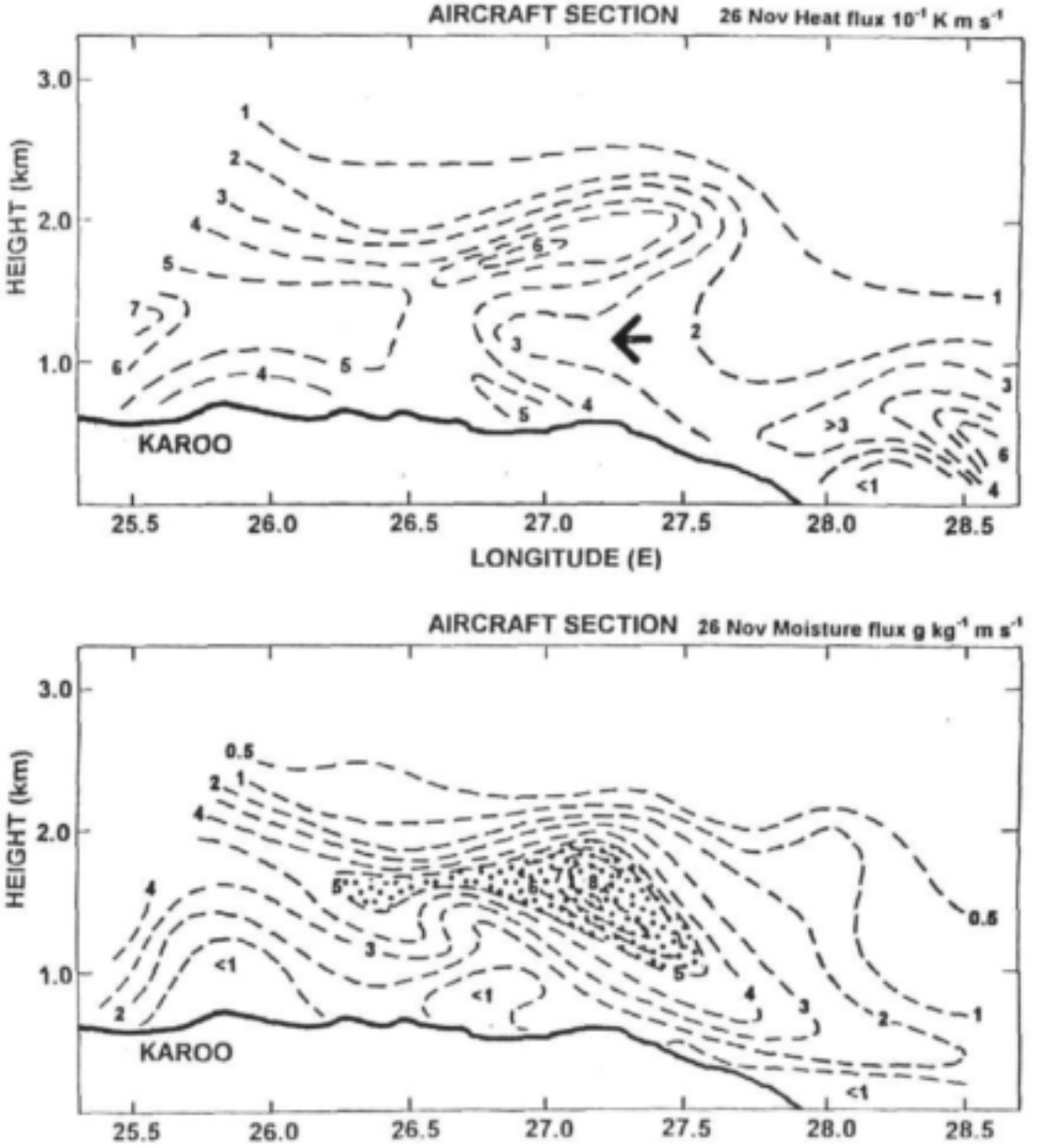

Figure 5.9: Aircraft section of covariances for heat (top. $\overline{w'T'}$) and moisture fluxes ($\overline{w'q'}$) for the easterly case of 26 November. Units and zonal wind direction are indicated. Shaded region indicates moisture fluxes > 5 g/kg m/s.

associated secondary circulations.

Surface flux estimates from 100 m aircraft data during the east wind case are shown in Figure 5.10. Moisture fluxes over the Agulhas Current and coastal mountains are double those over the inland desert and cold shelf water zone. Surface heat fluxes are generally 3 to 5 fold less than coincident moisture fluxes. The heat flux trends upward with inland distance as expected (Stull 1988), to become equivalent to the moisture flux over the Karoo desert. Flux values from the coastal weather station are about 50 % lower than aircraft (Figure5.5), owing to differences in sampling height and suppression of vertical eddies by the surrounding cooler sea surface.

Considering the turbulent perturbation parameters individually, it was found that vertical gusts (w') are lowest over the cold shelf waters. Large moisture perturbations (q') are confined to a shallow sub-cloud layer which is advected from the sea during easterly winds. The thin marine layer interacts with surface continental heating (T') to form convective plumes over the coastal mountainous escarpment. This buoyant air feeds developing cloud systems via mixing thermals. The moisture is available through a deeper atmospheric layer when ridging anticyclones support uplift at the top of the boundary layer. The inland penetration of moisture determines whether subsequent convective rains are limited to the coast or become widespread over the interior plateau.

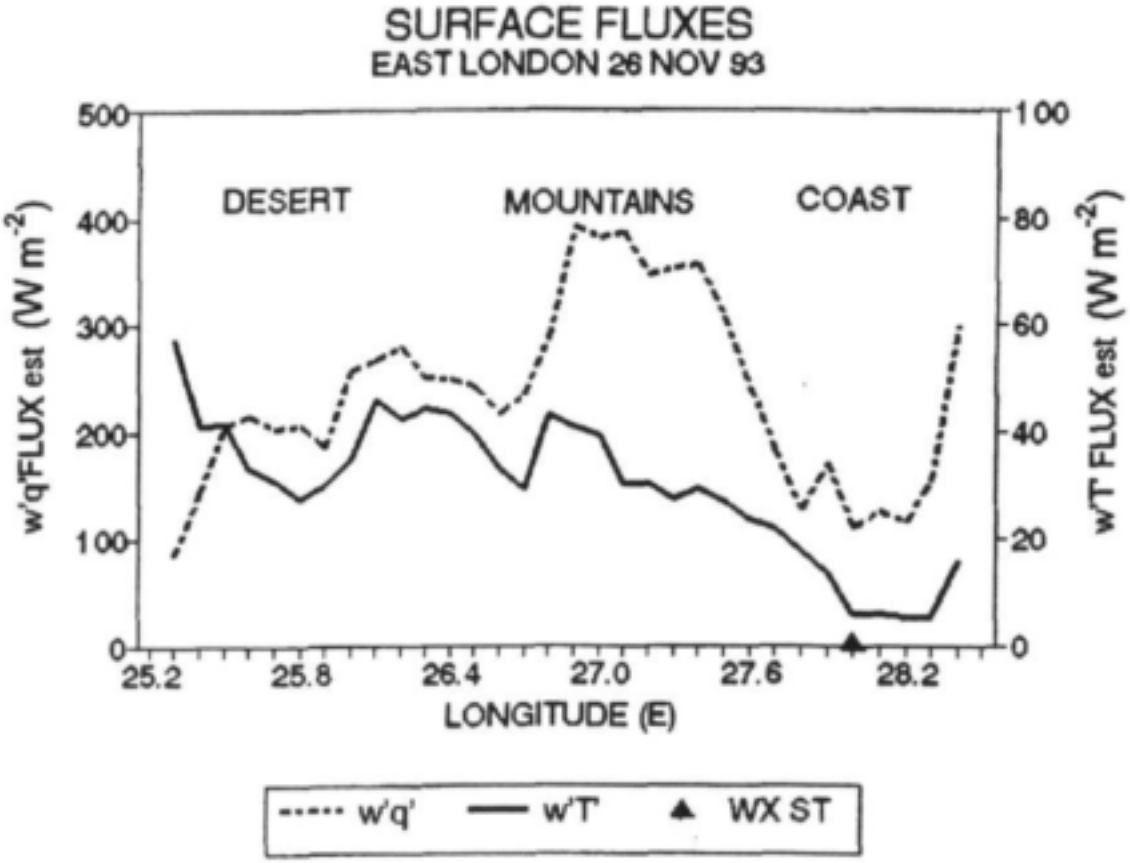

Figure 5.10: Surface flux measurements from lowest aircraft level (100 m above ground) along east-west leg on 26 November. $\overline{w'q'}$ and $\overline{w'T'}$ plots are constructed from 10 km bins. A three point running mean is applied.

Chapter 6

Fine-Time resolution measurements of atmospheric boundary layer properties between Cape Town and Marion Island.

6.1 Introduction

Calculation of the turbulent fluxes of momentum, latent and sensible heat requires the simultaneous measurement of wind speed, sea surface temperature, air temperature and air humidity. Except for humidity those parameters were already measured by a data acquisition and distribution system (DDS) and stored for further calculations. aboard the three research vessels, S.A. Agulhas, Africana and Algoa. The purpose of the project was to add a relative humidity probe to the existing on board system composed of a propeller anemometer, an air temperature probe and a thermosalinograph for sea surface temperature, to provide a low cost automatic, shipboard air-sea interaction measurement system.

The humidity probe was installed and underwent trials on the S.A. Agulhas during the Marion Island Relief winter cruise in 1994. For six weeks, in spite of the harsh conditions of the Roaring Forties, we had a good agreement between the relative humidity measured with our Vaisala probe and the relative humidity calculated from a wet bulb temperature sensor inside a traditional Stevenson screen. From these measurements the calculation of the turbulent fluxes of momentum, latent and sensible heat are used to describe the structure of the first hundred meters of the marine atmospheric boundary layer. During this cruise, radiosondes were launched by the South African Weather Bureau. Data from the radiosonde soundings complement the air-sea interaction measurement system and are used to understand the remainder of the marine atmospheric boundary layer. Because of the scarcity of ship time for air-sea interaction cruises the data coming from the Marion Island cruises are very valuable.

6.2 Results

6.2.1 Meteorological setting.

Results from the Marion Island Relief Cruise during late autumn (2 - 22 May) aboard the SA Agulhas are considered. A schematic of the ship track and the geographical disposition of the Agulhas Current as determined from a satellite SST composite can be found in Figure 6.1. Since very few cloud-free days occurred the composite has been constructed from a number of SST images spanning the entire duration of the cruise. The thermal envelope depicted here is thus only

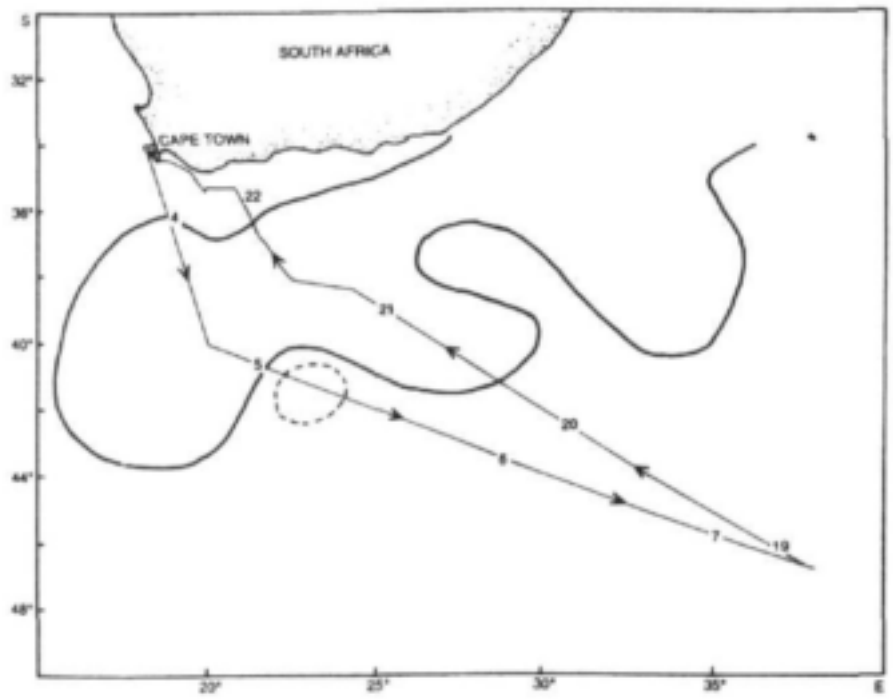

Figure 6.1: Schematic of the ship track and the geographical disposition of the Agulhas Current as determined from the satellite SST composite. Numbers indicate the ship's position on the eve of the cruise dates during May 1994.

approximate. The ship began steaming on 3 May reaching Marion Island by 7 May. For most of this period (3 - 5 May), an easterly flow persisted which owed its existence to a slow-moving transient anticyclone. The wind was blowing from the Agulhas Current region and had likely been previously modified. An approaching cold front on the evening of 5 May was realised by the following day. Zonal westerly flow characterised the period 6 - 8 May. The return leg began on 18 May. An assortment of pre-frontal and post-frontal conditions were then superimposed on mostly zonal westerly flow. On 21 May strong synoptic forcing on the leading edge of a ridging anticyclone behind a cold front gave rise to a "cold air outbreak". Quasi-meridional flow saw a cold, dry sub-polar air mass being advected northwards over the Agulhas Retroflection Region (ARR) during this period.

6.2.2 Intercomparison of results

Here we compare the values obtained from our automatic system with those of the manned SAWB operation. We will compare the parameters of air temperature, relative humidity and wind speed. It should be noted that the SAWB relative humidity is an indirect comparison and is dependent on the accuracy of the SAWB air temperature. Since there is a mismatch of time scales (ie. 1 minute vs 3 hours) we average the automatic (DDS) data for a ten minute period. Ten minutes averaging periods are chosen to coincide with those times corresponding to SAWB observations (ie. once every 3 hours). The resultant data set is small (n=57) and statistically limited. The results are shown in Figure 6.2 (data plotted as circles).

Air temperature, relative humidity and wind speed differences are mostly within 1°C, 10% and 5ms $^{-1}$. Investigating the differences as possible calibration drifts yielded no clear results. Wind speed values for the SAWB and DDS are derived from the same instrument (Koshin-Vane) and yet discrepancies of nearly 5ms $^{-1}$ are apparent. This is not a problem of averaging as a comparison of instantaneous values for all parameters (not

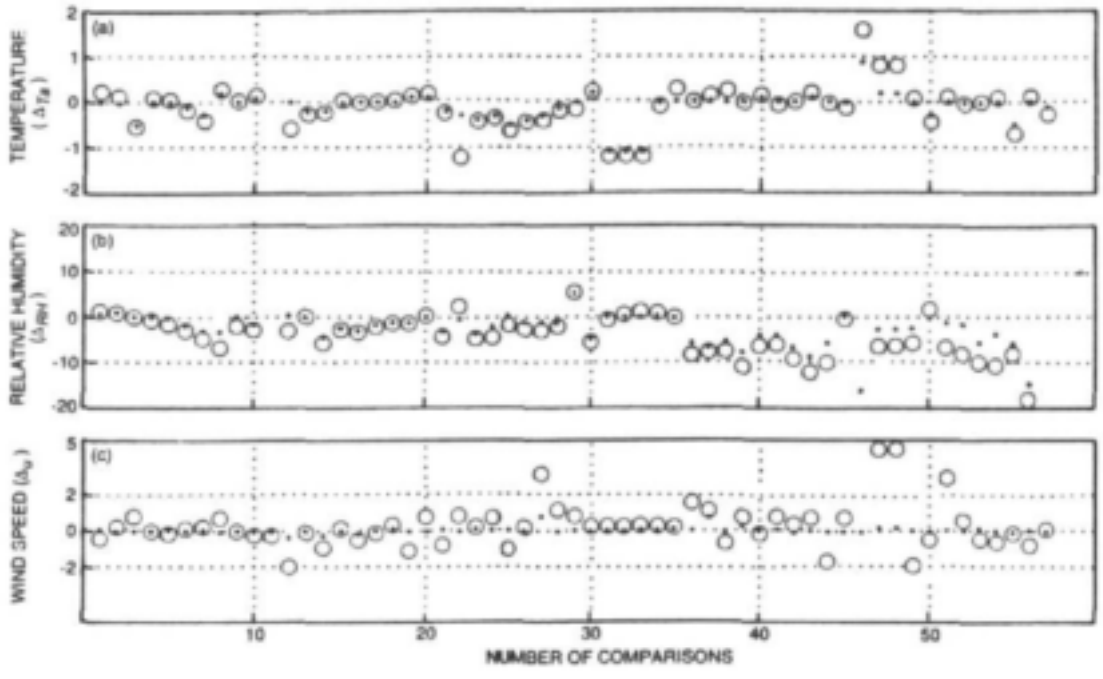

Figure 6.2: Differences between the one minute average DDS data and the instantaneous, three hourly Weather Bureau measurements of a) air temperature, b) relative humidity and c) wind speed, for the advance and return leg. Circles and dots denote the actual and minimum possible differences respectively

shown) yields the same results. The problem is one of sampling. SAWB values are instantaneous values read by the operator. Although they are intended to be representative of mean conditions it is clear that they are not. In order to demonstrate this, we also show the minimum possible difference by comparing SAWB values to automatic values using a twenty minute window on either side of the SAWB reading (shown as dots in Figure 6.2). Differences in T and RH reduce to 0.5°C and 5% respectively. Wind speed differences reduces to a negligible amount. The large errors in the instantaneous SAWB values have implications for previous studies that have utilised these data.

6.2.3 Fluxes of momentum, sensible and latent heat

Three cases have been selected for further study. The cases have been chosen to highlight the varying nature of air-sea transfer processes over the Agulhas Current and the usefulness of high-resolution data. We first present the surface measurements for the two legs. The fluxes and forcing parameters of inter est for the advance and return legs are shown in Figure 6.3 and Figure 6.4. respectively. Both time series refer to the area between the northern border of the Agulhas Current and the Subtropical Convergence (STC).

6.2.3.1 Advance leg

The advance leg (Figure 6.3) occurred during a period of weak anticyclonic synoptic forcing during which light easterly winds prevailed. The time series begins on the northern border of the ARR and ends o n the morning of 5 May. There is reason to believe that the ship's water intake was switched before the end of the time series making sea surface temperature measurements unreliable beyond this point. Since synoptic conditions began to change at midday on 5 May this portion was excluded from the easterly case analysis. Surface fluxes demonstrate fairly high short-term variability. Air-

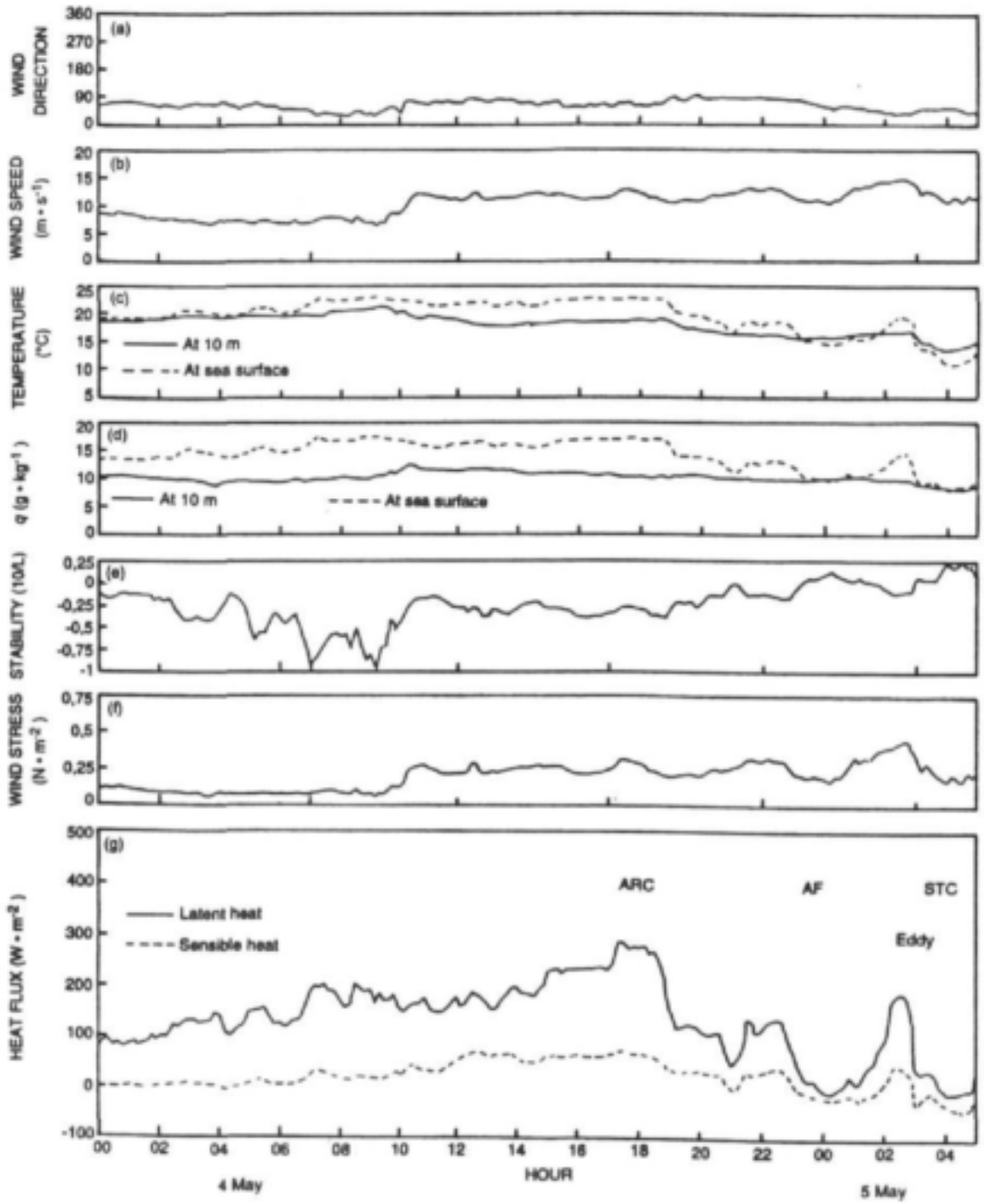

Figure 6.3: Time series of fluxes and parameters of interest for the advance leg. The parameters (from top to bottom) are: a) wind direction (—); b) wind speed (—) at 10 m; c) air temperature at 10 m (—) and sea surface skin temperature (- -); d) specific humidity at 10 m (—) and specific humidity at the sea surface (- -); e) stability parameter, $\zeta = 10/L$ (—); f) wind stress (—); g) Latent heat flux (___) and sensible heat flux (- -). The positions of the Agulhas Return current (ARC). Agulhas Front (AF). Warm-cored eddy (Eddy) and Sub Tropical Convergence (STC) are shown.

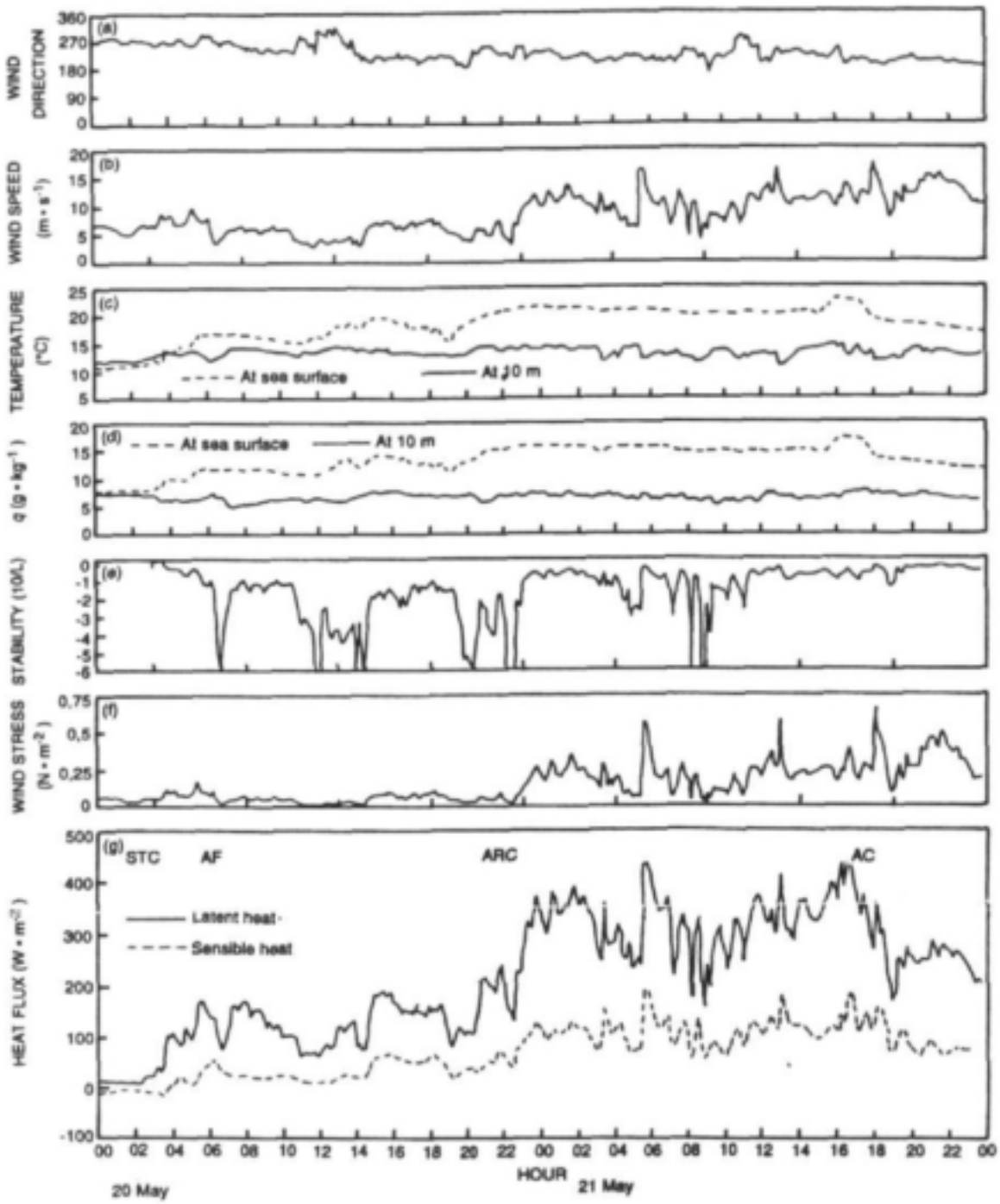

Figure 6.4: Time series of fluxes and parameters of interest for the return leg. a) wind direction (—); b) wind speed (—) at 10 m; c) air temperature at 10 m (—) and sea surface skin temperature (- -); d) specific humidity at 10 m (—) and specific humidity at the sea surface (- -); e) stability parameter, $\zeta = 10/L$ (—); f) wind stress (—); g) Latent heat flux (___) and sensible heat flux (- -). The positions of the Agulhas Return Current (ARC). Agulhas Front (AF), and Sub Tropical Convergence (STC) are shown.

Table 6.1: Fluxes and surface paramaters statistics.

Synoptic type	$\overline{Q_H}$	$\overline{Q_E}$	$\overline{Q_T}$	$max(Q_T)$	$\overline{\tau}$	$10/L$	σ_{Q_T}	σ_U
	Wm^{-2}	Wm^{-2}	Wm^{-2}	Wm^{-2}	$N.m^{-2}$		Wm^{-2}	ms^{-1}
Anticyclonic	28	158	186	359	0.19	-0.37	23	1.3
Frontal	41	145	186	500	0.19	-2.55	66	1.8
Cold-air outbreak	109	307	416	628	0.19	-0.95	82	2.4

sea gradients of T, q and u are initially small. Surface heat fluxes increase towards the core of the current and decrease rapidly toward the STC. The latent heat flux is almost exclusively responsible for the total heat flux (Table 6.1) and doubles over the Agulhas Return Current as maximum air-sea gradients of T and q are realised. It is likely that this air has only recently been modified by Agulhas Return Current waters (Figure 6.3).

The transition from the Agulhas Return Current to the STC is defined by a step-like SST pattern. The step-like fashion of this frontal region indicates that the Agulhas Return Current and the STC are some distance apart and hence will be referred to as the Agulhas Front (AF). A commensurate decrease in surface fluxes is realised. The increase in wind speed at t=11 hours on 4 May is related to a strengthening of the surface pressure gradients which reached a maximum on 5 May (not shown).

An interesting feature is the mesoscale feature described by a sharp jump in SST on the eve of 5 May. The SST at the core is 20 °C. Assuming that the ship covered the longest possible length then its maximum diameter is estimated at 43 km. This is a conservative estimate at best. Most likely this is an Agulhas Current Retroflection eddy. Eddies in this region have diameters of approximately 200 km (Lutjeharms and Valentine, 1988). Surface fluxes respond dramatically and winds increase by some 5 ms^{-1} and tail off on the periphery of the eddy. The mesoscale response of the wind is aptly demonstrated. Thereafter the SST declines steadily. Surface fluxes beyond the STC do little to destabilise the boundary layer and free convection is minimised.

6.2.3.2 Return leg

The return leg from Marion Island began on 18 May. The time series begins at the STC on 20 May and ends on the northern border of the Agulhas Current in the vicinity of the Agulhas Bank. During 20 May the ship crossed the STC, a more intense AF, and entered into the central ARR. An approaching cold front provided zonal and quasi-zonal westerly flow. On 21 May strong synoptic forcing on the leading edge of a ridging anticyclone behind a cold front gave rise to a "cold air outbreak". Quasi-meridional flow saw a cold, dry sub-polar airmass being advected northwards over the ARR during this period.

We begin the time series (Figure 6.4) in the region of the STC. The transition to the warm Agulhas Return Current is again defined by a number of step-like SST superimposed on a more intense AF. The wind was from the west and was almost parallel to the AF. Short term variability of the fluxes is again apparent. Over the main SST front, surface heat fluxes are seen to increase dramatically from a negligible amount to over 200 Wm^{-2}. Discontinuous jumps in the surface heat flux correspond to minor SST fronts and are superimposed on the overall increase in fluxes. The latter is attributed to the warmer SST and changing airmass characteristics. That the air-mass became more sub-polar is seen in the gentle decrease of T. On the eve of 21 May the ARR experienced an atypical "cold air outbreak" during strong southerly flow. Cold-air outbreaks are normally associated with zonal flow of continental air during the post-frontal stage (Mey et al.,1990 ; Bane, 1989). The short term variability of the fluxes is seen to increase dramatically as large air-sea temperature and humidity differences create a highly thermally unstable environment. It is

during this period that maximum turbulent heat fluxes of 628 Wm^{-2} were attained.

6.2.4 Air-sea transfer processes in the Agulhas Retroflection Region

In this section we demonstrate the usefulness of the high-resolution data in determinining the nature of air-sea transfer processes. Due to the rapid eastward tracking of synoptic sytems in the southern hemisphere the problem of non-stationarity arises. If a specific feature or interaction is to be investigated then this problem may be partially overcome by considering "stationary" synoptic conditions or small time intervals. In these cases a time series will be considered to constitute a series in space. Caution must be exercised when interpreting single radiosonde soundings as coherent structures (eg. plumes, thermals or rolls) may give a distorted view of the mean boundary layer depth (Stull, 1988). We will consider the response of the boundary layer under three synoptic types. The three synoptic situations to be considered are anticyclonic (easterly flow), frontal (westerly flow), and a cold-air outbreak (in this case, during post-frontal southerly flow).

6.2.4.1 Anticyclonic conditions.

6.2.4.1.1 Fluxes of momentum, sensible and latent heat During the advance leg the Agulhas Retroflection Region experienced light easterly winds under fairly strong anticyclonic forcing. Low surface heat fluxes were recorded (Table 6.1). Surface stability as given by the stability parameter at a standard height of 10 m, $\zeta = 10/L$, is dominated by the friction velocity u_* and is hence always near-neutral ($\overline{\zeta} = -0.37$). This does not imply the absence of buoyancy-driven mixing in the surface layer, simply that wind-driven mixing is a more important turbulent production term. Another measure of the nature of the turbulent heating of the boundary layer is the standard deviation of the total heat flux σ_{Q_T}, where $Q_T = Q_E + Q_H$. This is derived by first detrending the time series in order to eliminate the warming (cooling) effect of the Agulhas Current (STC). A value of $\sigma_{Q_T} = 23$ Wm^{-2} is obtained.

6.2.4.1.2 Profiles of temperature, humidity and wind. The two radiosonde soundings over the ARR are seen in Figure 6.5. We use θ_v, the virtual potential temperature, to describe the buoyancy structure and height of the boundary layer,z_i. θ_v includes the effect of humidity on the relative buoyancy of air parcels and is the preferred descriptor of the stability of the boundary layer (Stull, 1988). It is apparent from the profile of θ_v (Figure 6.5) that the entire boundary layer is slightly stable. With the exception of the first sounding, a coherent well-mixed layer is not evident. The constant flux layer, where superadiabatic lapse rates of U, T and q are expected to occur, is not always evident. The inversion layer is well defined and demonstrates the strong synoptic influence of the anticyclone. The mixed layer height, z_i of the Agulhas Current sounding (Agulhas Front sounding) is seen to end at 700 m (650 m). The profile of the mean wind, U describes a typical trade-wind profile. The positive wind shear and Ekman spiral (anticlockwise spiral) are clearly seen. Typically a wind speed maximum is attained at approximately 800 m. Since the boundary layer is mostly buoyantly stable, the small surface heat loss (Table 6.1) is insufficient to generate free convection. In the absence of this mixing mechanism and in the presence of a positive wind shear, it is likely that shear production of turbulence is responsible for most scales of mixing. From Table 6.2, we see that the boundary layer is warmest and most humid over the Agulhas Current. The warming (cooling) effect of the Agulhas Current (AF) is quite clear.

6.2.4.2 Frontal conditions

6.2.4.2.1 Fluxes of momentum, sensible and latent heat During the return leg the ship traversed the Agulhas Front, and entered over the Agulhas Return Current. Pre-frontal conditions were experienced during this period as the ship passed through the warm sector of the advancing front. Evidence for unstable conditions ($\overline{\zeta} = -2.55$) under this synoptic type are also provided

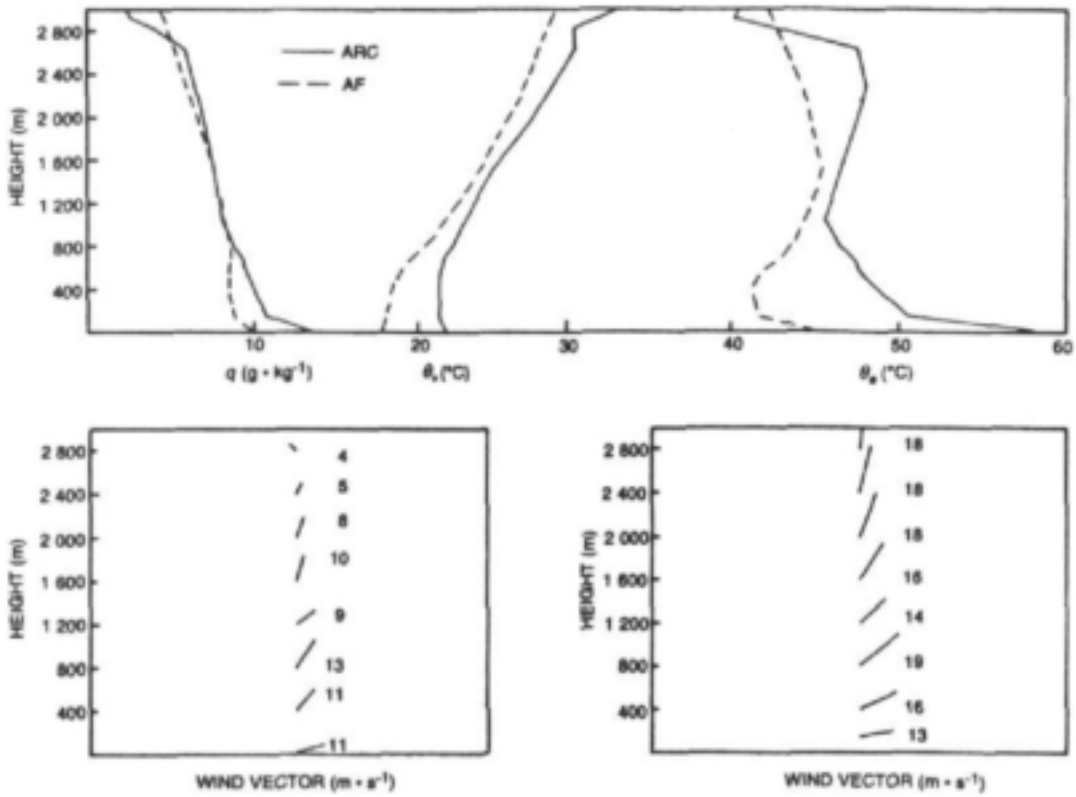

Figure 6.5: Radiosonde soundings over the Agulhas Retroflection Region during the advance (southbound) leg during anticyclonic flow: May 4 at 10:26 GMT (-) over the Agulhas return current and 23:46 GMT (- -) over the Agulhas Front. The set of plots (top) from left to right are the specific humidity. Virtual potential temperature and equavalent potential temperature. Wind vector plots (bottom) are May 4 at 10:26 GMT (left) and 23:46 GMT (right) with wind speeds given in ms^{-1}. Winds are drawn from the direction in which they come. The surface easterlies spiral anticlockwise to become northerly winds.

by the standard deviation of the detrended total heat flux time series (Table 6.1. Despite exhibiting greater variability, mean turbulent heat fluxes are very close to those for anticyclonic conditions.

6.2.4.2.2 Profiles of temperature, humidity and wind. The most interesting result for this case is found in Figure 6.6. Two radiosondes were released in the Agulhas Return Current area which show the mixed layer height, z_i to be approximately 800 m during this synoptic type. It is apparent that the stable boundary layer (SBL) over the Agulhas Front (first sounding) approaches a well-mixed convective boundary layer (second sounding). The cooling in the second sounding coincided with the arrival of the cold front. The boundary layer is both cooler and less humid (Table 6.2) than during the anticyclonic case which saw equivalent turbulent heat fluxes. Simple thermodynamic considerations dictate that the "atmospheric thickness" of the boundary layer for the anticyclonic case should be far greater. Subsidence, therefore is seen to determine the evolution of the boundary layer for the anticyclonic case. It is tempting to speculate that it may even affect the nature of atmospheric turbulence as seen from a comparison of σ_{Q_T}.

Table 6.2: Radiosonde statistics.

	Anticyclone		*Frontal*		*Cold-air outbreak*	
Time	10:46 4/05	23:46 4/05	06:45 20/05	10:59 20/05	10:49 21/05	23:40 21/05
$\overline{z_i}$ (m)	700	700	750 (SBL)	800	500 (TIBL)	900
$\overline{\theta_e}$ (°C)	49.8	42.2	29.0	28.0	24.4	24.7
$\overline{q}$ $(g.kg^{-1})$	10.4	8.8	4.9	4.9	4.1	4.3

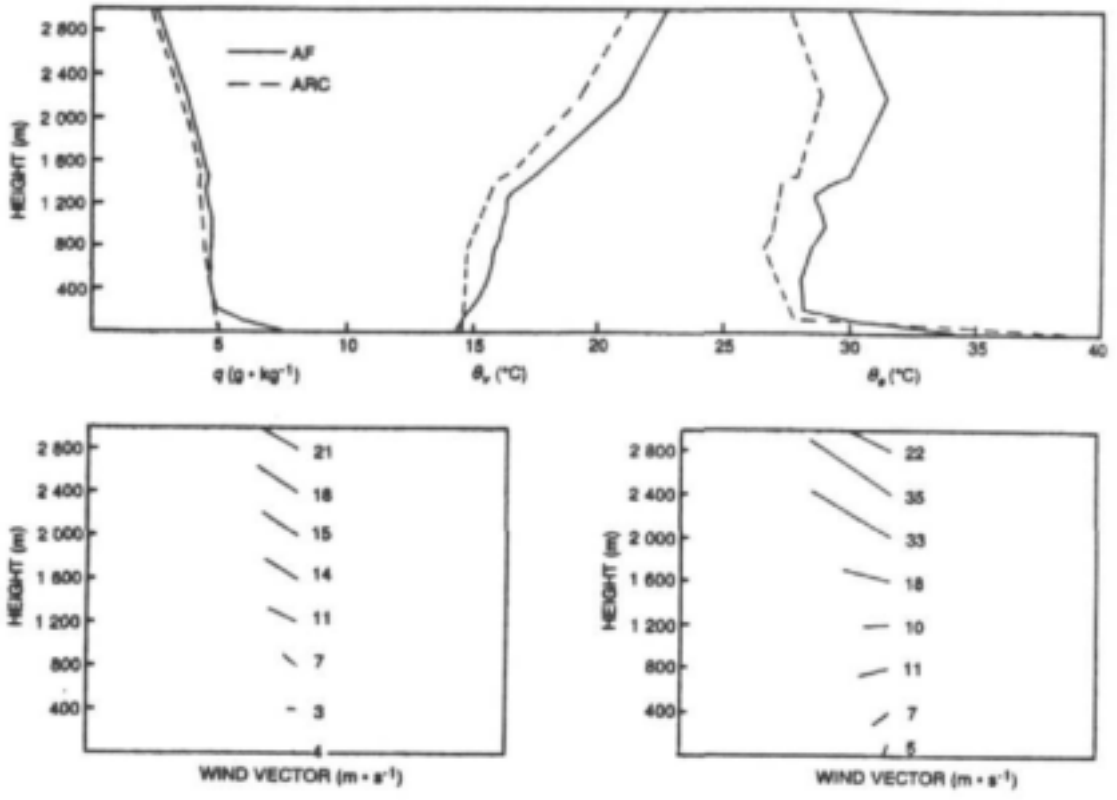

Figure 6.6: Same as Figure 6.5 but for the return (northbound) leg during frontal conditions May 20 at 06:45 GMT (-) over the AF and 10:59 GMT(- -) over the ARC. Wind vector plots are from left to right, 06:45 GMT and 10:59 GMT.

6.2.4.3 Cold-air outbreak

6.2.4.3.1 Fluxes of momentum, sensible and latent heat On 21 May strong synoptic forcing saw a ridging anticyclone sweep in cold post-frontal conditions over the ARR. Turbulent air-sea transfer processes are seen to be very different from the previous two cases. The surface layer is highly unstable, $\overline{\zeta} = -0.95$. Here we see that the generation of turbulent kinetic energy is dominated by buoyancy production (free convection). Fluxes of sensible and latent heat increase steadily in response to an increasingly warm sea surface. As the flow becomes more southerly, the airmass characteristics become sub-polar (and a concurrent decrease in T_a and q_a is realised). Evidence of highly unstable conditions are also provided by the horizontal gustiness of the wind and the large standard deviation of the detrended total heat flux time series ($\sigma_{Q_T} = 80.6$ Wm^{-2}) (Table 6.1). The wind gustiness is evidence of large perturbations in the vertical wind component w' and indicates that turbulent motion has a large vertical component (ie. free convection is taking place). Indeed, short-term variability of the wind and wind-stress is highly correlated with the latent and net heat flux. Under such conditions the properties of U, T_a and q will be freely mixed

within the boundary layer.

6.2.4.3.2 Profiles of temperature, humidity and wind. The response of the boundary layer to vigorous free convection is readily apparent (Figure 6.7). The boundary layer height grows

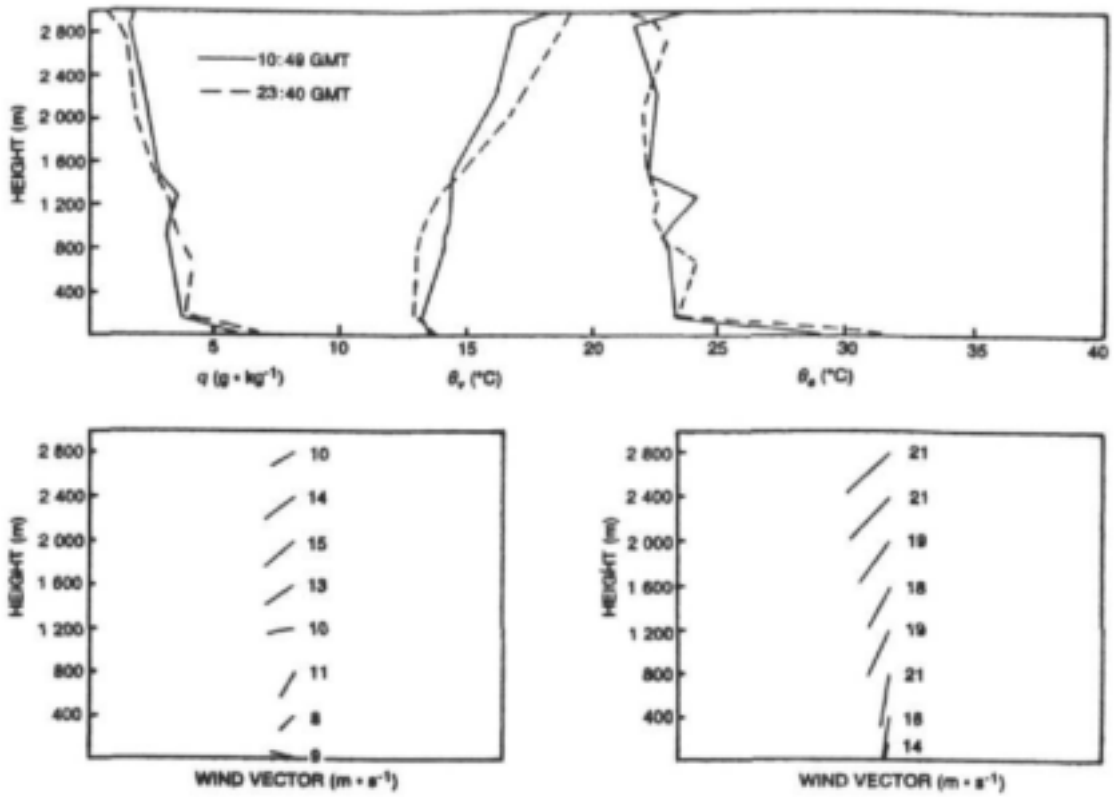

Figure 6.7: Same as Figure 6.5 but for the return (northbound) leg during a brief atypical cold-air outbreak. May 21 at 10:49 GMT (-) and 23:40 GMT (- -). Wind vector plots are from left to right, 10:49 GMT (-) and 23:40 GMT (- -).

from a convective thermal internal boundary layer (Stull, 1988) of 500 m to a well-mixed layer of 900 m (limit of convective thermals of 1250 m). We see that in more than any other case, the boundary layer contains and is defined by a well-mixed mixed layer. The parameters of θ_v, q and U are well-mixed. This supports our argument that mixing is dominated by free vertical convection. These results reveal the nature of vertical transfer processes within the boundary layer. Under strong free convection it is likely that entrainment of drier, free atmosphere air occurs as thermals "overshoot" the entrainment zone (Stull, 1988; Khalsa and Greenhut, 1989). Such energetic updrafts may also be compensated for by downdrafts of unmodified free atmosphere air originating above the inversion (Deardorff et al., 1969). Free-atmosphere air and undiluted boundary layer air undergo mixing in this entrainment zone and contribute to a poorly defined boundary layer-free atmosphere transition. The modified boundary layer air/entrained air may then be mixed toward the surface within downdrafts. This is the case for the second sounding where a thick entrainment zone (900 m - 1250 m) is associated with vigorous convection (Stull, 1988)).

6.3 Conclusion

An automatic system has been used for the first time in South African waters to derive the fluxes and parameters of interest, neccessary for air-sea interaction studies. A relative humidity sensor

was added to the DDS on the S.A. Agulhas. A high resolution data set may be obtained which is a real improvement over previously available datasets. In general results show good agreement between automatically logged and manually logged data. The usefulness of having higher resolution (1 minute) data has been proven. Varying statistics may now be generated which demonstrate the mesoscale variability of surface momentum and heat fluxes and their rapid response to changing environmental conditions. These data together with the manned SAWB radiosonde sounding operation have been used to distinguish the nature of boundary layer processes operating over the ARR. Three cases were investigated which show that air-sea transfer processes vary dramatically when stratified according to synoptic type. The data will be used to investigate frontally-induced secondary circulations over the frontal region south of the ARR. The South African Weather Bureau has susbsequently modified the radiosonde data acquisition system so as to acquire the finest possible vertical resolution by storing the raw data and improving the sonde tracking system. The operation will be repeated every year and the number of launches over the Agulhas Current is to be increased. With a good calibration monitoring program this low cost surface measurement system could be extended to include other suitable research platforms such as the SFRI research vessels, the S.A. Africana and S.A. Algoa. Together with the S.A. Agulhas these vessels average 200 days at sea each year between South Africa, the Antartic and South America, crossing interesting area such as the warm Agulhas and cold Benguela Currents.

Chapter 7

The Agulhas Current Air-Sea Exchange Experiment

7.1 Introduction

The marine atmospheric boundary layer (MABL) is of interest to both oceanographers and meteorologists. Close to the coast the MABL is inhomogenous with complex mesoscale circulations and land-marine interactions in response to large variability in sea surface temperature (SST). In the South African context, a better understanding of the MABL is needed to understand how ocean-atmosphere interactions control South African climate variability. Significant variation in boundary layer structure has been demonstrated in the Agulhas Retroflection Region (Jury and Walker, 1988; Mey *et al.*, 1990) and over the Agulhas Current (Jury and Courtney, 1991; Jury, 1993). Aircraft observations along a NW - SE cross-section of the northern edge of the Agulhas Current near the eastern Agulhas Bank (Jury and Courtney, 1991) have revealed a spatially organised thermodynamic and kinematic boundary layer structure during uniform, light, zonal (westerly) flow (Jury, 1993). It has been shown that under air flow parallel to the current, this may even lead to substantial cumulus cloud development over stretches of hundreds of kilometers along the current (Lutjeharms *et al.*, 1986).

The Agulhas Current Air-Sea Exchange Experiment (ACASEX) was a dedicated meteorological experiment designed to investigate atmospheric inhomogeneity across the Agulhas Current (Rouault *et al.*, 1995). The region south of Port Alfred, an area sufficiently removed from the coast so as to avoid coastal influences, was chosen as the location for the experiment. This coastal region exhibits very intense, but localised, upwelling inshore of the Agulhas Current creating extreme horizontal SST gradients not found elsewhere (Lutjeharms and Cooper, 1995). ACASEX consisted of a special research cruise aboard the R/V Algoa off Port Alfred and Port Elizabeth for the period 21 April to 3 May 1995 (Rouault *et al.*, 1995). 24 transects of the Agulhas Current were carried out in a mostly triangular cruise pattern (Figure 7.1). At least two transects were completed each day. Continuous surface meteorological measurements were undertaken in conjunction with radiosondes which were launched approximately 4 times a day. These ascents were timed to coincide when the vessel was over the shelf, SST front, current core and seaward regions, where possible. Oceanographic measurements using expendable bathythermograph probes (XBTs) and an acoustic doppler current profiler (ADCP) were carried out in support of this program. Standard meteorological measurements made by the South African Weather Bureau at Port Elizabeth and Port Alfred provided a land-based reference to assess the differences between the land and marine airmasses.

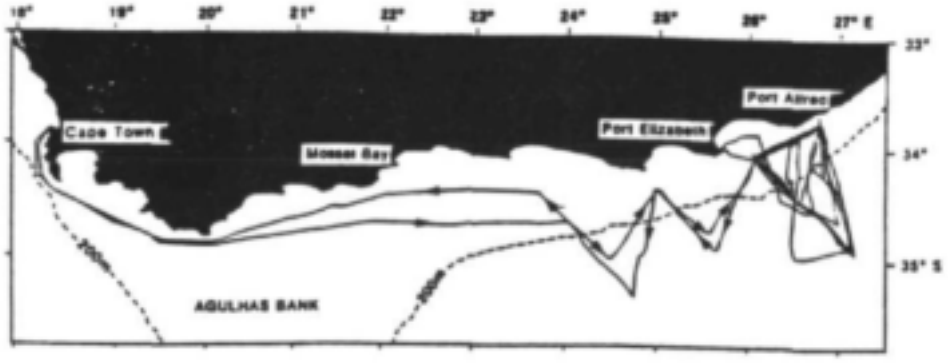

Figure 7.1: ACASEX - Schematic of the ship track (after Rouault *et al.*, 1995). The in shore edge of the Agulhas Current follows approximately the 200 m isobath.

7.2 An atmospheric moisture and thermal front in the boundary layer above the Agulhas Current

In this section we discuss the effects of the strong SST front across the inshore edge of the Agulhas Current on the surface turbulent fluxes and the structure of the marine atmospheric boundary layer during periods when air flow was parallel to the SST front. Shipboard meteorological measurements and radiosonde ascents are presented as case studies.

7.2.1 Background and meteorological setting

We present results for two contrasting wind regimes (westerly and easterly) where the wind is parallel to the axis of the SST front on the inshore edge of the current.

For the **westerly** wind case on April 24 maritime weather conditions were influenced by a weak low pressure passing east of the subcontinent Light, westerly geostrophic winds were indicated. Gentle surface westerly winds of 5-10 ms^{-1} were approximately parallel to the SST front (with a small component from cold to warm). The easterly winds of the previous two days had initiated upwelling in the study region. At the SST front a gradient of 3°C $(10\ km)^{-1}$ was observed. Shelf SSTs of 15°C compared with values found for the core of the current of ≤25°C. A schematic of the ship track may be found in Figure 7.2. The ship moved out of the current toward the shelf. A second transect was then undertaken in the seaward direction. The kink during this transect occurred during a radiosonde launch when the ship drifted out of the current into the shelf area. Upon reaching the seaward border (where SSTs ~20°C) a third transect was undertaken in the shelf direction.

On 29 April a ridging anticyclone brought easterly air flow (approximately parallel to the SST front) which then shifted to northeasterly (parallel to the axis of the SST front) the following day with the anticyclone being situated well east of the subcontinent. Three transects were undertaken on 29 April (Figure 7.4) and 30 April (Figure 7.6). These two days constitute the **easterly** case.

7.2.2 Results

7.2.2.1 Spatial variation of the surface fluxes

7.2.2.1.1 Westerly Case The surface fluxes and forcing parameters for the transects (Figure 7.2) during the **westerly** case are shown in Figure 7.3. An artificial kink at 08:00 GMT during a radiosonde launch is due to the ship drifting out of the current into the cool shelf area. Highest fluxes correspond to the current, lowest to the inshore region. Over the cool shelf z/L is neutral to stable corresponding to downward sensible and negligible latent heat fluxes (Table 7.1). Latent heat fluxes increase dramatically across the shelf edge. Mean values of the latent heat flux are a

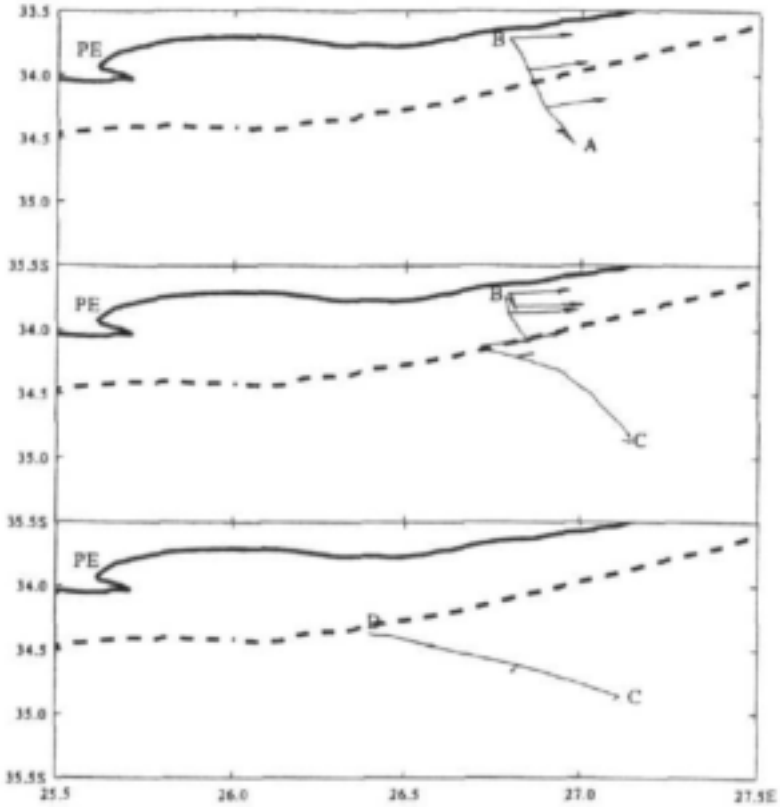

Figure 7.2: ACASEX 24 April - Schematic of the ship track showing transects, mean wind vectors (plotted every two hours), the 200 m isobath (dashed) and PE (Port Elizabeth). Labels denote the end-points of each transect as they appear in Figure 7.3. The first transect is shown in the top panel, second transect in the middle panel and so on.

Table 7.1: Air-sea flux statistics - 24 April. Averages are given for the shelf (SHELF) and Agulhas Current (AC). Q_T is the total heat flux ($Q_T = Q_H + Q_E$). The quantity $dSST/dy$ is the horizontal gradient of sea surface temperature perpendicular to the inshore SST front (i.e between the shelf and current).

	$\overline{\tau}$	$\overline{Q_H}$	$\overline{Q_E}$	$\overline{Q_T}$	$max(Q_T)$	$\overline{\zeta_{10}}$	$dSST/dy$
	$N.m^{-2}$			Wm^{-2}			$°C km^{-1}$
SHELF	0.08	-7	20	13	23	0.07	0.3
AC	0.08	49	184	233	353	-4.5	

Table 7.2: Air-sea flux statistics - 29 April.

	$\overline{\tau}$	$\overline{Q_H}$	$\overline{Q_E}$	$\overline{Q_T}$	$max(Q_T)$	$\overline{\zeta_{10}}$	$dSST/dy$
	$N.m^{-2}$			Wm^{-2}			$°C km^{-1}$
SHELF	0.14	-5	78	73	102	-0.01	0.2
AC	0.10	38	198	236	347	-3.0	

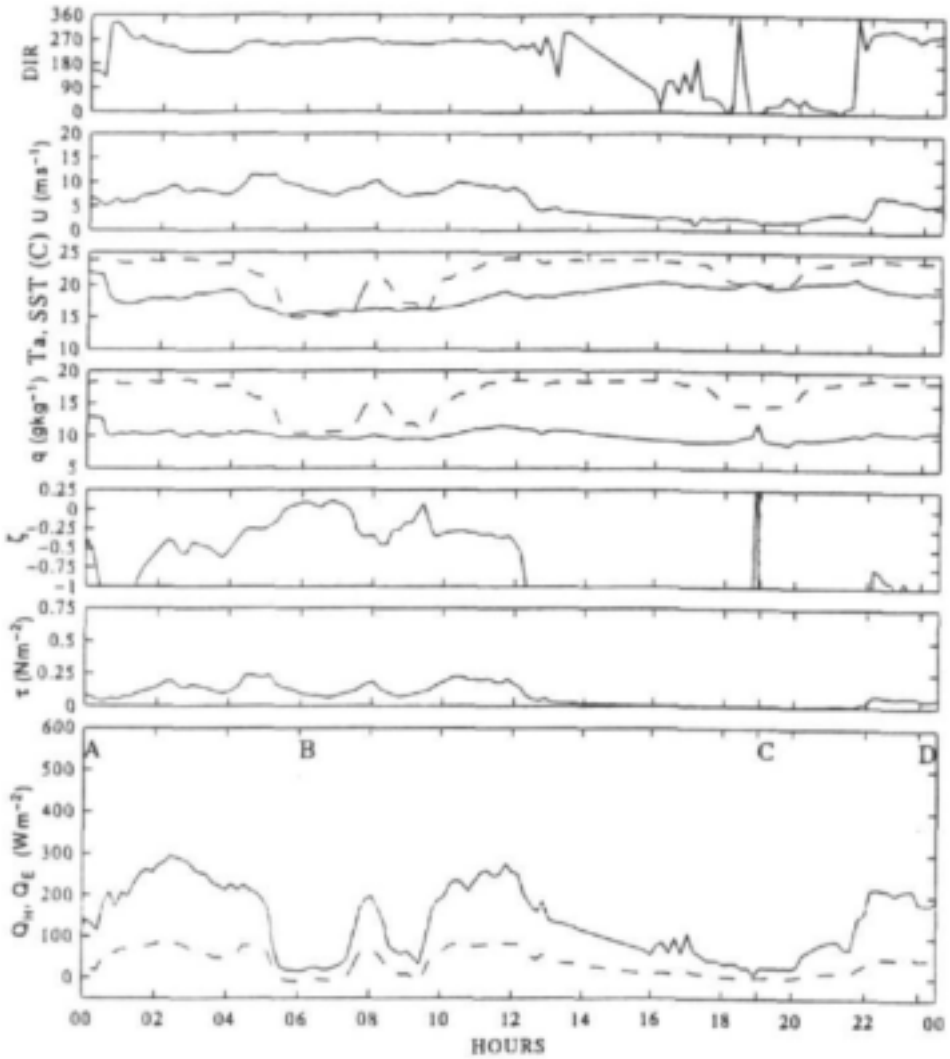

Figure 7.3: Time series of fluxes and parameters of interest during a ridging anticyclone - easterly flow - 29 April 1995. The parameters (from top to bottom) are: wind direction; wind speed (U) at 10 m; air temperature at 10 m (--) and sea surface skin temperature (- -); specific humidity at 10 m (--) and saturation specific humidity at the sea surface (- -); stability parameter, $\zeta 10 = 10/L$ (--); wind stress(--); latent heat flux (--) and sensible heat flux (- -).

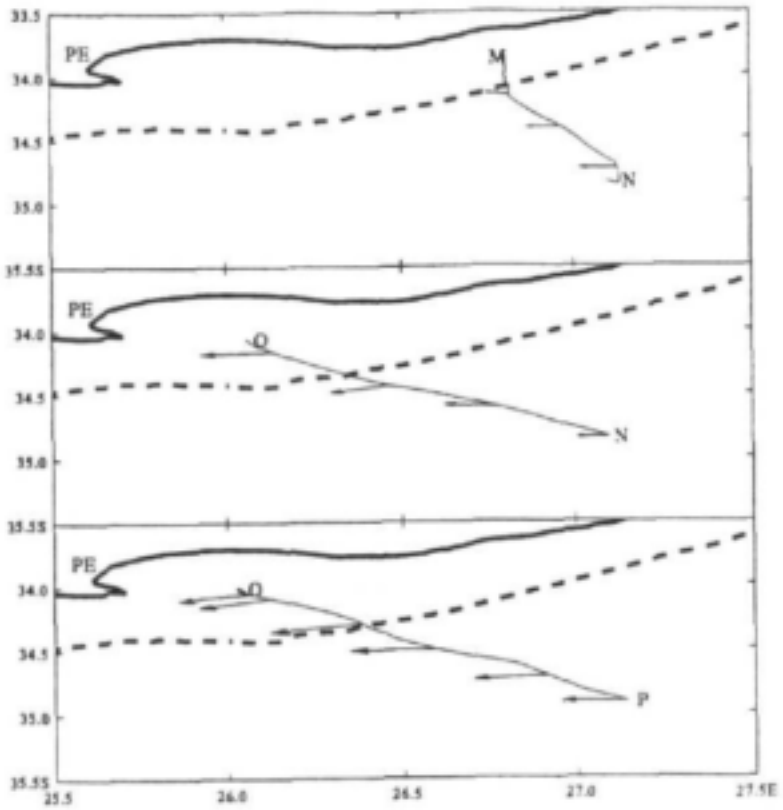

Figure 7.4: ACASEX 30 April - Schematic of the ship track showing transects and mean wind vectors (plotted every two hours), the 200 m isobath (dashed) and PE (Port Elizabeth). Labels denote the end-points of each transect as they appear in Figure 7.5. The first transect is shown in the top panel, second transect in the middle panel and so on.

factor of 7 greater over the current and are comparable to those found by Jury (1993) whilst no discernible relationship is found for the wind stress. This may be due in part to changing synoptic conditions during the second transect as seen from the remarkable and rapid decline of the wind speed over the current. Large, negative values of ζ 10 for this case are due to the small u_* and corresponds to a period of negligible wind stress.

It can be seen that for the weak westerly wind forcing studied here, low surface heat and momentum fluxes are unlikely to destabilise the surface layer. This suggests that thermals will not have any significant vertical extent. Furthermore the large horizontal surface heat flux gradient (Table 7.1) is expected to be instrumental in determining mean boundary layer characteristics across the inshore SST front.

7.2.2.1.2 Easterly Case Three transects were undertaken on 29 April (Figure 7.4). The sensible heat flux is small and positive over the current and negligible or negative over the shelf (Figure 7.5 and Table 7.2) whilst a dramatic increase in the latent heat flux occurs. A maximum turbulent heat flux of 347 Wm^{-2} during this case for the third transect is related to the wind speed increase. By 30 April surface northeasterly winds were parallel to the axis of the inshore SST front (Figure 7.6).

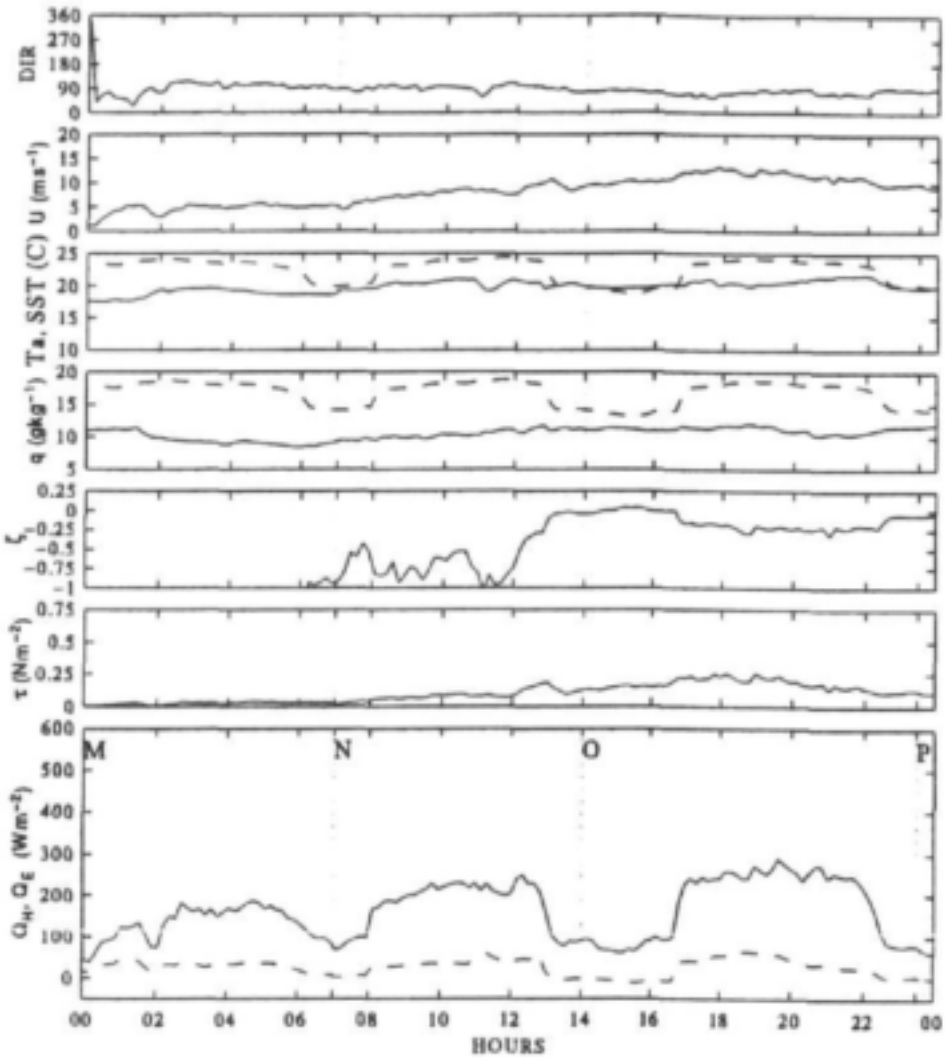

Figure 7.5: Time series of fluxes and parameters of interest during a ridging anticyclone - northeasterly flow - 30 April 1995. The parameters (from top to bottom) are: wind direction; wind speed (U) at 10 m; air temperature at 10 m (--) and sea surface skin temperature (- -); specific humidity at 10 m (--) and saturation specific humidity at the sea surface (- -); stability parameter, ζ 10 = *10/L* (--); wind stress(--); latent heat flux (--) and sensible heat flux (- -).

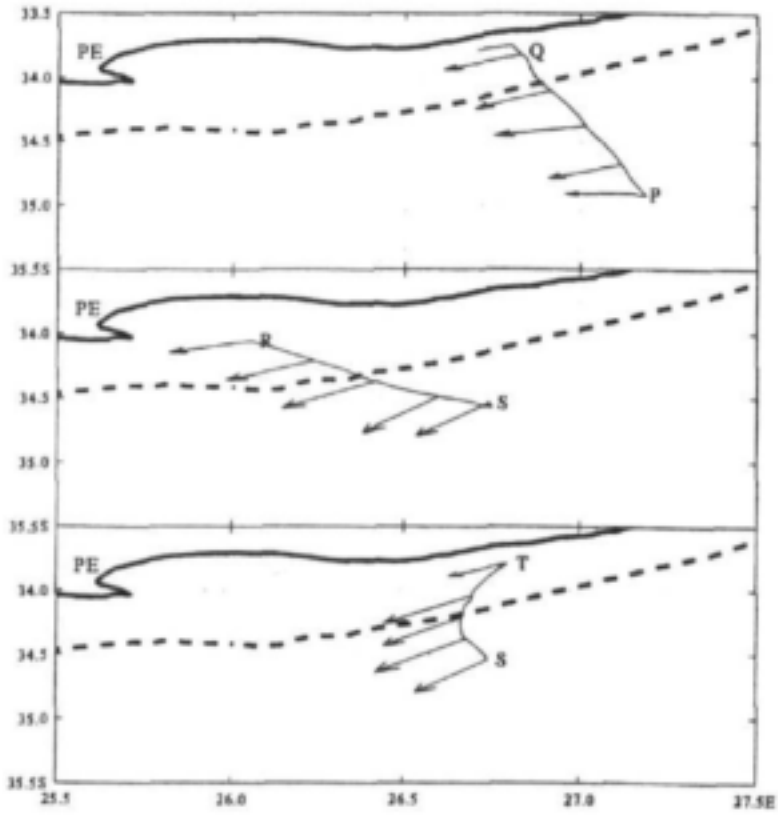

Figure 7.6: ACASEX 30 April - Schematic of the ship track showing transects and mean wind vectors (plotted every two hours), the 200 m isobath (dashed) and PE (Port Elizabeth). Labels denote the end-points of each transect as they appear in Figure 7.7. The first transect is shown in the top panel, second transect in the middle panel and so on.

During this period mean surface winds ($\bar{U}$=15 ms^{-1}) exceeded indicated geostrophic wind speeds (U_g=7.5 ms^{-1}) by a factor of 2. The geostrophic departure is greatest for the second transect and corresponds to a shift in the wind direction. Wind speed is closely correlated with SST with an unambiguous increase over the current and dramatic decrease over the shelf (Figure 7.7). Surface stability changes sign across the shelf edge. Mean wind stress and latent heat flux are a factor of 2 and 4 greater over the current respectively.

Alternating westerly and easterly wind stress facilitates onshore and offshore Ekman transport in the surface layers. This may control the variability in strength and position of the inshore SST front which in turn has implications for the large horizontal heat flux gradient across the SST front. XBT results during ACASEX have shown that kinematically-driven upwelling by the Agulhas Current may prime the system (Rouault *et al.*, 1995). Lower SSTs over the shelf region

Figure 7.3: Air-sea flux statistics - 30 April.

	$\overline{\tau}$	$\overline{Q_H}$	$\overline{Q_E}$	$\overline{Q_T}$	$max(Q_T)$	$\overline{\zeta_{10}}$	$dSST/dy$
	N.m^{-2}			Wm^{-2}			°Ckm^{-1}
SHELF	0.17	-31	58	27	92	0.13	0.3
AC	0.33	25	255	280	360	-0.09	

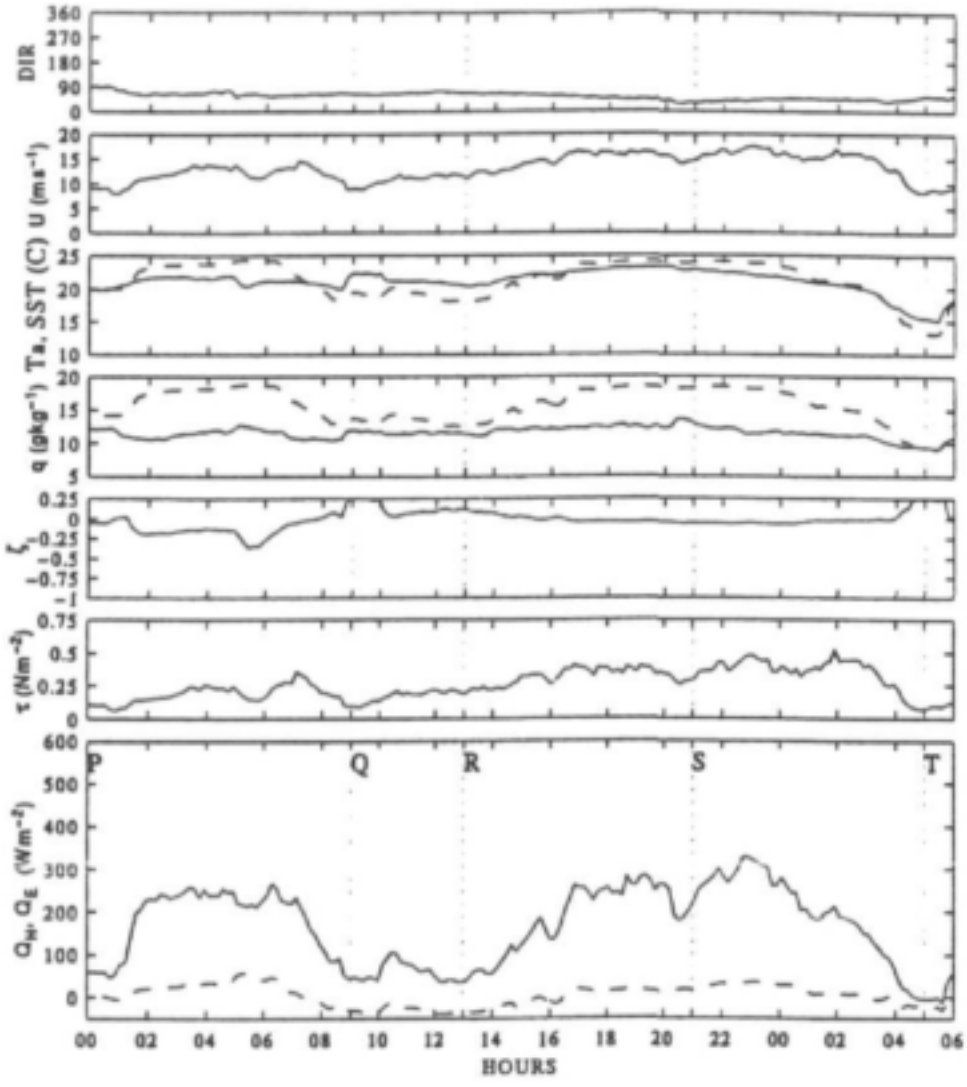

Figure 7.7: Time series of fluxes and parameters of interest during a ridging anticyclone - southerly flow - 28 April 1995. The parameters (from top to bottom) are: wind direction; wind speed (U) at 10 m; air temperature at 10 m (-) and sea surface skin temperature (- -); specific humidity at 10 m (-) and saturation specific humidity at the sea surface (- -); stability parameter $\zeta 10 = 10/L$ (-); wind stress(-); latent heat flux (-) and sensible heat flux (- -).

at the onset of the westerly case were related to the easterly wind stress of the previous two days . Westerly wind stress and onshore Ekman transport brought a subsequent reduction in intensity of the SST front (2°C(10 km)$^{-1}$) by 29 April. A progressive intensification of the SST gradient then occurred under easterly conditions such that a gradient in SST of 3.5°C(10 km)$^{-1}$ was observed during the third transect of 30 April (mean gradient of 3 °C(10 km)$^{-1}$).

In the above cases the latent heat flux constitutes the main component (80-90 %) of the surface turbulent heat exchange over the current. Surface destabilisation occurs across the inshore SST front which is characterized by a large horizontal latent heat flux gradient (Tables 7.1 to 7.3; Figures 7.3, 7.5 and 7.7). This suggests that the transition of the boundary layer from the current to adjacent inshore region defines a strong atmospheric *moisture* front and weaker *thermal* front. This hypothesis can easily be tested using the data from the radiosonde ascents conducted during ACASEX. A pattern of transition from a convective boundary layer to a stable (or relatively more stable) one will be shown to be a central theme in all cases and is in close agreement with the increase in surface fluxes.

7.2.2.2 Boundary layer structure

7.2.2.2.1 Westerly Case Figure 7.8 shows boundary layer differences over the shelf, inshore frontal region, current and seaward SST front for the first transect on 24 April. The q (and θ_e) profile over the shelf is suspect due to possible contamination of the RH sensor by sea spray during the radiosonde launch. This profile has been retained to illustrate the stabilisation due to θ.

The stable shelf profile is "capped" by an inversion (Figure 7.8). Destabilisation of the surface layer (in the inshore frontal region) then occurs as the first surface thermals mix vertically. Downwind (over the current core) a shallow, well-mixed profile is attained. The profile is not as convective as might be expected due to diminishing surface heat fluxes associated with decreasing wind speeds (Figure 7.3). Beyond the current on the seaward border, surface heat and momentum fluxes are negligible and a stable profile is attained. An increase in mean specific humidity, $\overline{q}$, potential temperature, $\overline{\theta}$, and equivalent potential temperature, $\overline{\theta}_e$, occurs from the shelf toward the current and decrease toward the seaward region (Table 7.4). Highest values occur over the current. The variation of mixed layer height, z_i, is less clear due to the difficulty in defining a mixed layer top for a stable boundary layer (Stull, 1988, p. 504-506).

Figure 7.9 shows boundary layer differences over the inshore front and current for the second transect. The pattern of stabilisation-destabilisation is repeated. The spatial variation of $\overline{q}$, $\overline{\theta}$ and $\overline{\theta}_e$ is unambiguous (Table 7.5) with differences of 1.7 gkg^{-1}, 3°C and 6.5°C apparent between the shelf and current.

7.2.2.2.2 Easterly Case Figure 7.10 follows the boundary layer structure across the current during easterly air flow (approximately parallel) to the SST front. An initially stable boundary layer (seaward front) is replaced by a convective boundary layer (current) and shallow convective boundary layer (shelf) with a concomitant deepening of 300 m over the current. The convective nature of the shelf boundary layer is due to the small oceanic heat loss in this region. Differences in $\overline{q}$, $\overline{\theta}$, and $\overline{\theta}_e$ (Table 7.6) are less accentuated due to the small cross-frontal wind component. Nevertheless the boundary layer is more moist and warmer over the current. Boundary layer profiles on 30 April in Figure 7.11 correspond to the shelf, SST front and current respectively. The northeasterly air flow was parallel to the SST front. The strong inversion in the MABL profile over the current is related to a strengthening of the subsidence field during the transect. A clear transition in stability (stable to convective structure) exists from the shelf toward the current while z_i increases by 200 m. The large thermodynamic differences ($\Delta_{\overline{q}} \simeq 3$ gkg^{-1}, $\Delta_{\overline{\theta}} \simeq 1$°C and $\Delta_{\overline{\theta}_e} \simeq 11$°C between the shelf SST front and current core clearly define an atmospheric moisture and thermal front across the inshore SST front (Table 7.7).

7.2.3 Conclusion

The response of the MABL to the sharp SST contrast on the inshore edge of the warm Agulhas Current was investigated in the Agulhas Current Air-Sea Exchange Experiment. The background weather was characterized by alongshore flow either as cool westerly winds or as warm easterly winds typical of winter cyclonic and summer anticyclonic conditions respectively.

The surface latent heat flux increased on average by a factor of 5 over the current whilst the sensible heat flux reversed sign. The large horizontal gradient in the surface heat fluxes across the SST front sets up a moisture and thermal front and transition in stability within the MABL. With the horizontal sampling it is not possible to describe the nature and position of the axis of this atmospheric front. However, it is likely to follow closely the surface heat flux profile. The orientation of the wind is important. The major-axis wind component for this region is parallel to the coast (Schumann, 1989). Thermodynamic differences are emphasized when the component of air flow across the SST front is minimized. Mean humidity differences of up to 3 gkg^{-1} were observed. Owing to the difficulty in defining a stable boundary layer z_i, the increase in MABL depth was sometimes ambiguous. A wind speed increase over the current and decrease over the shelf and seaward regions was observed to occur only on 30 April when the wind was parallel to the axis of the SST front. For the most part, however, rapidly changing synoptic conditions during the study period may have inhibited the establishment of any feedback in mesoscale circulations.

The Agulhas Current has frequently been linked to South African climate. Thus an emphasis has been placed on a useful quantification and characterization of the atmospheric boundary layer. Moisture uptake, mean thermodynamic properties and surface turbulent fluxes have been determined in the first dedicated shipboard study of the region. The results confirm the hypothesis that moisture and heat uptake above the Agulhas Current is substantial. This reserve of MABL moisture may enhance the convective potential of transient weather systems. The results here and of Jury (1993) have led to the unambiguous characterization of the boundary layer above the Agulhas Current as an area of high horizontal inhomogeneity. Large horizontal gradients of the surface turbulent fluxes have far-reaching implications. Airmass properties over the Agulhas Current are radically different from the seaward and shelf regions. Atmospheric general circulation models have been criticized for not taking into account boundary layer inhomogeneity (Brown and Foster, 1994; Foster and Brown, 1994). The boundary layer over the Agulhas Current must be considered to be an excellent example of a region of extreme horizontal inhomogeneity.

Improved horizontal and vertical sampling is needed to better understand feedback between coastal orography, the SST front, mesoscale circulations and transient weather systems. Therefore future research should involve both shipboard and aircraft measurements in a coordinated program during the climatologically important summer rainfall period.

Table 7.4: Boundary layer differences - 24 April - second transect. Locations of atmospheric profiles for the shelf (SHELF), current (AC) and seaward region (SEA) are labelled (R1-R4) in Figure 7.8.

	$\overline{z}_i$ (m)	$\overline{q}$ (gkg^{-1})	$\overline{\theta}$ (°C)	$\overline{\theta}_e$ (°C)	COMMENTS
SHELF (R1)	500	9.8	17.0	45.1	STABLE
AC (R2)	350	8.9	16.5	41.8	-
AC (R3)	250	10.2	18.1	47.5	SHALLOW-MIXED
SEA (R4)	350	8.4	18.9	43.4	STABLE

Table 7.5: Boundary layer differences - 24 April - third transect. Locations of atmospheric profiles for the shelf (SHELF), current (AC) and seaward region (SEA) are labelled (R4-R6) in Figure 7.9.

	$\overline{z}_i$ (m)	$\overline{q}$ (gkg^{-1})	$\overline{\theta}$ (°C)	$\overline{\theta}_e$ (°C)	COMMENTS
SHELF (R6)	200	8.4	15.8	41.5	STABLE
AC (R5)	300	10.1	18.8	48.0	MIXED
SEA (R4)	350	9.0	18.9	43.4	STABLE

Table 7.6: Boundary layer differences - 29 April Locations of atmospheric profiles for the shelf (SHELF) and current (AC) are labelled (R16-R18) in Figure 7.10.

	$\overline{z}_i$ (m)	$\overline{q}$ (gkg^{-1})	$\overline{\theta}$ (°C)	$\overline{\theta}_e$ (°C)	COMMENTS
SHELF (R16)	700	9.7	20.6	48.9	CONVECTIVE
AC^1 (R17)	1000	10.7	21.6	52.7	CONVECTIVE
AC^2 (R18)	800	10.11	22.5	52.2	MIXED/STABLE

Table 7.7: Boundary layer differences - 30 April. Locations of atmospheric profiles for the shelf (SHELF) and current (AC$^{1-2}$) are labelled (R20-R22) in Figure 7.11.

	$\overline{z}_i$ (m)	$\overline{q}$ (gkg^{-1})	$\overline{\theta}$ (°C)	$\overline{\theta}_e$ (°C)	COMMENTS
SHELF (R20)	500	9.5	22.5	50.4	STABLE
AC^1 (R21)	700	10.0	22.7	52.0	CONVECTIVE
AC^1 (R22)	500	12.8	23.5	61.2	MIXED/STABLE

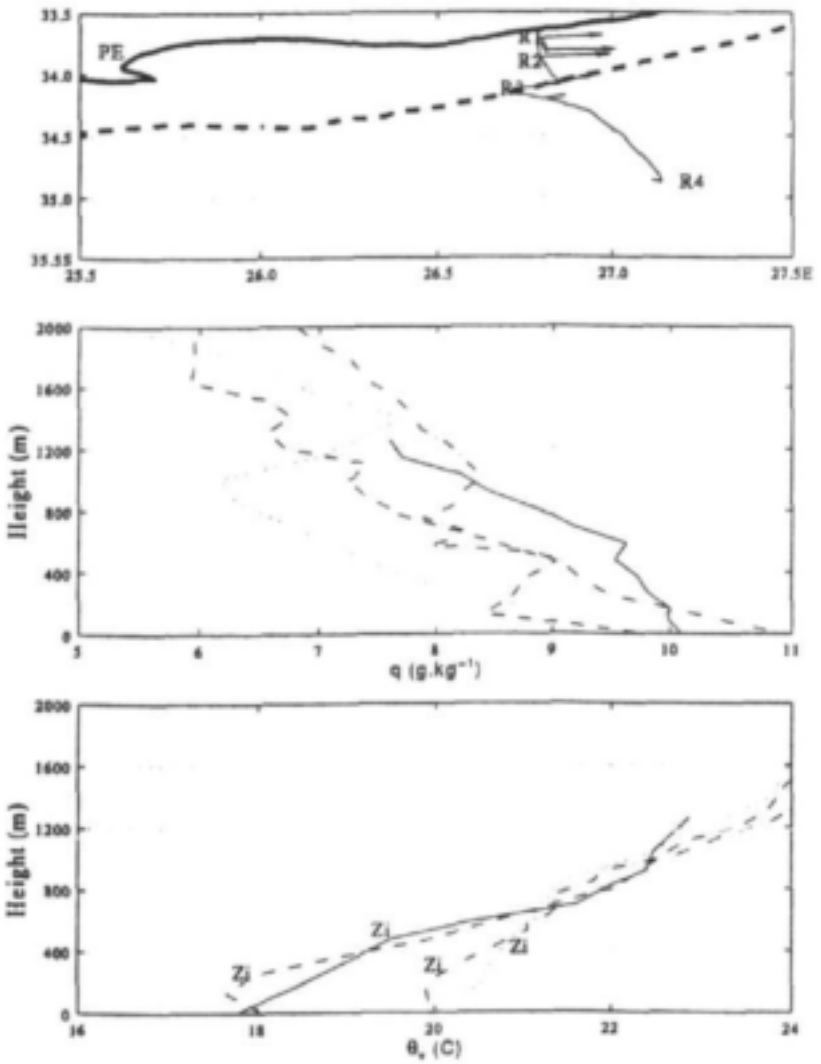

Figure 7.8: Atmospheric profiles showing boundary layer differences - 24 April - second transect. The plots are the locations (top), q (middle) and Θ_e (bottom); SHELF (R1) (-), AC (R2) (- -), AC (R3) (-.) and SEA (R4) (:). The approximate MABL height (z_i) is shown.

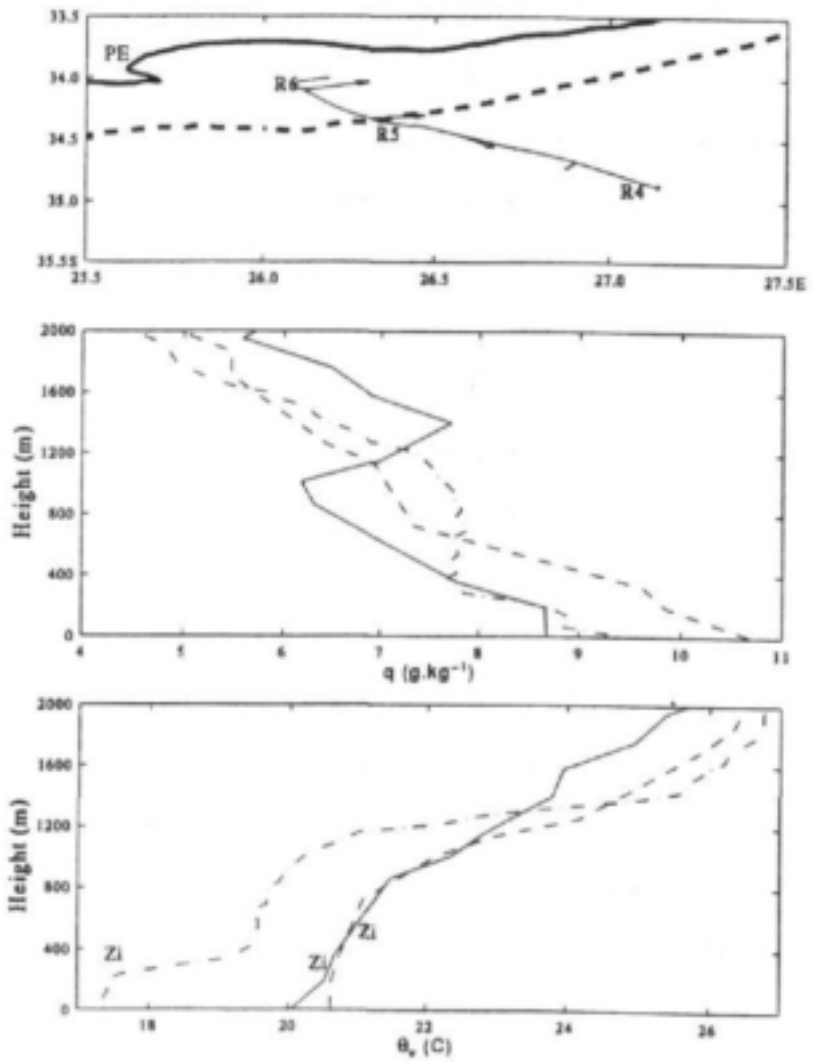

Figure 7.9: Atmospheric profiles showing boundary layer differences - 24 April - third transect. The plots are the locations (top), q (middle) and Θ_v (bottom); SEA (R4) (-), AC (R5) (- -), SHELF (R6) (-.)

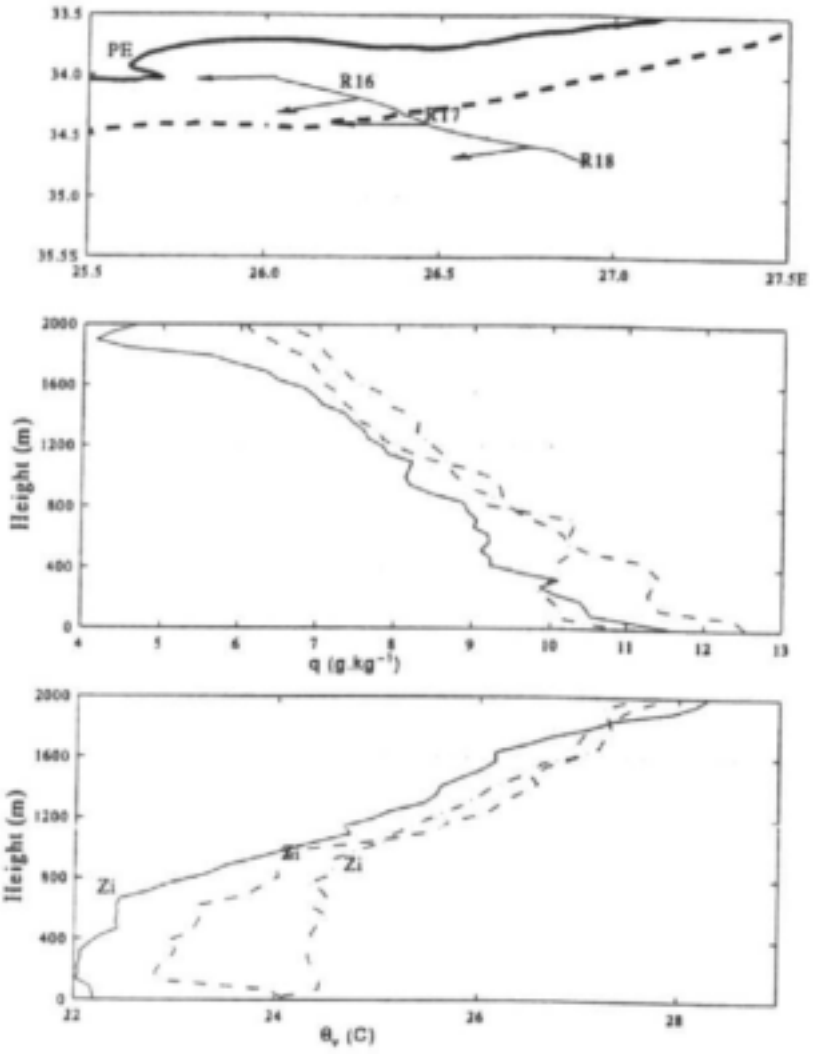

Figure 7.10: Atmospheric profiles showing boundary layer differences - 24 April. The plots are the locations (top), q (middle) and Θ_v (bottom); SHELF (R16) (-), AC^1 (R17) (- -), AC^2 (R18) (-.). The latter profile is on the current side of the seaward front.

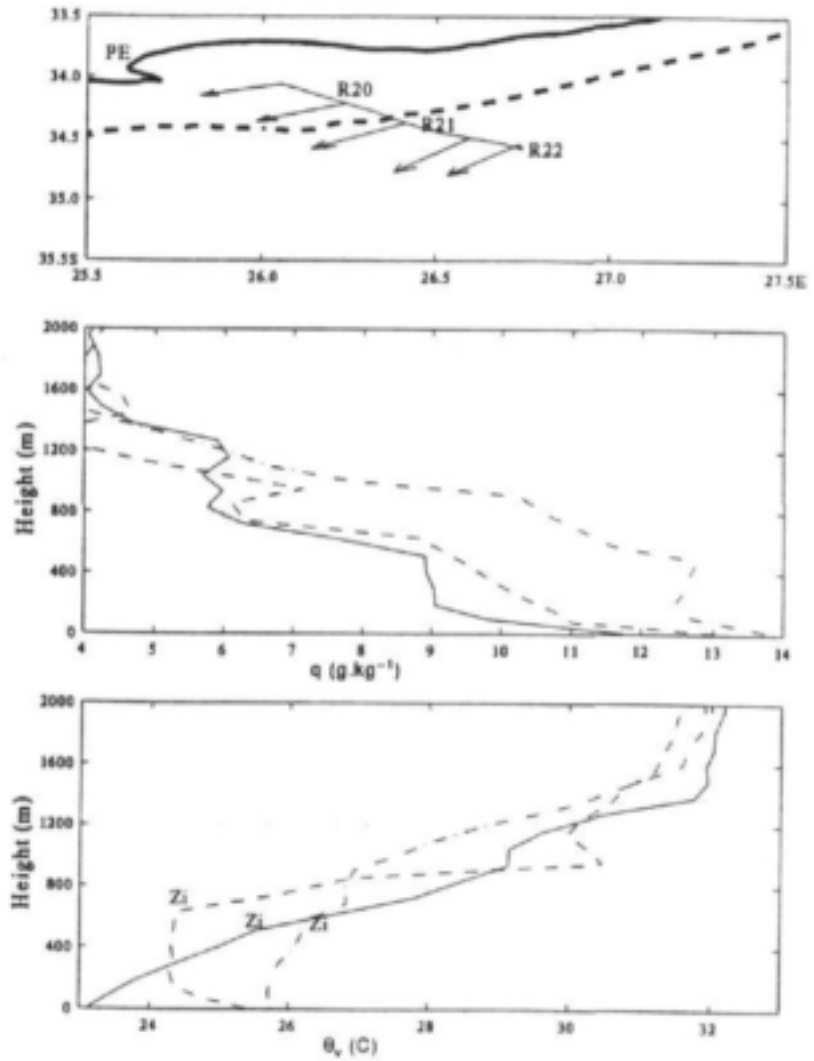

Figure 7.11: Atmospheric profiles showing boundary layer differences - 30 April. The plots are the locations (top), q (middle) and Θ_v (bottom); SHELF (R20) (-), AC[1] (R21) (- -), AC[1] (R22) (-.).

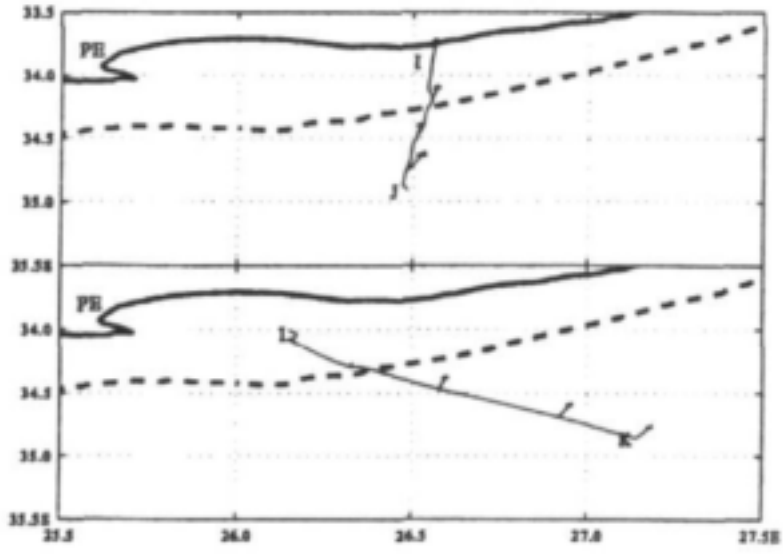

Figure 7.12: ACASEX 28 April - Schematic of the ship track showing transects, mean wind vectors (plotted every two hours), the 200 m isobath (dashed), PE (Port Elizabeth) and PA (port Alfred). Labels denote the end-points of each transect as they appear in Figure 7.13. The first transect is shown in the top panel and the second in the bottom panel.

7.3 Moisture uptake in the boundary layer above the Agulhas Current

In this section we focus on a period (28 April) when synoptic-scale atmospheric forcing brought maritime air toward the coast. The airflow was nearly perpendicular to the Agulhas Current which allowed us to study cumulative changes within the airmass.

7.3.1 Background and Meteorological Setting

Onshore flow was experienced as a result of a fairly strong ridge of high pressure behind a transient front. The maritime airmass had the open oceanic region to the south as its source region. Gentle southerly winds of 5-10 ms^{-1} were experienced. The westerly wind stress of the previous three days led to onshore Ekman transport of Agulhas Current waters and a subsequent reduction in intensity of the inshore SST front (2.0°C (10 km)$^{-1}$. This is in contrast to the maximum inshore SST gradient of 3.5°C (10 km)$^{-1}$ observed during easterly (upwelling-favourable) wind conditions. The inshore edge of the current is demarcated by the 200 m isobath.
The first transect I-J across the current was followed by a second oblique transect K-L towards the coast. The subsection J-K along the seaward edge is not shown.

7.3.2 Results

7.3.2.1 Spatial variation of the surface fluxes

The surface fluxes and forcing parameters for the two transects (Figure 7.12) are shown in Figure 7.13. An increase in the surface latent flux over the current is followed by a 6 times decrease over the shelf (Table 7.8). The surface sensible heat flux shows little variation. The relatively high latent heat flux over the shelf during the first transect is due to the intrusion of warm Agulhas Current waters. A decrease in wind speed over the shelf during the second transect may be due

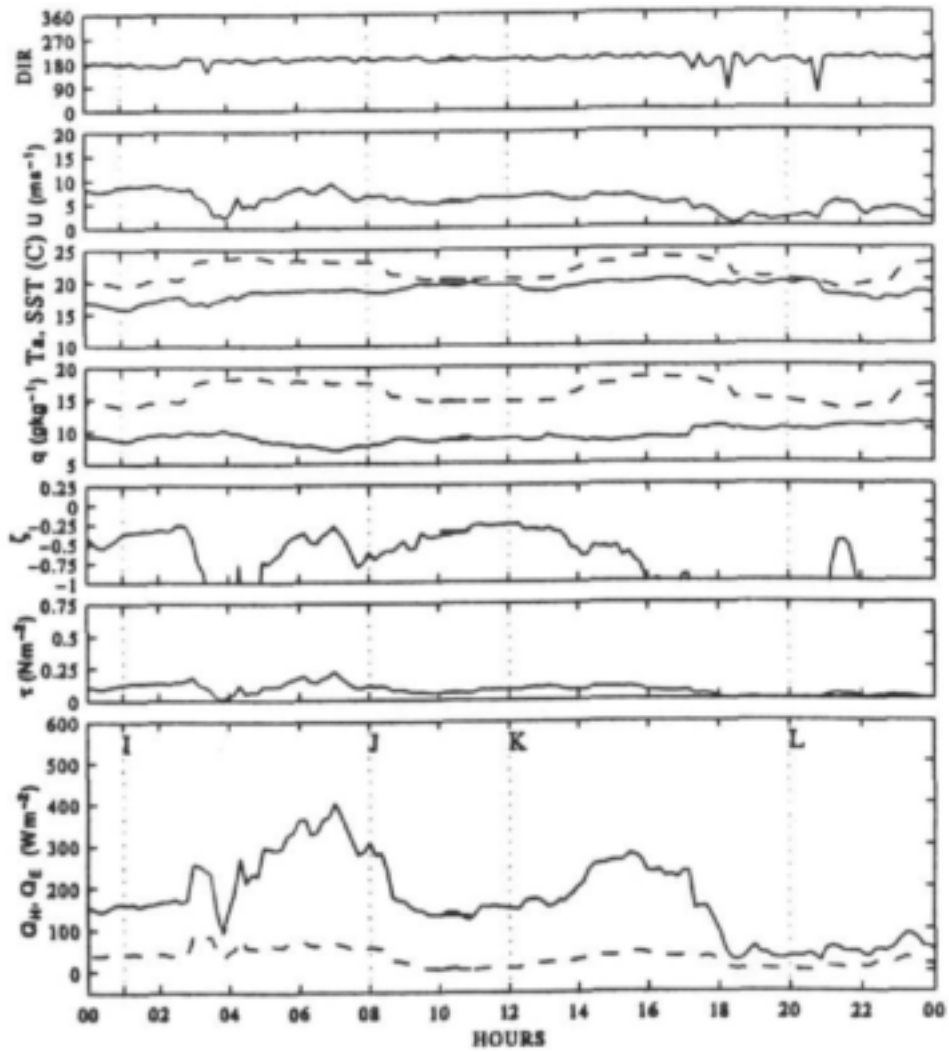

Figure 7.13: Time series of fluxes and parameters of interest during a ridging anticyclone - southerly flow - 28 April 1995. The parameters (from top to bottom) are: wind direction; wind speed (U) at 10 m; air temperature at 10 m (-) and sea surface skin temperature (- -); specific humidity at 10 m (-) and saturation specific humidity at the sea surface (- -); stability parameter, $\zeta 10 = 10/L$ (--); wind stress(-); latent heat flux (-) and sensible heat flux (- -). L is the Monin-Obukhov length. positive for stable conditions and negative for unstable conditions.

Table 7.8: Air-sea flux statistics - 28 April. Averages are given for the shelf (SHELF) Agulhas Current (AC), and seaward region (SAE). Q_T is the total heat flux ($Q_T = Q_H + Q_E$). The quantity $dSST/dy$ is the horizontal gradient of sea surface temperature perpendicular to the inshore SST front (top) and seaward STT front (bottom).

	$\overline{\tau}$	$\overline{Q}_H$	$\overline{Q}_E$	$\overline{Q}_T$	$max(Q_T)$	$\overline{\zeta}_{10}$	$dSST/dy$
	$N.m^{-2}$			Wm^{-2}			$^{\circ}C$
SHELF	0.01	6	40	46	71	-6.2	0.2
AC	0.10	52	268	320	469	-1.2	
SEA	0.10	31	163	194	274	-0.5	0.1

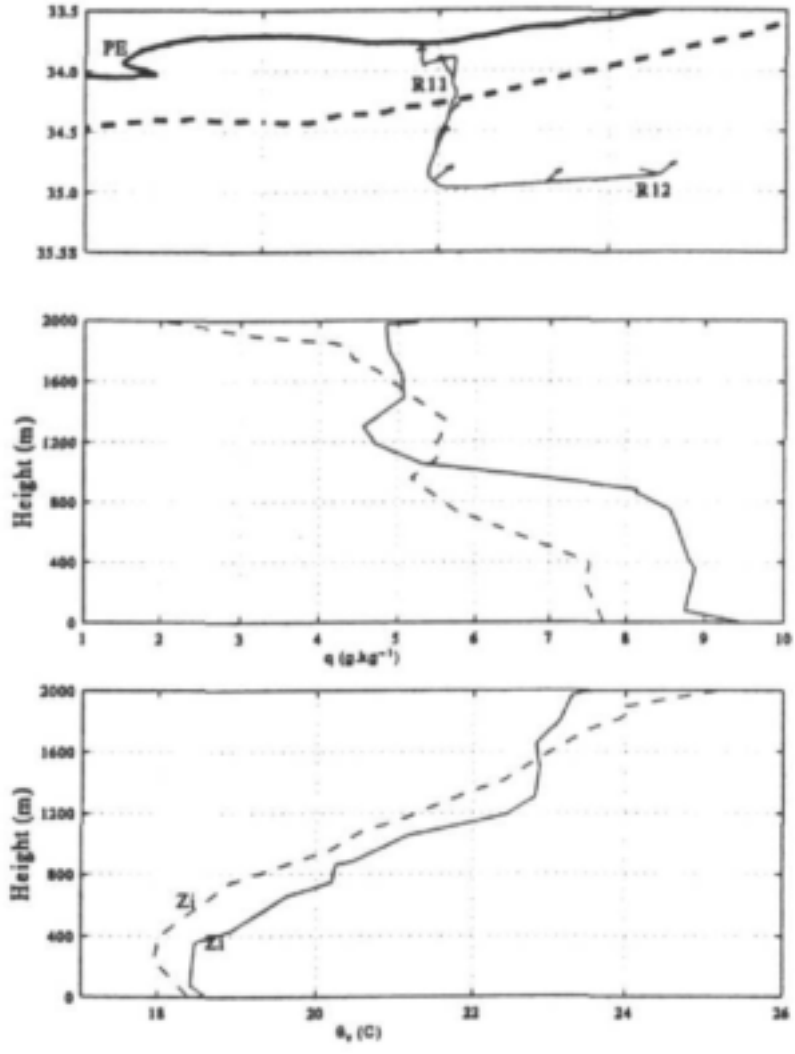

Figure 7.14: Atmospheric profiles showing boundary layer modification - 28 April -first transect. The plots are the locations (top), q (middle) and Θ_v (bottom); shelf R11) (-) and eaward border (R12) (- -). The approximate MABL height (z_i) is shown.

in part to changing synoptic conditions. In the above cases the latent heat flux constitutes the main component (80-90%) of the surface turbulent heat exchange over the current and indicates significant injection of moisture into the overlying atmosphere.

The reduction in the surface heat fluxes across the inshore SST front has implications for the convective potential of eddies.

7.3.2.2 Marine boundary layer modification

Thermodynamic differences in the MABL can be viewed from a Lagrangian perspective (i.e. an airmass with the initial properties of the seaward profile becomes modified as it moves over the current). The resultant airmass properties are that of the shelf profile.

A first indication of atmospheric moisture uptake can be seen from the results of the first subsection. Figure 7.14 shows atmospheric profiles and their locations over the seaward region and shelf for the subsection IJK. Significant moisture (q) differences occur below 1000 m. Whilst the convective limit of surface parcels for the seaward scenario (z_i=600 m) exceeds that of the

Table 7.9: Boundary layer differences, 28 April, first transect. $\overline{q}$, $\overline{\theta}$ and $\overline{\theta}_e$ are the MABL means of specific humidity, potential temperature and equivalent potential temperature. Values enclosed in parentheses are means for the first 1000 m. Locations of atmospheric profiles for the shelf (SHELF) and seaward region (SEA) are labelled (R11-R12) in Figure 7.14.

	z_i (m)	$\overline{q}$ (gkg^{-1})	$\overline{\theta}$ (°C)	$\overline{\theta}_e$ (°C)	COMMENTS
SHELF (R11)	400	8.9	16.9	42.4	CONVECTIVE/RESIDUAL LAYER
		(8.5)	(17.8)	(42.2)	
SEA (R12)	600	7.3	16.9	38.0	CONVECTIVE

Table 7.10: Boundary layer differences - 28 April - second transect. as in Table 7.9. Locations of atmospheric profiles for the shelf (SHELF), current (AC) and seaward region (SEA) are labelled (R12-R15) in Figure 7.14.

	z_i (m)	$\overline{q}$ (gkg^{-1})	$\overline{\theta}$ (°C)	$\overline{\theta}_e$ (°C)	COMMENTS
SHELF (R15)	300	8.9	19.2	45.0	STABLE/RESIDUAL LAYER
		(7.9)	(19.7)	(42.7)	
AC (R14)	1200	7.3	19.0	40.3	CONVECTIVE
		(7.4)	(18.8)	(40.4)	
AC (R13)	1400	6.7	19.6	39.1	CONVECTIVE
		(7.1)	(19.3)	(40.0)	
SEA (R12)	800	7.0	17.1	37.3	CONVECTIVE
		(6.7)	(17.5)	(36.8)	

shelf scenario (z_i=400 m), a comparison of the moisture profiles shows the seaward area to have a layer well-mixed in q until only 400 m. The deep moisture layer over the shelf (800 m) exists as a residual layer (Stull, 1988). Moisture in this case acts as a passive tracer and indicates the former vertical extent of eddies whilst the θ_v profile indicates rapid convective adjustment over the shelf. Table 7.9 summarizes the thermodynamic differences. $\overline{q}$ and $\overline{\theta}_e$ are $\simeq$1.5 gkg^{-1} and $\simeq$4.5 °C greater over the shelf. Since integrating to varying boundary layer heights yields a somewhat biased comparison of $\overline{q}$, $\overline{\theta}$ and $\overline{\theta}_e$, we integrate to the approximate limit of z_i (in this case 1000 m) to obtain a more meaningful comparison. Integrating to 1000 m yields $\Delta_{\overline{q}} \simeq$2 gkg^{-1} and $\Delta_{\overline{\theta}_e} \simeq$5.5 °C. This is equivalent to a 27 % increase in mean specific humidity and precipitable water vapour content.

Owing to its possible climatological importance this case merits further attention. Results from the second transect, KL, on 28 April can be seen in Figure 7.15. As air moves from the seaward region over the current vigorous convective mixing results in the boundary layer deepening by 400 m. The convective nature of the MABL is then eroded as the airmass moves over the cool shelf. The humidity mixed layer depth (not neccessarily equal to the limit of surface convection z_i) increases toward the shelf, varying from 800 m (over the core) to 1200 m (near the SST front). A residual humidity layer over the shelf is once again found to exist (between 600 m and 1400 m). Without exception, the boundary layer becomes warmer and more humid as air is advected over the current (Table 7.10). Boundary layer values of $\overline{q}$ and $\overline{\theta}_e$ for air over the shelf are approximately 2 gkg^{-1} and 6°C greater than over the current.

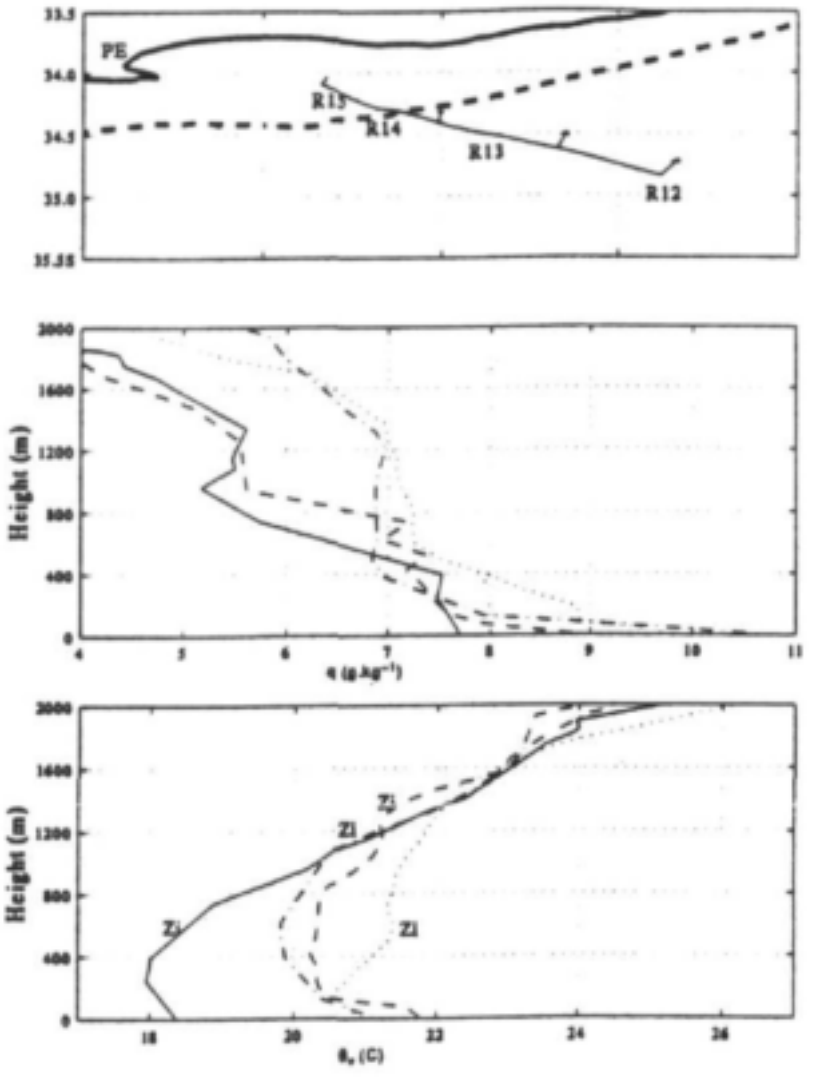

Figure 7.15: Atmospheric profiles showing boundary layer modification - 28 April -second transect. The plots are the locations (top), q (middle) and Θ_v (bottom); seaward border (R12) (-), current core (R13) (- -), current near the inshore SST front (R14) (-.) and shelf (R15) (:). The approximate MABL height (z_i) is shown.

7.3.2.3 Onshore vs alongshore winds

Radiosonde observations at the coast (Port Elizabeth) provided a land-based reference to assess the differences between land and marine airmasses. This is especially useful for a comparison of boundary layer structure during onshore and alongshore winds. During alongshore winds dry, cool conditions over the shelf and warm, moist conditions over the current are separated by an atmospheric front which lies above the inshore SST front. Onshore winds lead to cumulative moisture uptake by the boundary layer. In the latter case land-sea differences of moisture are expected to be small. The comparison is complicated by several factors, namely the height (60 m above mean sea level), location (a few kilometers inland), local topographic effects and diurnal variations, and the fact that the observation times did not always suitably coincide. Thus while a $\overline{q}$ comparison is quite instructive a comparison of boundary layer height and mean temperature ($\overline{\theta}$ and $\overline{\theta}_e$) is not useful.

Figure 7.16 shows the spatial variation of boundary layer structure and specific humidity during periods of alongshore winds. In the first panel (24 April) westerly winds were approximately parallel to the inshore SST front. The effect of surface heating during the day at PE is evident. A well-mixed layer is capped at 500 m. At night, however, a stable (nocturnal boundary) layer was present (Figure 7.17). The presence of a stable boundary layer leads to difficulty in defining an appropriate boundary layer top (Stull, 1988). In contrast, the boundary layer structure above the current did not show any discernible diurnal variation, only a spatial variation consistent with the spatial variation of the surface heat fluxes. $\overline{q}$ decreases from the current towards the coast. A similar spatial pattern is revealed on 29 April and 30 April during alongshore easterly (middle panel) and northeasterly winds (bottom panel). Mean moisture content decreases towards the coast, being lowest at PE.

Mean moisture differences are minimized during onshore winds. Figure 7.17 illustrates the spatial variation of $\overline{q}$ for the second transect on 28 April. In this case the limit of integration for $\overline{q}$ at PE was chosen as the limit of humidity mixed-layer (750 m). Coast-shelf differences of $\overline{q}$ are negligible. This is in agreement with the simple conceptual model of cumulative moisture uptake proposed for onshore winds (Walker, 1990).

7.3.3 Conclusion

Surface heat and moisture uptake and resultant boundary layer modification was investigated during a period of onshore wind forcing on 28 April during the Agulhas Current Air-Sea Exchange Experiment (ACASEX). A slow ridging anticyclone gave rise to moderate onshore winds which were approximately perpendicular to the Agulhas Current.

A doubling of the surface latent flux over the current was followed by a 6 times decrease over the shelf whilst the sensible heat flux showed little variation. The latent heat flux constituted the main component (80-90 %) of the surface turbulent heat exchange over the current resulting in substantial injection of moisture into the overlying atmosphere. Not surprisingly, the mean potential temperature ($\overline{\theta}$) of the MABL showed little variation whilst the mean specific humidity ($\overline{q}$) increased substantially by up to 2 gkg^{-1} ($\simeq$ 25 %) along the air flow trajectory. A progressive accumulation of MABL moisture was accompanied by a consistent deepening of the humidity mixed layer. The MABL deepened rapidly as air moved from the seaward region over the current, becoming shallow and stable over the shelf. This indicates rapid convective adjustment of convective eddies to the spatial heat flux gradient. Over the shelf a residual moisture layer acted as a tracer of the former vertical extent of convective eddies. It has been shown that during alongshore winds an atmospheric front over the inshore SST front separates boundary layer air above the shelf and current. Land-based observations support this simple conceptual model describing onshore and alongshore wind regimes.

Statistical results have led to the assertion by many investigators that moisture uptake above the Agulhas Current is substantial during periods when the direction of wind forcing is toward the

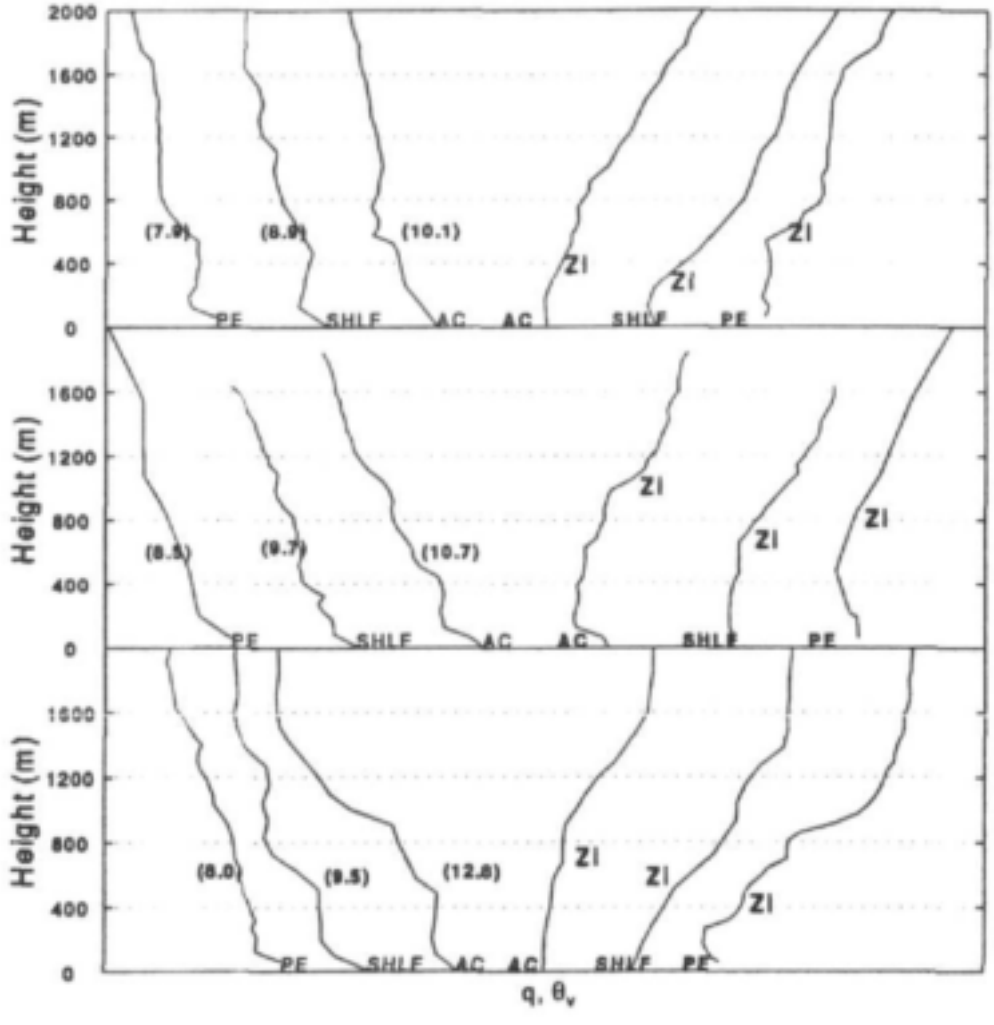

Figure 7.16: Boundary layer structure of $\overline{q}$ (left) and Θ_v (right) over the current core (AC), shelf (SHLF) and near midday at Port Elizabeth (PE) on 24 April (top), 29 April (middle) and 30 April (bottom). The plots have been scaled and offset to aid visualization. Values of q (enclosed in parentheses) are given.

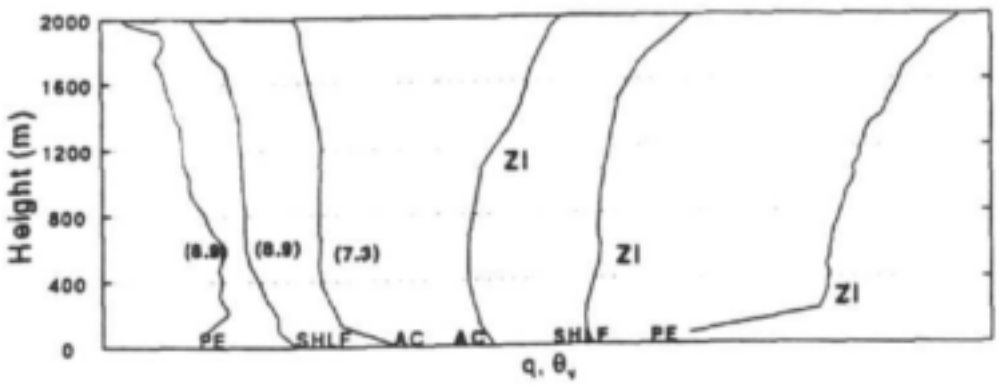

Figure 7.17: Boundary layer structure of q (left) and Θ_v (right) over the current core (AC), shelf (SHLF) and near midnight at Port Elizabeth (PE) on 28 April during the second transect. The plots have been scaled and offset to aid visualization. Values of q (enclosed in parentheses) are given.

coast and may significantly enhance moisture convergence over the interior of South Africa. These results strengthen this argument.

7.4 Cumulus cloud formation above the Agulhas Current

During the Agulhas Current Air-Sea Exchange Experiment (ACASEX), south of Port Alfred, substantial cumulus formation was observed above the Agulhas Current. Clear conditions over the shelf were replaced by active, coupled cumuli over the current and partly cloudy conditions over the seaward border. Radiosonde ascents and satellite images are used to describe this transition during a period of anticyclonic ridging. Negligible or even downward heat fluxes occurred over the shelf whilst strong atmospheric heat and moisture fluxes were observed over the current. This was reflected in the overlying atmosphere by a transition in stability of the boundary layer and potential cumulus formation. An inversion capped the boundary layer whilst a second, higher-level subsidence inversion was found which acted to limit the vertical development of cumulus clouds and therefore the redistribution of heat and moisture above the boundary layer.

7.4.1 Introduction

One of the main reasons for discrepancies between different General Circulation Models is the difference in cloud feedback and parametrization schemes (Cess et al., 1990). The study of clouds has been the focus of various international experiments and a priority of the World Meteorological Organisation and World Climate Research program. The occasional presence of cloud lines above the Agulhas Current has received very little attention in the local literature. Differences in sea surface temperature (SST) between the cool waters over the continental shelf and the warm Agulhas Current (Pearce, 1977) offer the possibility of a mesoscale circulation system that can interact with transient weather systems (Jury, 1993). Indeed satellite images frequently show the presence of a line of deep cumulus clouds organised in the alongshore direction over the Agulhas Current either as singular cloud lines or as cloud streets. Lutjeharms et al (1986) have shown that cloud lines form preferentially during the final stages of a ridging anticyclone and occasionally demonstrate a distinct diurnal cycle that suggests a seaward extension of the early morning land-sea breeze regime. A dramatic transition in cumulus was observed during the experiment during a period of anticyclonic ridging. Clear conditions over the shelf were replaced by active, coupled cumuli over the current and partly cloudy conditions over the seaward border.

7.4.2 Theoretical considerations

The boundary layer is the lower domain of the atmosphere that responds to surface forcings on timescales of an hour or less. A close coupling exists between cumulus clouds and boundary layer thermals (Stull, 1988). Although it is difficult to formulate a simple working definition for the boundary layer top it coincides with the lowest inversion separating boundary layer air from air having the properties of the free-atmosphere. Observations during ACASEX suggest that cumulus clouds are a ubiquitous feature above the Agulhas Current during most synoptic situations. This is not readily visible from satellite images, however, during the stratiform conditions of transient mid-latitude depressions. In contrast, cumuli are easily visible during the clear trade-wind conditions associated with the final stages of anticyclonic ridging. It is important to distinguish between a singular cumulus cloud line (e.g. Jury and Walker, 1988) and the occurrence of a broad band of cumulus which delineates the position of the Agulhas Current. The former is due to a local mesoscale circulation such as a land-sea breeze. We will establish a simple theoretical framework for the latter by way of an example. To illustrate the potential for cumulus development we use the convective available potential energy (CAPE). This is simply the amount of convective energy that is available to an ascending air parcel within a cloud. Figure 7.18 explains the the derivation

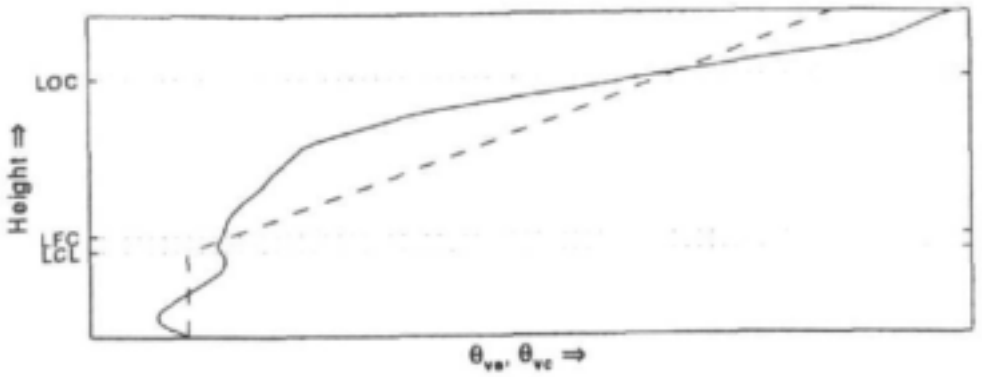

Figure 7.18: Schematic example of the use of the convective available potential energy above the shelf on 29 April. θ_{Ve} is the environmental atmospheric profile of the virtual potential temperature (solid line). θ_{vc} is a trace of an ascending air parcel as virtual potential temperature (dashed line).

of CAPE. The virtual potential temperature, θ_v of an air parcel is inversely related to its density. The additional subscripts c and e denote the cloudy air parcel and the environment. An ascending air parcel initially follows a dry adiabat (vertical dashed line) from the surface until the lifting condensation level (LCL), a reasonable approximation of cloud base. It then follows the wet adiabat (sloping dashed line) as latent heat is released during condensation. The virtual potential temperature of the cloudy air parcel, θ_{vc} is unsaturated below cloud base but takes into account the liquid water content above cloud base. The air parcel begins its ascent at the surface where it is initially positively buoyant since it is less dense than the environment (i.e. $\theta_{vc} > \theta_{ve}$). If the ascending parcel overshoots the area of negative buoyancy above the capping inversion, where it is heavier than the environment (i.e. $\theta_{vc} < \theta_{ve}$), then it might rise to the level of free convection (LFC) where it is again positively buoyant. A cloud that reaches its level of free convection is classified as an active cloud. The parcel continues to ascend under its own buoyancy until the limit of convection (LOC). The area of positive buoyancy is integrated to yield the convective available potential energy. If the CAPE is large and the air parcel has sufficient inertia to overcome the initial area of negative buoyancy this indicates a large potential for cumulus formation. Although this example gives an upper limit on CAPE, it demonstrates the close coupling between boundary layer structure, thermals and cumulus convection. Many convective thermals, however, have undiluted cores allowing the actual cloud base to be close to the lifting condensation level calculated from surface-layer air.

7.4.3 Meteorological setting

On 28 April an anticyclone began ridging around the subcontinent behind a transient mid-latitiude depression. Southerly, onshore winds advected maritime air towards the coast. The following day, easterly winds were approximately parallel to the current whilst a concomitant lowering of the subsidence inversion occurred. By 30 April, the wind had rotated to northeasterly, parallel to the current, with a further lowering of the subsidence inversion.

7.4.4 A transition in cumulus

A distinct atmospheric feature during ACASEX was the persistent layer of cumulus clouds over the current, clear conditions over the shelf and scattered cumulus over the seaward border (Figure 7.19). The sequence of satellite images in Figure 7.20 corresponds to the period 28 to 30 April. On 28 April an assortment of stratiform and cumuliform clouds are present. Cloudless conditions are to

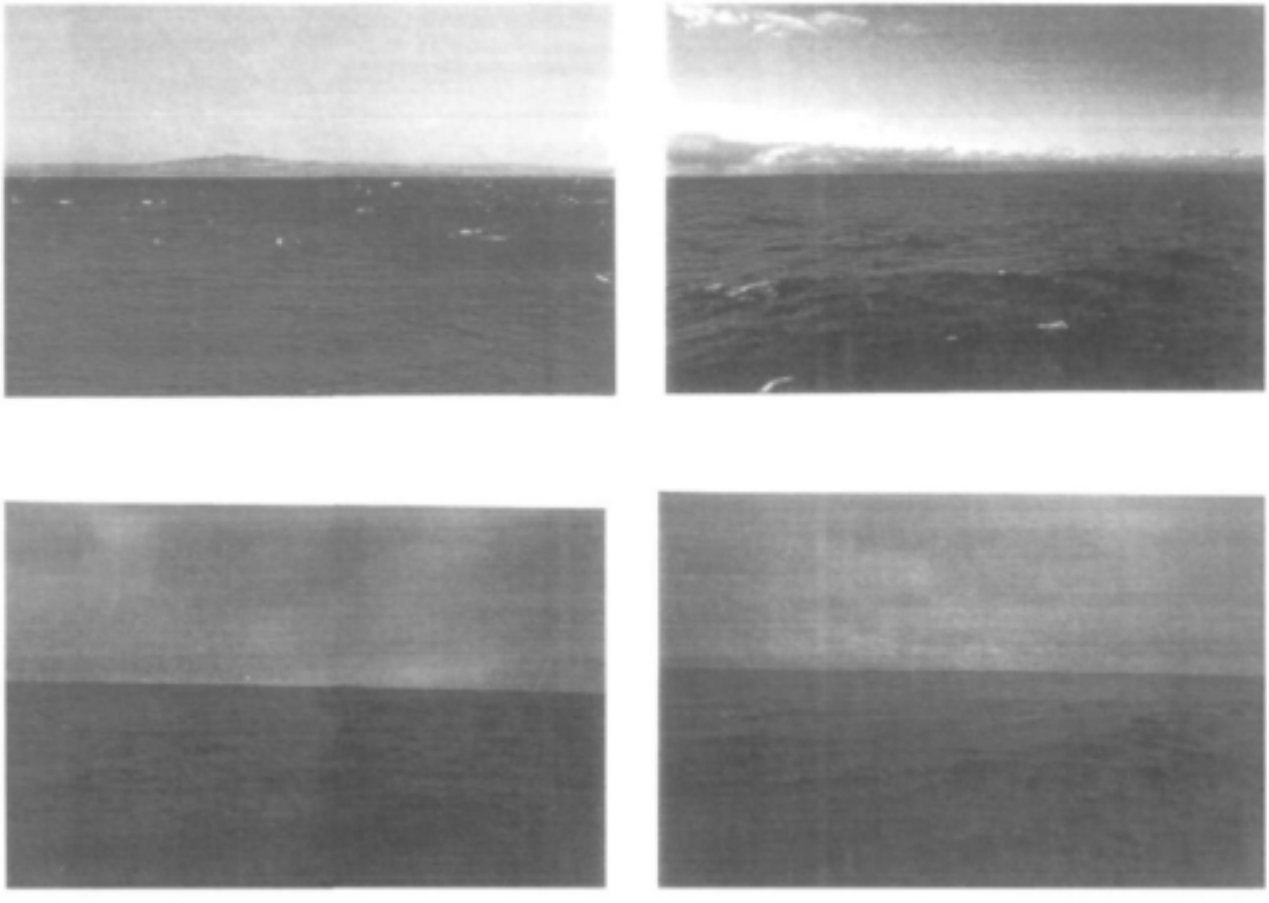

Figure 7.19: Photographs of cumulus formation over the shelf, Agulhas Current and seaward regions on 29 April. The photographs are: (a) facing west toward the coast from the shelf (cloudless conditions) , (b) facing east toward the Agulhas Current from the shelf (where the edge of the current is clearly demarcated by cumulus formation), (c) cumulus formation over the Agulhas Current, (d) facing seaward from the current where cumulus becomes more scattered.

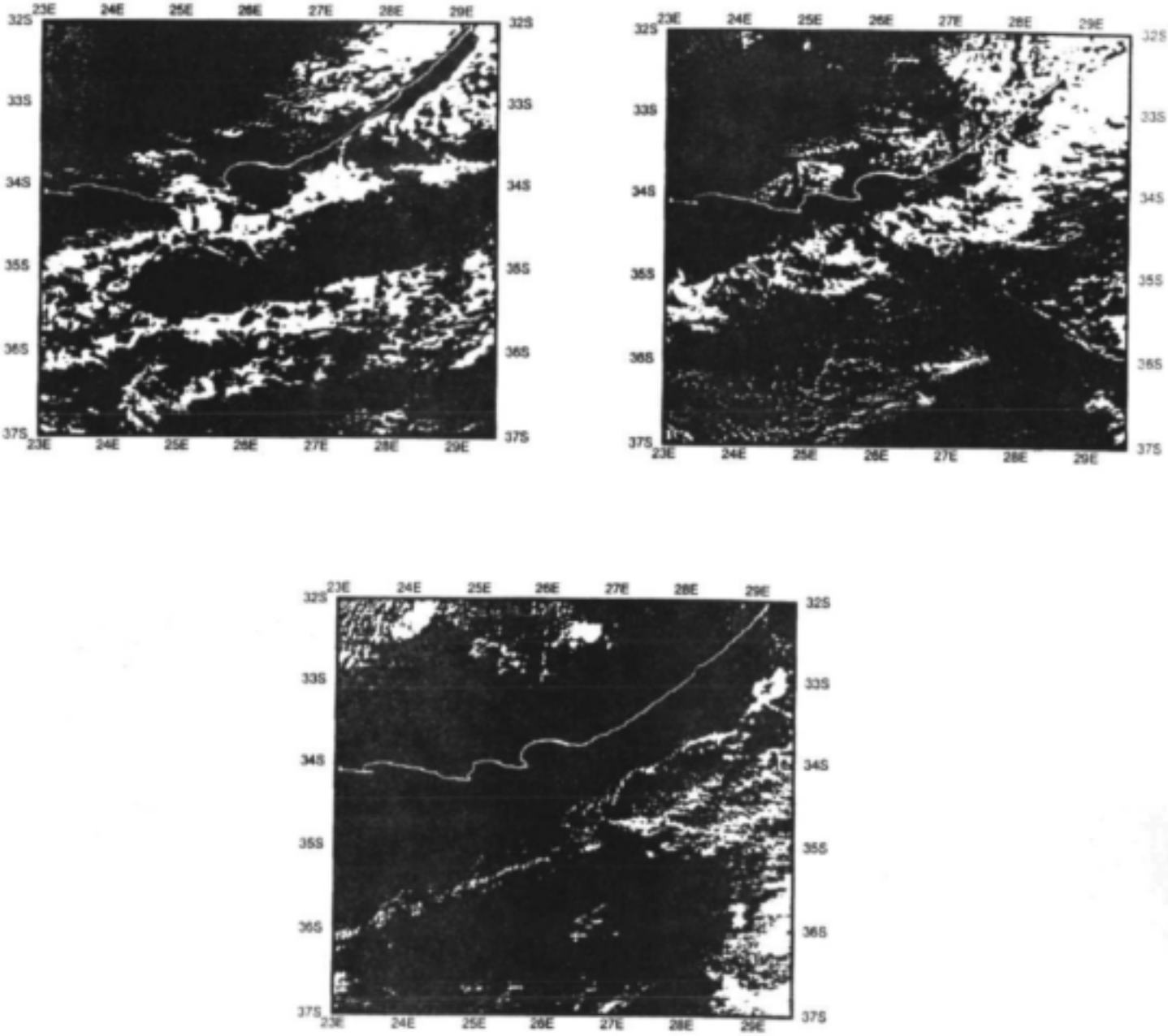

Figure 7.20: Sequence of images showing the spatial pattern and temporal evolution of cumulus clouds above the Agulhas Current on (a) 28 April, (b) 29 April and (c) 30 April

be found in the vicinity of the Agulhas Bank, Algoa Bay and along a portion of the east coast. There is some evidence for cumulus development above the current. By 29 April a clear band of cumulus delineated the position of the current which is flanked by clear skies above the shelf and seaward of the current. On the following day the cumulus cloud band, aligned with the current core, became less distinct with an apparent decay in the downstream wind direction.

7.4.5 Evolution of convective available potential energy

It is possible to investigate the spatial and temporal variation of cumulus clouds by examining the CAPE. Atmospheric profiles over the shelf, current and seaward region illustrate the spatial variation of CAPE on 28 April (Figure 7.21). Surface thermals over the seaward region do not attain a level of free convection as potential cloud parcels are always negatively buoyant above the lifting condensation level. As an example, consider an air parcel that has risen to a height of 1000 m. The air parcel has already reached its lifting condensation level, indicated by the change in slope of the dashed line. At 1000 m the cloudy air parcel is heavier than the environment shown by the solid line (i.e. $\theta_{vc} < \theta_{ve}$). Above the current surface thermals attain their lifting condensation level within the boundary layer (i.e. there is no negatively buoyant overshoot). In this case the cumulus clouds are convectively coupled to the surface forcing. Thus moisture is vertically redistributed above the boundary layer. The limit of cumulus convection is determined by the height and strength of the subsidence inversion. Shallow cumulus convection is possible over the shelf. Sufficient inertia is required to overcome the negatively buoyant overshoot above the inversion. This may occur periodically and lead to scattered cumulus formation. The spatial cumulus pattern above the current is not well-defined due to the orientation of the wind (Figure 7.20). Thus active cumuli which develop above the current are advected toward the coast and become decoupled.

The pattern is repeated with some variation on 29 April when winds were easterly and hence approximately parallel to the current. A strengthening and lowering of the subsidence inversion occurred. Potential cumulus formation is absent over the seaward region since surface thermals are always negatively buoyant (Figure 7.21). Over the current, deep cumulus convection is again coupled to the surface. CAPE is weak over the shelf edge where cumulus convection was absent. On 30 April dry northeasterly winds were parallel to the Agulhas Current. Over the shelf CAPE is absent due to a strong inversion and stable boundary layer which supresses convection (Figure 7.21). Above the current surface thermals contain sufficient moisture and energy such that cloud base occurs near the inversion. This explains the observed weak cumulus clouds. In this case, maximum potential for cumulus development corresponds to the current core. The degree of coupling between cumulus convection and surface forcing is determined by the surface heat and moisture flux and atmospheric stability. Moist air parcels will become quickly saturated during ascent. If the boundary layer is convective the area of negatively buoyant overshoot is minimised. A clear transition in atmospheric stability occurs (θ_{ve} in Figure 7.21). Over the shelf and seaward border the boundary layer is stable. Above the current a convective boundary layer is capped by an inversion which limits dry adiabatic convection. A closer inspection of Figures 7.21 reveals a similar pattern i.e. an increase in boundary layer stability away from the current toward the shelf and seaward border.

7.4.6 *Conclusion*

During the Agulhas Current Air-Sea Exchange Experiment a transition in cumulus was observed above the Agulhas Current during a period of anticyclonic ridging. In-situ data have allowed the reliable determination of the boundary layer structure in the first dedicated study of its kind in the region. Clear conditions over the shelf were replaced by active, coupled cumuli above the current and partly cloudy conditions above the seaward border. Negligible or even downward heat exchanges occur over the shelf whilst strong atmospheric heat and moisture gains occur over the current. This sets up a transition in stability of the boundary layer and potential cumulus formation.

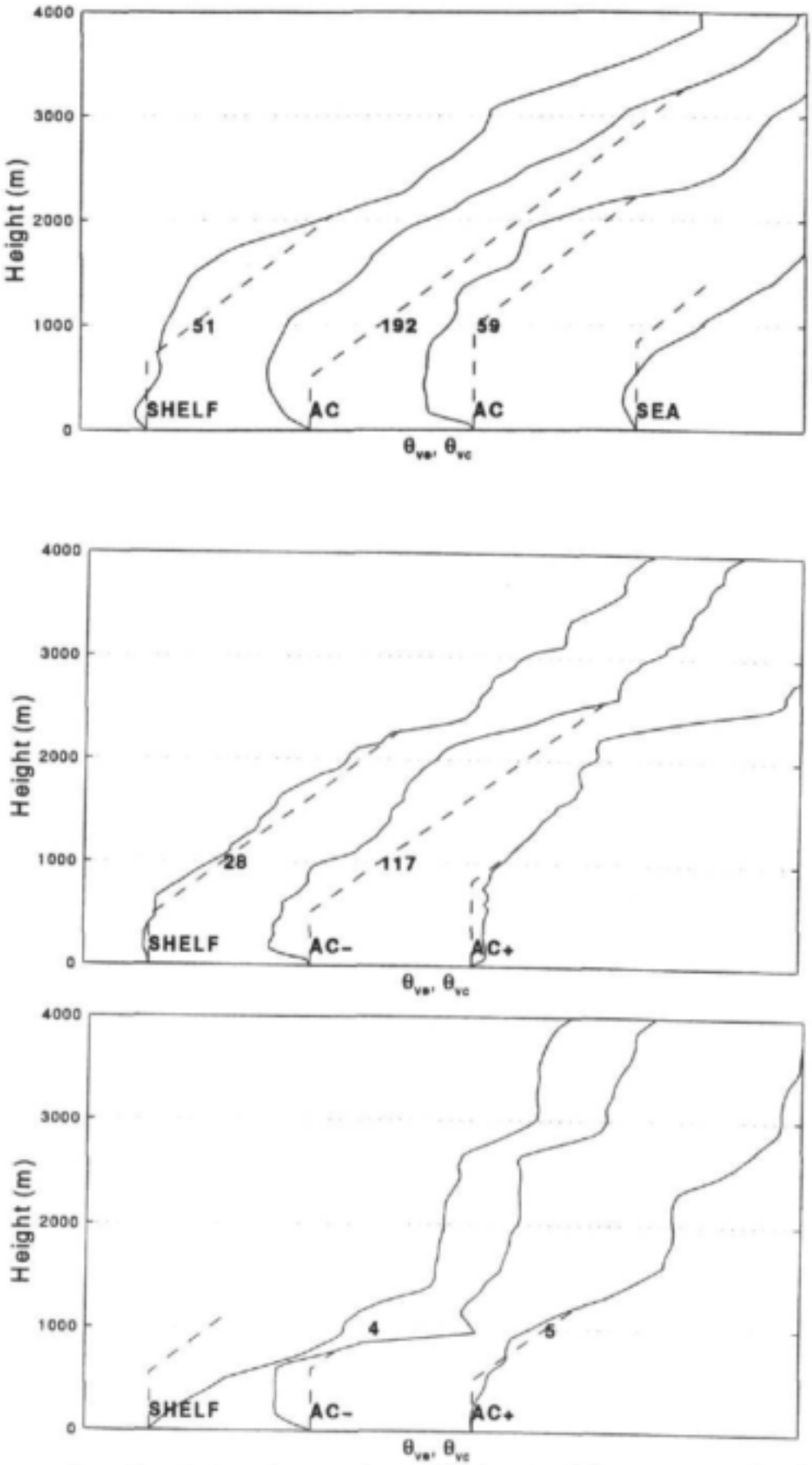

Figure 7.21: Spatial variation of convective available potential energy over the Agulhas Current on (a) 28 April, (b) 29 April and (c) 30 April over the shelf (SHELF), current (AC) and seaward border (SEA). The plots are the environmental (θ_{vc}) profile (-) and ascending air parcel (θ_{vc}) profile (- -), offset to aid visualisation. The CAPE (in $m^2.s^{-2}$ is also given with each profile.

Thermodynamic considerations adequately account for this cumulus transition. The vertical extent of cumulus is influenced by the atmospheric stability and limited by the subsidence inversion. Thus cumulus cloud lines also demonstrate a temporal evolution which is determined by the wind and subsidence field of the ridging anticyclone. This is important since the atmospheric boundary along the inshore edge of the current defines an atmospheric moisture front. The transition in cumulus may increase the vertical extent of this atmospheric moisture front through vertical redistribution of heat and moisture.

Chapter 8

Conclusion and Recommendations

This five year research program was designed to investigate the physical mechanisms of ocean-atmosphere interaction in the Agulhas Current and how the Agulhas Current affect the weather through this ocean-atmosphere interaction.

The first goal of this program was to perform high quality measurements above the Agulhas Current and to use up to date methods to quantify the air-sea interaction. Because turbulent fluxes are supposedly constant in the first 100 meters of the atmosphere, meteorological measurements made aboard a ship at one height allow the calculation of the turbulent fluxes and the vertical profile of wind speed, temperature and humidity in that layer. Radiosondes can then be used to link those surface measurements to the remainder of the atmosphere.

Once the latent and sensible heat fluxes are calculated, one needs to calculate the radiative heat fluxes to obtain the net heat flux at the sea surface. This parameter has a direct effect on the sea surface temperature, a parameter whose variation has been linked to South African climate variability.

The radiative budget was obtained by measuring the incoming short wave and long wave radiation at the sea surface and by calculating the outgoing long wave and short wave radiation. The first two quantities vary substantially as a function of time, ship position, cloud cover and atmospheric water vapor and have therefore to be measured to get a good estimate of the net heat budget at the surface. The outgoing longwave radiation is calculated with good accuracy as a function of the sea surface temperature. The outgoing short wave radiation was taken as a function of the incoming measured short wave radiation. The Eppley pyranometer (incoming short wave) and pyrgeometer (incoming long wave) gave us total satisfaction and we recommend their use.

The most important parameter and the most difficult to calculate is the turbulent latent heat flux, proportional to the water vapor flux at the sea surface. It is a function of wind speed, sea surface temperature and air temperature and humidity. It cannot be measured directly but can be derived using various methods from the measurement of wind speed relative to the ocean, sea surface temperature, air temperature and air specific humidity.

It is the measurement of the air humidity which is difficult mainly because of the contamination of the probes with sea spray and aerosols. To measure the humidity we tested a fast response hygrometer OPHIR and a slow response Vaisalla humidity and temperature probe. The Ophir did not give us satisfaction and we do not recommend its use. The Vaisalla probe was satisfactory and we recommend its use. We also recommend this low cost probe to be installed on the fleet of Sea Fisheries research vessell.
This probe could be added to the existing set of meteorological measurement devices aboard the research vessel S. A. Agulhas to provide an automatic, unmanned, air-sea interaction system. Measurement during the Marion Island relief cruises across the Agulhas Current with this new intrumentation can be complemented by radiosonde releases made by the South African Weather Bureau.

Moreover two of the methods used to calculate the turbulent fluxes, the inertial-dissipation method and the covariance methods require fast response instruments (at least 20 measurements per second) and make the measurement a technical challenge. The third method, the bulk method, only required slow response devices (measurements every 10 second) but these have to be averaged over a period of about 10 mn. This methods requires information on the ship's position, heading and velocity and the current velocity to calculate the absolute wind speed.

During the project we evaluated those methods and came the following conclusion. The inertial dissipation and the eddy covariance methods are technically difficult to implement, especially for the calculation of the sensible and latent heat fluxes. We had good result with the calculation of the wind stress using the inertial dissipation methods. A clear advantage of the inertial dissipation method to calculate the wind stress is that you just need to measure the relative wind speed which means that one does not need to have information

concerning the current velocity, the ship position and speed and the absolute wind speed which are mandatory for the bulk methods. We have tested an hybrid method where the wind stress is calculated with the inertial dissipation methods and the latent heat fluxes with the bulk methods.

We recommend the use of the Gill ultrasonic anemometer jointly with the use of the Vaisalla HMP35 humidity and temperature probe. This allow the use of the bulk method and the hybrid method jointly. The bulk method will provide long time series of the air sea exchange and the hybrid method will provide an better estimate of the wind stress and will allow a better calculation of the fluxes when ocean current velocity measurements are not available. To calculate the radiative budget we recommend the use of the Eppley pyranometer and pyrgeometer.

The system was made portable and can also be used for coastal meterology. The system was installed on the research vessel S.A Agulhas and tried with success during a 6 weeks cruise (the SAAMES 3 cruise) in the Roaring Forties during the 1993 winter. The system was then used in a coastal meteorology experiment in November 1993 and set up on a mast on top of a lighthouse at the end of a jetty. The highlight of the program was the Agulhas Current Air-Sea Exchange Experiment (ACASEX). It was the first dedicated air-sea interaction experimental cruise in the Agulhas Current. It took place during autumn 1995 to study the influence of the Agulhas Current on the atmospheric marine boundary layer.

We also took part in 2 cruises of opportunity, the ACE cruise in 1995 and the ACE recovery cruise in 1996. Being guests on foreign research vessel, it was not convenient to use our system and we used their meteorological instruments to collect data above the Agulhas current.

Most of our measurements have shown that the core of the Agulhas current, about 50 km wide, transfers about 5 time as much water vapour to the atmosphere as the surrounding water all year long. Moreover the structure of the marine atmospheric boundary layer in the first 1000 m is very different offshore, above the core of the current and above the colder inshore water. The atmospheric stability parameter is usually unstable above the current (highly convective condition) stable above the inshore cold water and near neutral offshore. This creates an important heterogeneity at the mesoscale. This heterogeneity will create a problem for General Circulation Models whose hypothesis of homogeneous turbulence between 2 grids points (usually, 300 to 100 km) will be seriously challenged south of Africa.

The SAAMES 3 was a multi-disciplinary cruise on the research vessel S. A. Agulhas during the austral winter of 1993. The aim of the physical oceanographic component of the research cruise was to identify a warm eddy south of the Subtropical Convergence in the region south of Africa and to investigate its interaction with the Subtropical Convergence, with the ambient Subantarctic water masses and with the overlying atmosphere. Mesoscale oceanic features are believed to have considerable effects on the overlying atmosphere, notwithstanding their relatively small lateral dimensions. Air-sea interaction measurements were made jointly with radiosonde launches and oceanographic measurements. These observations were made in winter, further enhancing the already strong ocean-atmosphere contrasts. The eddy was a substantial source of heat for the atmosphere as a result of latent heat fluxes of up to 500 Wm^{-2}, sensible heat fluxes of up to 350 Wm^{-2} and low short wave radiation inputs due to cloud coverage. The vertical heat flux from the ocean to the atmosphere in these mesoscale oceanic features is an order of magnitude higher than shown in climatology. Satellite altimetric data suggest that the eddy remained relatively stationary for a number of months. ERS-1 satellite wind measurements from this period show that the eddy had a persistent influence on the mesoscale wind field, increasing wind speeds whenever high differences between air and sea temperatures created unstable atmospheric conditions and high values of turbulent heat flux. Modification of air-sea interaction characteristics across the Agulhas Front, with a temperature gradient of 8 °C, were investigated during the cruise. It showed large differences of the air-sea exchange from the warm side to the cold side leading to decreases in wind strength on the colder sides.

The East London 1993 experiment was a multi-disciplinary study of the lower atmospheric environment west of East London in November 1993. The study region falls in a transition zone between a dry region to the west and sub-humid vegetated areas bordering the Agulhas Current to the east. Instrumented aircraft surveys were flown between the southeastern Karoo and the warm SW Indian Ocean. Meanwhile measurements were taken at the East London harbour jetty with our air-sea interaction measurement system. Cool upwelled water along the coast lies adjacent to sea surface temperatures > 24 °C offshore, where gale force winds were measured by the aircraft. Aircraft and radiosonde data quantified the depth of the atmospheric moist layer and reveal how the sub-humid front is shifted east-west by large scale weather systems. Some aircraft sections illustrate sharp spatial gradients and changes in surface fluxes

of the order of 100 $Wm^{-2}.(10\ KM)^{-1}$. Inland penetration of moisture depends on background zonal winds and depth of the marine layer. Aircraft turbulent covariance estimates are used to identify high surface heat fluxes over the inland arid Karoo. During easterly winds, moisture fluxes are greatest over vegetated coastal mountains in a plume 2 km deep. Surface moisture fluxes over the Agulhas Current and coastal mountains are double those over the cold inshore waters and inland desert. The injection of moist unstable air increases the convective potential, during ridging anticyclone weather conditions.

The Marion Island Relief Cruises are part of a routine annual program to supply the base on Marion Island. Calculation of the turbulent fluxes of momentum, latent and sensible heat requires the simultaneous measurement of wind speed, sea surface temperature, air temperature and air humidity. Except for air humidity, these parameters are measured and stored aboard the three research vessels, S.A. Agulhas, Africana and Algoa. These vessels average approximately 200 days at sea each year and could gather valuable air-sea interaction data. Our seas are too rough to have an array of air-sea interaction buoys such as the Tropical Atmosphere Ocean array of buoys deployed in the Pacific during TOGA. This provides ample motivation for a shipboard, automatic air-sea interaction monitoring scheme. The simple addition of an air humidity probe to the existing suit of instruments on any of these platforms completed a low-cost, automatic, air-sea interaction measurement system. A relative humidity probe was installed aboard the S.A. Agulhas to provide such a system in 1994. Radiosonde releases made by the South African Weather Bureau aboard this vessel linked the surface forcing to the remainder of the atmosphere providing invaluable data above the Agulhas Current at a very low cost and without having to spend 6 weeks to gather 4 days of data.

The Agulhas Current Air-Sea Exchange Experiment (20 April to 5 May, 1995) was the first dedicated air sea interaction cruise to investigate the horizontal variability of ocean atmosphere interaction over the Agulhas Current and adjacent sea. ACASEX resulted in a thorough investigation of the exchange between ocean and atmosphere, the net heat budget of the ocean, the structure of the marine atmospheric boundary layer as well as the behavior of the Agulhas Current and the upwelling cell at Port Alfred for different wind conditions. Approximately 20 transects across the Agulhas Current were carried out in the area where the Agulhas Current separates from the coast, namely between Port Elizabeth and Port Alfred. To link surface measurements to the marine atmospheric boundary layer, radiosondes were launched 4 times a day. Oceanographic measurements were carried out in support of this program. Surface heat fluxes increased by over 200 Wm^{-2} over the current from a negligible amount over the shelf whilst the sensible heat flux reversed sign. A characteristically stable boundary layer over the cool shelf waters was replaced by an unstable convective boundary layer over the current. For both westerly and easterly wind cases the mean specific humidity and potential temperature of the boundary layer increased significantly with a concomitant boundary layer deepening over the current.

In the presence of alongshore winds an atmospheric moisture and thermal front developed over the inshore SST front. This is attributed to the horizontal gradient in the surface heat fluxes at the time.

When air is advected towards the coast the surface latent heat flux increased from approximately 160 Wm^{-2} over the seaward border to 270 Wm^{-2} over the current (approximately 80-90 km wide) and decreased dramatically to approximately 40 Wm^{-2} over the cool shelf. This spatial heat flux gradient is reflected in the overlying atmosphere by a transition in atmospheric stability from the warm current to the cool continental shelf. A convective boundary layer over the current is replaced by a stable boundary layer over the cool shelf where a deep residual moisture layer indicated the former vertical extent of convective eddies. A progressive accumulation of moisture occurred within the boundary layer as the airmass is advected over the current. Mean specific humidity and precipitable water vapour content in the boundary layer over the shelf were 20-25% higher than over the seaward border of the current. The results give credence to the assertion by many investigators that moisture uptake above the Agulhas Current may contribute significantly to moisture convergence and rainfall over the interior of South Africa.

During the cruise a transition in cumulus was observed above the Agulhas Current during a period of anticyclonic ridging. Clear conditions over the shelf were replaced by active, coupled cumuli above the current and partly cloudy conditions above the seaward border. Negligible or even downward heat exchanges occur over the shelf whilst strong atmospheric heat and moisture gains occur over the current. This sets up a transition in stability of the boundary layer and potential cumulus formation. Thermodynamic considerations adequately account for this cumulus transition. The vertical extent of cumulus is influenced by the atmospheric stability and limited by the subsidence inversion. Thus cumulus cloud lines also demonstrate a temporal evolution which is determined by the wind and subsidence field of the ridging

anticyclone. The transition in cumulus may increase the vertical extent of this atmospheric moisture front through vertical redistribution of heat and moisture.

Another important result was that neglecting the speed of the Agulhas Current in the calculation of the wind stress, sensible and latent heat flux could lead to important mis-estimation of those fluxes. The mistake would be the same as a mistake induced by a 2 m/s error in the wind speed measurement.

Results of the kind produced by this project may be used to parameterize ocean-atmosphere processes for ocean regions of importance for South Africa. Doors have been opened for fruitful international collaboration in this regard.

Even though the aims of this project were comprehensively addressed, the extent of the results obtained was necessarily limited with respect to both time and space. Further challenges lie in using such local-scale data in conjunction with remotely-sensed data, to quantify processes operating over larger ocean areas.

To this end, it is recommended that the research be continued, with the following objectives in mind:

1. To develop an adequate understanding of the role of ocean-atmosphere interactions in regulating rainfall and drought in South Africa.
2. To develop a satellite-based methodology to study and monitor the hydrological cycle from ocean evaporation to the advection of water vapour over southern Africa.
3. To use the *in situ* measurement techniques developed and data acquired during the completed project to validate satellite observations and model output that are useful in predicting rainfall over southern Africa.
4. To acquire more information on the mechanisms causing sea surface temperature variability in those regions where such anomalies are linked to drought in southern Africa.
5. To develop satellite remote sensing applications for the weather forecaster, the climate forecaster and the water resource manager.

Chapter 9

Project output

RESEARCH ARTICLES

Jury, M.R. and Lutjeharms, J.R.E.: 1993, Die struktuur en aandrywingskragte van die 1991-1992 droogte in suidelike Afrika. Suid-Afrikaanse Tydskrif vir Natuurwetenskap en Tegnologie, 12, 8-16.

Jury, M.R., Valentine, H.R. and Lutjeharms, J.R.E.: 1993, Influence of the Agulhas Current on Summer rainfall on the southeast coast of South Africa. Journal of Applied Meteorology, 32, 1282-1287.

Rouault, M. and Lutjeharms, J.R.E.: 1994 , Air-sea interaction in the marine atmospheric boundary layer: a new South African research venture. South African Journal of Science, 90, 11-12.

Lutjeharms, J.R.E, Lucas, M.I., Perissinotto, R., van Ballegooyen,R. C. and Rouault M.: 1994, Oceanic processes at the Subtropical Convergence: report of research cruise SAAMES 3. South African Journal of Science, 90, 367-370.

Rouault, M., Lee-Thorp, A. M., Ansorge, I. and Lutjeharms, J.R.E.: 1995, The Agulhas Current Air-Sea Exchange Experiment. South African Journal of Science, 91, 493-496.

Andreas, E.L., Edson, J.B., Monahan, E.C., Rouault, M. Smith, S.: 1995, The spray contribution to net evaporation from the sea: A review of recent progress. Boundary Layer Meteorology, 72, 3-52.

Jury, M., Rouault, M., Weeks, S. and Shormann, M.: 1997, Atmospheric boundary layer fluxes and structure across a transition zone in Southeastern Africa. Boundary Layer Meteorology, 83, 311-330.

Rouault, M. and Lee-Thorp, A. M.: 1997, Fine-Time resolution measurements of atmospheric boundary layer properties between Cape Town and Marion Island. South African Journal of Marine Science, 17, 281-296.

Rouault, M. and Lutjeharms, J.R.E.: 1997, Air-sea exchange over an Agulhas eddy at the Subtropical Convergence. The Global Atmosphere and Ocean System, in revision.

Lee-Thorp, A. M., Rouault, M. and Lutjeharms, J.R.E.: 1997, Moisture uptake in the boundary layer above the Agulhas Current: a case study. Journal of Geophysical Research, in press

Lee-Thorp, A. M., Rouault, M. and Lutjeharms, J.R.E.: 1997, Cumulus cloud formation above the Agulhas Current. South African Journal of Science, in press

Rouault, M., Lee-Thorp, A. M., Ansorge, I. and Lutjeharms, J.R.E.: 1997, Observations of the

atmospheric boundary layer above the Agulhas Current during alongcurrent winds, Journal of Physical Oceanography, in press

CONFERENCE PROCEEDINGS

Rouault, M., Lutjeharms, J. R. E. and Van Ballegooyen, R. C.: 1994, Air-sea Interaction at the Subtropical Convergence South of Africa. Proceedings of Second International Conference on Air-Sea Interaction and Meteorology and Oceanography of the Coastal Zone, 22-27 September 1994, Lisbon, Portugal, pp 32-33.

Rouault, M., Lee-Thorp, A. M. and Lutjeharms, J. R. E.: 1994, New Research Initiative on Air-Sea Interaction in South Africa. Proceedings of Second International Conference on Air-Sea Interaction and Meteorology and Oceanography of the Coastal Zone, 22-27 September 1994, Lisbon, Portugal, pp 254-255.

Lutjeharms, J.R.E., Jury, M.R., and Mason, S.J.: 1995, Oceanic influence on southern Africa's climate. Global Environmental Change: implication for southern Africa, regional conference, Program and Abstract, 24-26, April 1995, Pretoria, pp 92-94.

Rouault, M., Lee-Thorp, A. M. and Lutjeharms, J.R.E.: 1996, Boundary Layer Modification Above The Agulhas Current. Proceeding of Conference on Meteorology and Oceanography of the Coastal Zone, 76th American Meteorological Conference, 28 January-2 February, Atlanta, 1996, pp 116-119.

Rouault, M., Lee-Thorp, A. M. , Lutjeharms, J. R. E. and Ansorge, I.: 1996, Air Sea interaction Above the Agulhas Current. Invited paper, Proceedings Eigth Conference on Air-Sea Interaction, 76th American Meteorological Conference, 28 January-2 February, 1996, Atlanta, pp 1-6.

Rouault, M., Lee-Thorp, A. M. and Lutjeharms, J.R.E.: 1997, The Agulhas Current Air Sea Exchange Experiment. Fifth International Conference on Southern Hemisphere Meteorology and Oceanography, 7-11 April 1997, Pretoria, South Africa, Preprints, pp 314-315.

Lee-Thorp, A. M., Rouault, M. and Lutjeharms, J.R.E.: 1997, Air-sea interaction effects in the boundary layer above the Agulhas Current. Fifth International Conference on Southern Hemisphere Meteorology and Oceanography, 7-11 April 1997, Pretoria, South Africa, Preprints, pp 318-319.

Majodina, M., Jury, M. R. and Rouault, M.: 1997, Tropical air- sea interaction duringacruise in the central Indian Ocean. Fifth International Conference on Southern Hemisphere Meteorology and Oceanography, 7-11 April 1997, Pretoria, South Africa, Preprints, pp 364-365.

CONFERENCE ABSTRACTS.

Rouault, M. and Lutjeharms, J.R.E.: 1993, New research initiative on air sea interaction. Eighth Southern African Marine Science Symposium. 17-22 October 1993. Langebaan, South Africa.

Rouault, M. and Lutjeharms, J.R.E.: 1993, New Research Initiative on Air-sea Interaction. Tenth Annual Conference, South African Society of Atmospheric Science, 13-14 October, 1993, Pretoria.

Rouault, M., Lee-Thorp, A. M., Ansorge, I. and Lutjeharms, J.R.E.: 1995, The Agulhas Current air-sea exchange experiment, South African Society of Atmospheric Science Annual Conference, 25-37 October 1995, Pretoria.

Rouault, M.,Lutjeharms, J.R.E., Jury, M. R. and Lee-Thorp, A. M.: 1995, Air-sea interaction

research in South Africa, South African Society of Atmospheric Science Annual Conference, 25-27 October 1995, Pretoria.

Majodina, M., Rouault, M. and Jury, M. R.: 1996, Tropical air-sea interactions during a cruise in the Central Indian Ocean. 9th Southern African Marine Science Symposium, 21-23 November 1996, Cape Town.

Rouault, M., Lee-Thorp, A. M., Ansorge, I. and Lutjeharms, J.R.E.: 1996, The Agulhas Current Air-Sea Exchange Experiment, 9th Southern African Marine Science Symposium, 21-23 November 1996, Cape Town.

Lee-Thorp, A. M., Rouault, M. and Lutjeharms, J.R.E.: 1996, Air-sea interaction in the Agulhas Current System. 9th Southern African Marine Science Symposium, 21-23 November 1996, Cape Town.

Ansorge, I. , Lutjeharms, J. R. E., Roberts, M., Cooper, J. and Rouault, M.: 1996, Variability of the eastern Agulhas Bank upwelling cell. Benguela Dynamics Symposium, 25-27 November 1996, Programme, Abstracts & Directory, p. 23.

Rouault, M., Lee-Thorp, A. M. and Lutjeharms, J.R.E.: 1997, Differences between ERS1, ECMWF, state of the art meteorological measurements and voluntary observing ships in the Agulhas Current. Annales Geophysicae, European Geophysical Society, Part II Hydrology, Oceans, Atmosphere & Nonlinear Geophysics, Supplement II to Volume 15, p. C409.

TECHNICAL REPORTS

Rouault, M., Lee-Thorp, A. M., Ansorge, I., Lutjeharms, J. R. E.: 1996, Data report on the Agulhas Current Air-sea Exchange Experiment, April-May 1995. University of Cape Town Report 97-1, 160 pp.

Bibliography

[1] Albrecht, B. A., Fairall, C. W., Thomson, D. W., White, A. B., Snider, J. B. and Schubert, W. H.: 1990, Surface based remote sensing of the observed and the adiabatic liquid water content of stratocumulus clouds, *Geophys. Res. Let.*, **17**, 89-92.

[2] Bane, J. M. Jr: 1989, Results From the Genesis of Atlantic Lows Experiment, Physical Oceanographic Studues: Introduction, *J. Geophys. Res.*, **94**, 10685.

[3] Bang, N. D.: 1970, Dynamic interpretations of a detailed surface temperature chart of the Agulhas Current retroflexion (sic) and fragmentation area, *S. Afr. Geograph. J.*, **52**, 67-76.

[4] Barnston, A. G., Thiao, W. and Kumar, V.: 1996, Long-lead forecasts of seasonal precipitation in Africa using CCA. *Weather and Forecasting*, **11**, 4, 506-520.

[5] Beardsley, R. C., Dorman, C. E., Friehe, C. A., Rosenfield, L. K. and Winant, C.D.: 1987, Local atmospheric forcing during the Coastal Ocean Dynamics Experiment, 1, A description of the marine atmospheric boundary layer and atmospheric conditions over a northern Californian upwelling region, *J. Geophys. Res.*, **92**, 1467-1488.

[6] Bentamy, A., Quilfen, Y., Gohin, F., Grima, N., Lenaour, M. and Servain, J.: 1996, Determination and validation of average wind fields from ERS-1 scaterrometer measurements. *Global Atm. Oc. Sys.*, **4**, 1-29.

[7] Betts, A. K. and Albrecht, B. A.: 1987, Conserved variable analysis of the convective boundary layer thermodynamic structure over the tropical oceans, *J. Atm. Sci.*, **44**, 83-99.

[8] Betts, A. K. and Bartlo, J.: 1991: The density temperature and the dry and wet virtual adiabats, *Mon. Weather Rev.*, **119**, 169-175.

[9] Blanc, T. V.: 1987, Accuracy of bulk-determined flux, stability and sea surface roughness, *J. Geophys. Res.*, **92**, 3867-3875.

[10] Bolton, D.: 1980, The computation of equivalent potential temperature, *Mon. Weather Rev.* **108**, 1046-1053.

[11] Brown, R.A. and Foster, R.C.: 1994, On PBL models for general circulation models, *J. Global Atmos. Oc. Sys.*, **2**, 163-183.

[12] Buck, A. L.: 1981, New equations for computing vapor pressure and enhancement factor, *J. Appl. Meteo.*, **20**, 1527-1532.

[13] Budyko, M. I.: 1963, Atlas of heat balance of the world, Glabnaia Geofiz. Observ., [Also: Guide to the atlas of the heat balance of the earth, Translation by I A Donehoo, 1963, U S Weather Bureau WB/T-106, Washington D C].

[14] Bunker, A. F.: 1976, Computations of surface energy flux and annual air-sea interaction cycles of the North Atlantic Ocean, *Mon. Weather Rev.*, **104**, 1122-1140.

[15] Cess, R. D., Potter, G. L., Blanchet, J. P., Boer, G. J., Del Ginio, A., Deque, D.M., Dymnikov, V., Galine, V., Gates, W. L., Ghan, S. J., Kiehl, J. T. A., Lacis, A., Le Treut, M., Li, Z. X., Liang, X. Z., Mcavaney, B. J., Meleshko, V. P., Mitchell, J. F. B., Morcrette, J. J., Randall, D. A., Rikus, L., Roeckner, A.,Royer, J. F., Schlese, U, Scheinin, D. A., Slingo, A., Sokolov, A. P., Taylor, K. E., Washington, W. M., Wetherald, R. T., Yagai I. and Zhang, M. H.: 1990, Intercomparison and interpretation of climate feedback processes in 19 atmospheric general circulation models, *J. Geophys. Res.*, **95**, 16601-16605.

[16] Comrie, A. C.: 1988, Growth structure and prediction of the thermal internal boundary layer, MSc thesis, Univ. Cape Town.

[17] Davidson, K. L., Boyle, P. J., Gautier, C., Hanson, H. P., and Khalsa, S. J. S.: 1991, Medium- to large-scale atmospheric variability during the Frontal Air-Sea Interaction Experiment, *J. Geophys. Res.*, **96**, 8531-8551.

[18] Deardorff, J. W., Willis, G. E. and Lilly, D. K.:, 1969, Laboratory investigation of non-steady penetrative convection, *J. Fluid Mecha.*, **35**, 7-31 pp.

[19] DeCosmo, J., Katsaros, K. B., Smith, S. D., Anderson, R. J., Oost, W. A., Bumke, K. and Chadwick, H.,: 1996, Air-sea exchange of water vapour and sensible heat: The Humidity Exchange Over the Sea (HEXOS) results, *J. Geophys. Res.*, **101**, 12001-12016.

[20] Edson, J.B., Fairall, C.W., Larsen, S.E. and Mestayer, P.G.: 1990, Study of the inertial-dissipation technique for computing air-sea fluxes, *J. Geophys. Res.*, **96**, 10689-10711.

[21] Fairall, C.W., Edson, J.B., Larsen, S.E. and Mestayer, P.G.: 1990 Inertial-dissipation air-sea flux measurements: A prototype system using realtime spectral computations, *J. Atmos. Oceanic Tech.*, **7**, 425-453.

[22] Fairall, C.W., Bradley, E. F., Rogers, D. P., Edson, J. B. and Young, G. S.: 1996, Bulk parametrization of air-sea fluxes for TOGA COARE, *J. Geophys. Res.*, **101**, 3747-3754, 1996.

[23] Fitschen, L. J. and Gay, L. W.:, 1979, Environmental Instrumentation, Springer-Verlag, New York.

[24] Friehe, C. A., Shaw, W. J., Rogers, D. P., Davidson, K. L., Large, W. G., Stage, S. A., Crescenti, G. H., Khalsa, S. J. S., Greenhut, G. K., and Li, F.: 1991, Air-sea fluxes and surface layer turbulence around a sea surface temperature front, *J. Geophys. Res.*, **96**, 8593-8609.

[25] Foster, R.C. and Brown, R.A.: 1994, On large-scale PBL modelling: surface wind and latent heat flux comparisons, *J. Global Atmos. Oc. Sys.*, **2**, 199-219.

[26] Gamo, M., Yamamoto, S. and Yokoyama, O.: 1982, Airborne measurements of the free convective internal boundary layer during the sea breeze, *J. Meteorol. Soc. Japan*, **60**, 1284-1298.

[27] Gill, A. E.: 1982, Atmosphere-Ocean Dynamics, Academic Press, London, 622 pp.

[28] Gutowski, W. J. Jr., Otles, Z. and Chen, Y.: 1997, Effect of ocean-surface heterogeneity on Climate Simulation. Submitted to J. Clim.

[29] Harrison, M. S. J.: 1984, A generalized classification of South African summer rain-bearing synoptic systems, *Int. J. Clim.*, **4**, 547-560.

[30] Holton, J. R.: 1972, An introduction to dynamic meteorology, second edition, Academic Press, San Diego, California.

[31] Jury, M. R.: 1993, A thermal front within the atmospheric boundary layer over the Agulhas Current south of Africa: Composite aircraft observations, *J. Geophys. Res.*, **99**, 3297-3304.

[32] Jury, M. R.: 1994, A review of the meteorology of the eastern Agulhas Bank, *S. Afr. J. Sc.*, **90**, 109-113.

[33] Jury, M. R.: 1995, A review of research on ocean-atmosphere interactions and South African climate variability, *S. Afr. J. Sci.*, **91**, 289-294.

[34] Jury, M.R. and Walker, N. D.: 1988, Marine boundary layer modification across the edge of the Agulhas Current, *J. Geophys. Res.*, **93**, 647-654.

[35] Jury, M.R. and Courtney, S.: 1991, A transition in weather over the Agulhas Current, *S. Afr. J. Mar. Sci.*, **10**, 159-171.

[36] Jury, M. R. and Levey, K.: 1993, The climatology and characteristics of drought in the eastern Cape of South Africa, *Int. J. Clim.*, **13**, 629-641.

[37] Jury, M. R., Valentine, H. R., and Lutjeharms, J. R. E.: 1993a, Influence of the Agulhas Current on summer rainfall along the southeast coast of South Africa, *J. Appl. Meteorol.*, **32**, 1282-1287.

[38] Jury, M. R., Diab, R. D., and Schormann, M.: 1993b, An aircraft study of mesoscale surface wind patterns and associated meteorological conditions over Cape St Francis South Africa, *J. Appl. Meteorol.*, **32**, 1647-1655.

[39] Katsaros, K.B., Donelan, M.A., Drennan, W.M., and Howard, K.M.: 1994, Surface fluxes and their relation to planetary boundary layer structure, in Proceedings of *Air-Sea Interface Symposium, Radio and Acoustic Sensing, Turbulence and Wave Dynamics*, Marseille, France, June 24-30, 1993.

[40] Khalsa, S.J.S. and Greenhut, G.K.: 1989, Atmospheric turbulence structure in the vicinity of an oceanic front, *J. Geophys. Res.*, **94**, 4913-4922.

[41] Lee-Thorp, A.M.: 1996, The atmospheric boundary layer above the Agulhas Current, MSc Dissertation, University of Cape Town.

[42] Lenschow, D. H.: 1986, Aircraft measurements in the boundary layer, in *Probing the Atmospheric Boundary Layer*, ed. D. H. Lenschow, Amer. Meteorol. Soc., Boston, 39-55.

[43] Liu, W.T., Katsaros, K.B. and Businger, J.A.: 1979, Bulk parametrization of air-sea exchanges of heat and water vapour including the molecular constraints at the interface, *J. Atmos. Sci.*, **36**, 1722-1734.

[44] Lutjeharms, J. R. E. and van Ballegooyen, R. C.: 1984, Topographic control in the Agulhas Current system, *Deep-Sea Res.*, **31**, 1321-1337.

[45] Lutjeharms, J.R.E., Mey, R.D. and Hunter, I.T.: 1986, Cloud lines over the Agulhas Current, *S. Afr. J. Sci.*, **82**, 635-640.

[46] Lutjeharms, J. R. E. and Valentine, H. R.: 1988, Eddies at the Sub-Tropical Convergence south of Africa, *J. Phys. Ocean.*, **18**, 772-774.

[47] Lutjeharms, J. R. E. and Gordon, A. L.: Shedding of an Agulhas Ring observed at sea, *Nature*, **325**, 138-140.

[48] Lutjeharms, J. R. E., Lucas, M. I., Perissinotto, R., van Ballegooyen, R. C. and Rouault, M.: 1994, Oceanic processes at the Subtropical Convergence; report of research cruise SAAMES III. *S. Afr. J. Sci.*, **90**, 367-370.

[49] Lutjeharms, J.R.E. and Cooper, J.: 1998, Upwelling inshore of the Agulhas Current, submitted to *Cont. Shelf Res.*

[50] McCreary, J. P. Jr., Kundu, P. K. and Molinari, R. L.: 1993, A numerical investigation of dynamics, thermodynamics and mixed-layer processes in the Indian Ocean, *Prog. in Oceanogr.*, **31**, 3, 181-244.

[51] Mason, S. J.: 1995, Sea surface temperature - South African rainfall associations, 1910 - 1989, *Int. J. Climatol.*, **15**, 119-135.

[52] Mesiä, H.: 1993, Humicap, 20 years of excellence, *Vaisala News*, **129**, 6-8.

[53] Mey, R.D., Walker, N.D and Jury, M.R.: 1990, Surface heat fluxes and marine boundary layer modification in the Agulhas Retroflection Region, *J. Geophys. Res.*, **95**, 15997-16015.

[54] Olson, D. B. and Evans, R. H.: 1986, Rings of the Agulhas Current. *Deep-Sea Res.*, **33**, 27-42.

[55] Pearce, A.F.: 1977, Some features of the upper 500 m of the Agulhas Current, *J. Mar. Res.*, **35**, 731-751.

[56] Preston-Whyte, R. A. and Tyson, P. D.: 1988, The atmosphere and weather of Southern Africa, Oxford University Press, Cape Town, South Africa.

[57] Quilfen, Y.: 1993, ERS-1 scatterometer off-line products: calibration/validation results and case studies, Proc. IGARSS 1993, Japan, 1750-1752.

[58] Raynor, G. S., Sethuraman, S. and Brown, R. M.: 1979, Formation and characteristics of coastal internal boundary layers during onshore flows, *Boundary-Layer Meteorol.*, **16**, 487-514.

[59] Rigg, G. M., van Ballegooyen, R. C., Attwood, C., Newton, S., Lucas, M. and Lutjeharms, J. R. E.: 1992, Data report on the first cruise of the South African Antarctic Marine Ecosystems Study (SAAMES-I), April - May 1992. University of Cape Town, Department of Oceanography, Report DO-92-01, 1992.

[60] Rouault, M., Lee-Thorp, A.M., Ansorge, I., and Lutjeharms, J.R.E.,: 1995, The Agulhas Current Air-Sea Exchange Experiment, *S. Afr. J. Sci.*, **91**, 493-496.

[61] Said, F. and Druilhet, A.: 1991, Experimental study of the atmopheric marine boundary layer from in-situ aircraft measurements: variability of boundary conditions and eddy flux parameterization, *Boundary-Layer Meteorol.*, **57**, 219-249.

[62] Schumann, E.H.: 1989, The propagation of air pressure and wind systems along the South African coast, *S. Afr. J. Sci.*,**85**, 382-385.

[63] Schumann, E. H., Perrins, L. A. and Hunter, I. T.: 1982, Upwelling along the south coast of the Cape Province, South Africa, *S. Afr. J. Sci.*, **78**, 238-242.

[64] Sethuraman, S., Brown, R. M., Raynor, G. S. and Tuthill, W. A.: 1979, Calibration and use of a sailplane variometer to measure vertical velocity fluctuations, *Boundary-Layer Meteorol.*, **16**, 99-105.

[65] Smith, S. D.: 1988, Coefficients for sea surface wind stress, heat flux and wind profiles as a function of wind speed and temperature, *J. Geophys. Res.*, **93**, 15467-15472.

[66] Stull, R. B.: 1988, An introduction to boundary layer meteorology, Kluwer Academic Publishers, Dordrecht, The Netherlands.

[67] Sweet, W., Fett, R., Kerling, J. and LaViolette, P.: 1981, Air-sea interaction effects in the lower troposphere across the north wall of the Gulf Stream, *Mon. Weather Rev.*, **109**, 1042-1052.

[68] Tanga, L. V.: 1992, Rainfall disparities in the eastern Cape, MSc thesis, Univ. Fort Hare, Alice.

[69] Tennant, W. J.: 1996, Influence of Indian Ocean sea surface temperature anomalies on the general circulation of southern Africa, *S. Afr. J. Sci.*, **92**, 289-295.

[70] Tjernström, M.: 1991, Airborne observations of thermal mesoscale circulations in the coastal marine boundary layer, *J. Geophys. Res.*, **96**, 20499-20520.

[71] Tucker, C. J.: 1978, A comparison of sensor bands for vegetation monitoring. *Remote Sens.*, **44**, 1369-1380

[72] Uys, C. J.: 1983, Rainfall variations at Fort Hare (1970-1982), MSc thesis, Univ. Fort Hare, Alice.

[73] Van Ballegooyen, R.C., Grundlingh, M. L. and Lutjeharms, J. R. E.: 1994, Eddy fluxes of heat and salt from the southwest Indian Ocean into the southeast Atlantic Ocean: a case study. *J. Geophys. Res.*, **99**; 4053-14070.

[74] Walker, N.D.: 1990, Links between South African rainfall and temperature variability of the Agulhas and Benguela Current systems, *J. Geophys. Res.*, **95**, 3297-3319.

[75] Walker, N.D. and Mey, R.D.: 1988, Ocean atmosphere heat fluxes within the Agulhas Retroflection Region, *J. Geophys. Res.*, **93**, 15473-15483.

[76] Wyngaard, J. C.: 1986, Observational Strategies, in Probing the Atmospheric Boundary Layer, ed. D. H. Lenschow, Amer. Meteorol. Soc., Boston, 269 pp.

[77] Xie, L., Pietrafesa, L. J. and Raman, S.: 1996, Mesoscale air-sea interaction over the continental shelf off the Carolina coast. *Global Atm. Oc. Sys.*, **4**, 65-88.

[78] Yelland, M. and Taylor, P. K.: 1996, Wind stress measurement from the open ocean. *J. Phys. Oceanogr.*, **26**, 541-558.

[79] Zemba, J. and Friehe, C.A.: 1987, The marine atmospheric boundary layer jet in the Coastal Ocean Dynamics Experiment, *J. Geophys. Res.*, **92**, 1489-1496.